Sveriges lantbruksuniversitet
Swedish University of Agricultural Sciences

Department of Soil and Environment

Carbonaceous aerosols and trace metal deposition in high-latitude snow –

A comparative study in Sweden and Alaska

Anika Pinzner

Master's Thesis in Environmental Science
EnvEuro – European Master in Environmental Science

Examensarbeten, Institutionen för mark och miljö, SLU
2019:07

Uppsala 2019

Carbonaceous aerosols and trace metal deposition in high-latitude snow – A comparative study in Sweden and Alaska

Anika Pinzer

Supervisor: Youen Grusson, Department of Soil and Environment, SLU
Assistant supervisor: Anders Svensson, University of Copenhagen, Niels Bohr Institute, Center for Ice and Climate
Assistant supervisor: Christian Zdanowicz, Department of Earth Sciences, Uppsala University
Assistant supervisor: Martin Stuefer, Geophysical Institute, Atmospheric Sciences University of Alaska Fairbanks,
Examiner: Jon Petter Gustafsson, Department of Soil and Environment, SLU

Credits: 30 ECTS
Level: Second cycle, A2E
Course title: Independent Project in Environmental Science – Master´s thesis
Course code: EX0431
Programme/Education: EnvEuro – European Master in Environmental Science 120 credits
Course coordinating department: Soil and Environment

Place of publication: Uppsala
Year of publication: 2019
Cover picture: 2017, Denali National park, photo by: Anika Pinzer
Title of series: Examensarbeten, Institutionen för mark och miljö, SLU
Number of part of series: 2019:07
Online publication: http://stud.epsilon.slu.se

Keywords: now, PM, carbon particles, pXRF, Arctic, subarctic, EC/OC, LAHM, PSAP, TOT, ICP-MS, filter, contamination, albedo

Sveriges lantbruksuniversitet
Swedish University of Agricultural Sciences

Faculty of Natural Resources and Agricultural Sciences
Department of Soil and Environment

Abstract

This study investigates the advantages and disadvantages of several destructive and non-destructive analytical methods that can be employed to characterize airborne particulate matter (PM) deposited in seasonal snow. To this end, a comparative study was conducted on PM obtained from snowpack surveys in two Arctic/subarctic regions of Northern Sweden and Interior Alaska, USA. This study measured and characterized carbonaceous particles (CPs) in snow-filtered PM using three different optical analytical methods: a Particle Soot Absorption Photometer (PSAP), a Thermo-Optical Transmittance (TOT) analyser, and a Light-Absorbing Heating Method (LAHM) instrument. The study additionally tested the applicability of a portable X-Ray Fluorescence (pXRF) analyser for quantifying the particulate trace metal content in the snow. The ratios of analytes from the measurements performed with the pXRF were also compared with the ratios of elements from bulk chemical analyses by Inductively Coupled Plasma Mass Spectrometry (ICP-MS). Snow meltwater was filtered with two filtration set-ups (syringe and vacuum-pump) on two differently sized tissuquartz filters (25 mm and 50 mm). The analysis of CPs suggests a higher correlation between the measurements of PSAP/TOT in comparison to LAHM/TOT measurements. The lower association between LAHM and TOT were i.a. assumed to derive from heterogeneities of the loading of the filter material especially on the smaller 25 mm filters produced by syringe-filtration. Organic carbon (OC) and elemental carbon (EC) values derived from TOT measurements gave insight into possible emission sources in different geographic regions of Sweden and Alaska. High OC values in rural Alaska suggested the influence of wood smoke on the particle composition in the snow. The chemical analysis of the empty and blank tissuquartz filters used for filtration showed high base elemental concentrations. Despite these high initial values of the filter matrix, an analysis of the two inbuilt calibrations 'GeoMining' and 'GeoExploration' showed that both calibrations measure relatively precisely. pXRF calibration 'GeoExploration' further yielded higher count rates and thus is more suitable for trace metal analysis filters than calibration 'GeoMining.' The correlation of ICP-MS vs. pXRF further showed no significant relationship between the measurements of the two methods. Yet, for filters with high filter loadings the relative concentration pattern (RCP) of the pXRF measurements reflected the chemical composition of the respective sample environment. This suggests that further investigations into using pXRF for snowpack analyses could be a valuable time- and cost-effective tool for the analysis of chemical composition of snow.

Keywords: PM, carbon particles, trace metals, pXRF, Arctic, subarc-tic, EC/OC, LAHM, PSAP, TOT, ICP-MS, filter, contamination, albedo

Popular Science Summary

Snow has many important functions: It serves as animal habitat, enables transportation (e.g. by dogsled), regulates the climate and yields water for almost two billion people worldwide. Even though snow is primarily composed of water, snow-flakes can scavenge small particles emitted by natural or anthropogenic sources and deposit them on the snowpack. Such particles, also called particular matter (PM), can also be deposited via settling of particles on the snow or other forms of dry deposition. Of concern are particles which contain carbon, and which are therefore dark in colour. Dark particles take up more energy than ice crystals in snow and can therefore lead to an earlier beginning of the snow melt season. Another concern is the level of trace metals in PM which, in certain amounts, can be toxic to humans, animals, and plants once released to streams and waterbodies.

To analyse and characterize the different components of PM in snow, snow samples were taken in Northern Sweden and Interior Alaska in places with varying human influence and proximity to different emission sources. The snow was subsequently melted and filtered with two different filtration set-ups and the resulting loaded quartz filters were analysed using five methods. To measure carbonaceous particles (CP) in snow, three methods were applied, and the respective results compared. The methods were based on different physical principles (thermal or optical), and thus introduced different uncertainties into their measurements. It was found that a lesser load of particles on the filters is preferable for the analysis of CP. Snow samples were screened for trace metals using two methods, one of which was rather exploratory in design, as the respective method hasn't been widely applied to such filter material yet. Some of the snow samples showed concerning high concentrations of certain elements which could be related to the environmental setting in which the samples were taken. It was also shown that filtering snow meltwater with a vacuum pump instead of a syringe produced more homogeneous filter loadings.

Due to the increase of human activities in Arctic and subarctic regions and the important ecosystem functions of snow, quantifying the different impurities in snow can help increase understanding and prediction of snow melt rates as well as ecosystem responses to change.

Declaration of Authorship

I, Anika PINZNER, declare that this thesis titled, “Carbonaceous aerosols and trace metal deposition in high-latitude snow: A comparative study in Sweden and Alaska” and the work presented in it are my own.

I confirm that:

- This work was done wholly or mainly while in candidature for a research degree at the above-mentioned Universities.
- Where I have consulted the published work of others, this is always clearly attributed.
- Where any part of this thesis has previously been submitted for a degree at this University or any other institution, this has been clearly stated.
- Where I have quoted from the work of others, the source is always given. With the exception of such quotations, this thesis is entirely my own work.
- I have acknowledged all main sources of help.

Signed: _____

Date: _____

Table of contents

List of tables

Appendix - Tables

List of figures

Appendix - Figures

Abbreviations

AC	Atmospheric Circulation
Al	Aluminium
AK	Alaska
AMAP	Arctic Monitoring and Assessment Programme
AO	Arctic Oscillation
Ar	Argon
ARM	Atmospheric Radiation Measurement
As	Arsenic
Ba	Barium
BC	Black Carbon
BCe	Black Carbon equivalent
Ca	Calcium
Cd	Cadmium
CO	Carbon monoxide
CP	Carbon/ carbonaceous particle
Cu	Copper
Cr	Chromium
CV	Coefficient of variation
DI	Deionized
E	GeoExploration
eBC	Equivalent Black Carbon
EC	Elemental Carbon
EDXRF	Energy dispersive X-Ray Fluorescence
EEA	European Environmental Agency
EPA	United States Environmental Protection Agency
Est.BC	Estimated Black Carbon
Fe	Iron
FID	Flame ionization detector

H_2O_2	Hydrogen peroxide
HF	Hydrofluoric acid
Hg	Mercury
HNO_3	Nitric acid
ICP-QP-MS	Inductively Coupled Plasma Quadrupole Mass Spectrometer
IUPAC	International Union of Pure and Applied Chemistry
K	Potassium
LAHM	Light-Absorption Heating Method
LAI	Light absorbing impurity
LED	Light emitting diode
LOD	Limit of Detection
LRTAP	Long-Range Transboundary Air Pollution
M	GeoMining
MAC	Mass absorption cross sections
MD	Mineral Dust
mL	Millilitre
Mg	Magnesium
Mn	Manganese
MS	Mass Spectrometry
Na	Sodium
Ni	Nickel
NSIDC	National Snow & Ice Data Center
NO_X	Nitrogen oxides
NO_3-	Nitrate
O_3	Ozone
OC	Organic Carbon
Pb	Lead
PM	Particulate Matter
Ppm	Parts per million
PSAP	Particle Soot Absorption Photometer
pXRF	portable X-Ray Fluorescence
Rb	Rubidium
RCP	Relative concentration pattern
Refl	Reflectance
RSD	Relative standard deviation
SD	Standard deviation
Sb	Antimony
Se	Selenium
SLCP	Short-lived Climate Pollutant
SMHI	Swedish Meteorological and Hydrological Institute

SO_2	Sulfur dioxide
SO_4^{2-}	Sulfate
Sr	Strontium
SW	Sweden
SWE	Snow water equivalent
TC	Total Carbon
TOT	Thermal-Optical Transmittance
Trans	Transmittance
USGS	U.S. Geological Survey
V	Vanadium
VOCs	Volatile Organic Contaminants
WHO	World Health Organization
Zn	Zinc

1 Introduction

The changing state of the global atmosphere has received a great deal of scientific and, increasingly, political attention during the last decades. Rising global temperatures caused by 'climate forcers' such as atmospheric levels of carbon dioxide (CO_2), methane (CH_4) and ozone (O_3) have been the focus of climatic concerns. In parallel with this, there has also been a growing concern about deteriorating air quality in many parts of the world, which affects climate as well as the health of humans and that of the ecosystems they depend upon. According to new data from the World Health Organization (WHO), nine out of ten people worldwide breath contaminated air, with an estimated 4.2 million premature deaths per year caused by ambient air pollution alone (WHO, 2018). The United States Environmental Protection Agency (EPA) identifies six 'criteria air pollutants', which are deemed specifically harmful to human health and the environment (EPA, 2018). Besides noxious gases such as sulphur dioxide (SO_2), carbon monoxide (CO) and nitrogen oxides (NO_X), ground-level O_3, lead (Pb) and particulate matter (PM) are cited on the infamous list (ibid; NIH, 2018).

In this context, PM or aerosol describe a mixture of both solid and liquid particles suspended in air, such as soot, dust, or smoke, which can be either natural or emitted from anthropogenic sources (UCAR, 2019; EPA, 2018). These particles or droplets can vary greatly in size, with some particulates being so big and dark that they create a haze which is visible to the naked eye, while others can only be detected through an electron microscope (EPA, 2018; IVHHN, 2018). Despite their differences in chemical composition and surface properties, a distinction is oftentimes made between inhalable particles with a diameter <10 µm (PM_{10}) and particles with a diameter <2.5 µm ($PM_{2.5}$). The sources of aerosol are manifold: some are emitted directly in particulate form from sources such as forest fires, soil dust, sea spray, mines or smokestacks (primary aerosols), while others are formed as a result of chemical reactions between gaseous pollutants in the atmosphere, emitted e.g. by cars, industries or power plants (secondary aerosols) (UCAR, 2019). In addition to the potential of fine PM to severely irritate and damage respiration pathways and cause or

amplify heart diseases, some aerosols can consist of, or contain, toxic substances. Examples include certain toxic metals, which can be associated with power plant or vehicular emissions, and volatile organic contaminants (VOCs) such as carcinogenic benzopyrene, often associated with soot (Valavanidis et al., 2008; Dickhut et al., 2000).

The geographic dispersion of polluting aerosols is partly determined by their size and partly by prevailing weather conditions. Gravity forces larger particles to quickly settle to the ground near emission sources (gravitational settling), mostly in a matter of hours, whereas smaller and lighter particles (~<1 μm), can stay suspended in air for weeks and months at a time and thus travel much longer distances (102 -103 km; UCAR, 2019). Some aerosols, such as black carbon (BC; a refractory type of soot) can be efficiently removed from the atmosphere by wet deposition in rain, fog droplets, ice grains, or snow (Paramonov et al., 2011). Snowflakes are especially efficient aerosol scavengers and even a moderate snowfall can deposit a substantial number of particulates on the ground surface (Bourgeois & Bey, 2011).

At its annual peak extent, the perennial and seasonal snow cover occupies ~30% Earth's surface (NSIDC, 2019). It is an important natural resource having great impact on Earth's global and regional climate (Mankin et al. 2015), supporting a unique ecosystem (Callaghan et al., 2011; Starr and Oberhauser, 2003), and impacting economic livelihoods (Ghaderi et al., 2013). Seasonal snowpacks constitute a vital source of drinking water (NSIDC, 2019) with about 1.9 billion people worldwide depending heavily on runoff from snowmelt (Mankin et al., 2015). However, the expanding global human population, increasing fossil fuel soot emissions, increasing anthropogenic activities (e.g., resource extraction), and a warming climate are now raising concerns about rising urban and rural pollution levels in snow and snow meltwater (Law and Stohl, 2007). Airborne contaminants deposited over the course of a single year (seasonal snow) or several years (perennial snow) can be released by melt into surface waters or undergo chemical transformations creating different types of hazardous contaminants, such as the toxic metal mercury (Hg) which can be subject to transformations to form the potent neurotoxin methylmercury (MeHg) (Dupuis, 2017; Larose et al., 2013). Additionally, light-absorbing (i.e., dark) airborne PM, such as dust or soot, deposited on snow alters the radiative properties of snowpacks which can lead to significant increases in melt rates, particularly in spring (Schmitt et al. 2015). The amount and the different types of PM deposited on snow cover may vary with geographical location, meteorological conditions and atmospheric composition (Paramonov et al., 2011). In certain regions such as the Arctic or the Andes, the accumulation of PM on snow can have significant impacts on both people and ecosystems considering the multitude of functions and ecosystem services of snow as well as its widespread distribution. With the rapidly changing climate in the high-latitudes human activities in those regions are expected to

increase substantially in the near future, which gives rise to concerns of increasing snow cover pollution in the Arctic and subarctic regions (Huntington et al., 2007).

1.1 Motivation and Objectives

Sources of airborne contaminants and their transport pathways to the polar regions have been the subject of several studies (Fischer, 2011; CACAR II, 2003; AMAP, 1998; Barrie et al. 1992). Particulate contaminants deposited in the snowpack can affect its physical properties (e.g., albedo) and be released in snowmelt, adversely impacting freshwater and marine ecosystems (AMAP, 1998). This is of particular concern for local populations, who may be exposed to hazardous levels of contaminants in drinking water or in their traditional fish/game diet. Light-absorbing impurities (LAIs) deposited in snow may also hasten snow melt onset in northern regions, which can have both local (hydrological) and global (albedo feedback) impacts.

The perennial and seasonal snow cover is widespread at high latitudes in winter, which makes it a convenient sampling medium to investigate geographical differences in the deposition of airborne particulate contaminants (Orr et al., 2019). However, at present few comprehensive surveys of airborne particulate matter (PM) in snow exist for the Arctic and subarctic regions. Existing published surveys of this sort are primarily local in character and have been carried out using a variety of methods, making any intercomparison difficult (Caritat et al., 2005). Systematic surveys of airborne PM in snow across parts of the Arctic and/or subarctic using standardized protocols would give deeper insight into inter-annual and spatial trends in PM deposition, and can be used to validate air pollutant model simulations. Findings can also inform policy makers on the efficacy of atmospheric pollution reduction measures and help local northern communities to anticipate the impact of possible changes in snow cover duration and melt onset.

This study investigates the pros and cons of several destructive and non-destructive analytical methods that can be employed to characterize airborne PM deposited in seasonal snow. To this end, a comparative study was conducted on PM obtained from snowpack surveys in two Arctic/subarctic regions of Northern Sweden and Interior Alaska, USA. These two regions are affected by different local and distant sources of natural and anthropogenic contaminants (e.g., residential heating emissions of soot). The first objective of the study was to measure and characterize carbonaceous/ carbon particles (CPs) in snow-filtered PM using three different optical analytical methods: a Particle Soot Absorption Photometer, a Thermo-Optical Transmittance (TOT) analyser, and a Light-Absorbing Heating Method (LAHM). The second objective of this study is to the test the applicability of a portable X-Ray

Fluorescence (pXRF) analyser for quantifying the particulate trace metal content in the snow. The presence of particulates emitted either naturally or through human activity can affect estimates of the radiative impact of CPs in snow. Measurements performed with the pXRF were also compared with bulk chemical analyses by Inductively Coupled Plasma Mass Spectrometry (ICP-MS), which is a standard method for quantifying the trace metal composition in PM.

The key research questions of this study are:

i) What is revealed about CP in snow when considering different techniques (TOT vs PSAP, TOT vs LAHM), especially regarding the incertitude of measurements?

ii) What are the differences in the levels of CPs deposited in snow between two northern regions with differences in intensity and types of PM emissions?

iii) How do those levels of CP compare to previous published data from other high-latitude regions?

iv) What can be learned from comparing trace metal levels of empty and blank filters?

v) How consistent and reproducible are pXRF measurements of trace metals in filtered snow?

vi) To which extent do the different pXRF calibration settings affect results?

vii) Does pXRF detect differences in the relative abundance of trace metals that can be related to conditions between sites?

viii) Can the pXRF data be classified into different groups with similar characteristics that can be related to the type of environment where the samples were collected?

ix) How do pXRF measurement performed compare to the ICP-MS?

2 Background

The regions studied in this report are mostly covered under what the Arctic Monitoring and Assessment Programme (AMAP) defines as ‘Arctic’ for the purpose of their assessment reports, based on natural and political-/ administrative borders and parameters (Fig. 1) (AMAP, 1998). According to the Köppen-Geiger climate classification, Interior Alaska and Northern Sweden would however rather be considered the ‘subarctic’. Yet, some samples were collected in higher elevations, which could, on a micro-scale, be considered ‘Arctic’ conditions again. This report will thus mainly refer to the regions under investigation as ‘northern latitude regions’, applying the various terms according to the respective context.

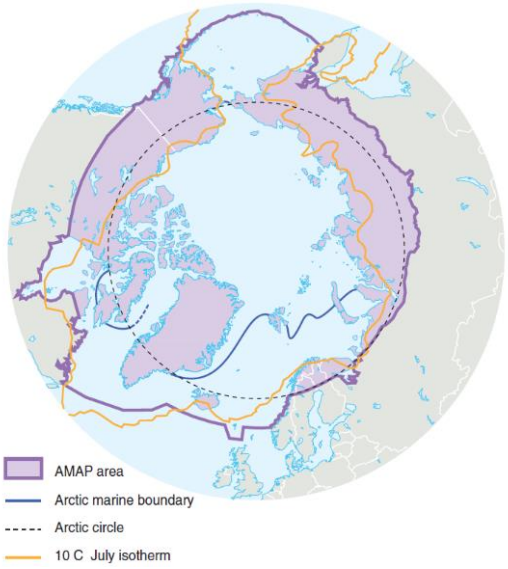

Figure 1. The Arctic as defined in the AMAP assessment reports, the 10°C isotherm as temperature delimitator of the Arctic (after Stonehouse 1989), and the Arctic marine boundary (AMAP, 1998).

2.1 Atmospheric Pathways to the Northern Regions

The Arctic was long considered to be a pristine region with an exceptionally clean atmosphere. It was not until the 1980s that the hazy belts in the Arctic air and dark deposits on snow were identified as airborne aerosol of sulphate (SO_4^{2-}) and soot (particulate black carbon), transported and deposited to these remote areas from major pollution sources in the mid-latitudes (AMAP 2005; Law and Stohl, 2007; AMAP, 1998). This discovery, as well as the detection of other high levels of contaminants in the air of this thought-to-be pristine environment, made scientists increasingly aware of long-range transport of pollutants to the polar regions and stimulated research on the pathways of airborne contaminants (ibid). The airborne transport of pollutants in aerosol form is fast compared to other contamination pathways, but varies strongly throughout the seasons (Groth Grube, 2011; AMAP, 2009). Despite ongoing research efforts in recent decades, some uncertainty remains regarding the sources and atmospheric pathways of aerosols to northern latitudes (Shindell et al., 2008). This is in part due to the fact that atmospheric pathways are highly complex and variable, and shaped by a multitude of global, regional and local factors, such as large-scale pressure systems, precipitation, and air and ocean temperatures (Sherrell et al., 2000). In this regard, studies of global climate change scenarios indicate that the trends in the delivery of aerosol to the northern polar region are likely to change and their variability is to increase even further in the future (AMAP 2005; AMAP, 1998).

The fundamental driver of the polar climate system is the negative net radiation budget of the Arctic. It causes very low temperatures especially during the winter months (low pressure system), drives the heat exchange and thus the winds between these high and mid-latitudes and hence the polar jet stream (AMAP, 2005). This latitudinal energy exchange is highly dynamic, as the Earth's macro-scale topography and Coriolis force lead to regional and local specific climate conditions (ibid). In addition, the atmospheric circulation pattern over the mid-to-high latitudes of the Northern Hemisphere (NH), the 'Arctic Oscillation (AO)', also termed 'Northern Hemisphere Annual Mode (NAM)', changes substantially over the course of the years (Fig. 2) (NOAA, 2019; Dahlman, 2009). As shown in figure 2 and 3, the AO can take on positive (AO^+) and negative (AO^-) phases (AMAP, 2005). The AO^+ phase is characterized by lower-than-average air pressure over the Arctic basin or polar cap coupled with higher-than-average pressure anomalies in the ocean basins of the northern Pacific (Aleutian Low) and Atlantic Ocean (Icelandic Low) (NCSU, 2018; Dahlman, 2009) (Fig. 3). The location of the jet-stream is farther north in this phase, which is largely associated with cold temperatures in the Arctic region and milder temperatures and fewer cold air outbreaks in lower latitudes (ibid). The AO^- phase, on the other hand, describes a high-pressure anomaly over the Arctic basin

or polar cap (Beaufort High) and a lower-than-average atmospheric pressure system in the respective ocean basins, which lets the jet stream shift southward (ibid). During an AO^--phase, colder-than average temperatures and snowstorms often govern lower latitudes while milder weather is expected in the Arctic. With these variations in the location and amplitude of atmospheric pressure systems, associated wind pattern change substantially. The AO can therefore be considered an atmospheric mixing index (Thompson et al., 2002). During the AO^+ phase the relatively stable low-pressure system over the polar basin allows for only very little exchange of atmospheric masses between the Arctic and lower latitudes (mid-latitudes and subtropics) (ibid). The AO^- phase however, allows for increased mixing of atmospheric masses between the Arctic and lower latitude, leading to a stronger inflow of air from major pollution sources in Europe, Asia, or North America (AMAP, 2005).

Keeping seasonal and interannual variations in mind, the atmospheric pressure pattern as well as orographic barriers and ocean currents form a large-scale air circulation with three major atmospheric pathways to the northern region. The (south) westerly winds between Iceland and Scandinavia, eastern Siberia and Alaska, and central Siberia (Fig. 4).

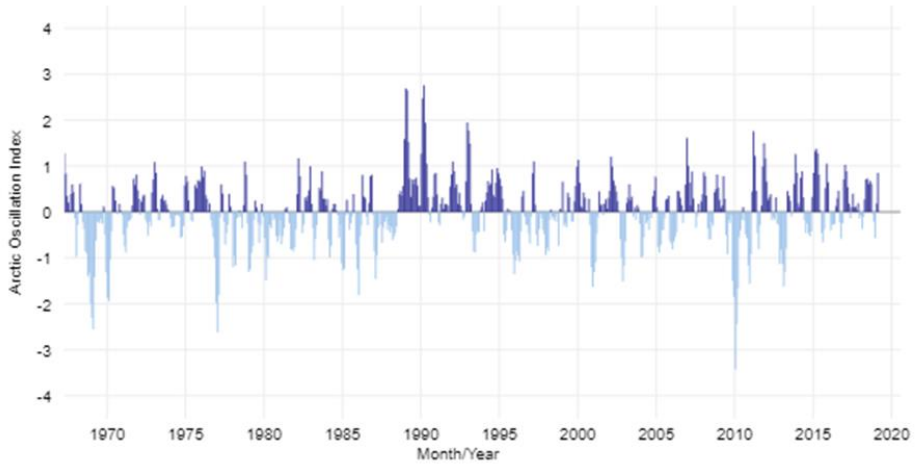

Figure 2. Positive and negative AO phases since 1965 (NOAA, 2019).

Another factor governing airborne particle transport in the North, is a phenomenon termed the 'Arctic Dome' (Norwegian Polar Institute, 2014; Law & Stohl, 2007). The decreasing temperatures in winter and thus the increase in pressure of the lower atmosphere (stable Polar High) are forming a "surface of constant potential temperature" (Law & Stohl, 2007, p. 1537), separating the polar lower troposphere from higher stratospheric layers (ibid). This 'dome', the very cold and dense

air, is creating a transport barrier which can become so strong that, for some time of the year, the lower troposphere is almost entirely separated from lower latitude and higher altitude air masses (Law & Stohl, 2007; Norwegian Polar Institute, 2014). Hence, during this time it is mostly local emission sources from within the boundaries of the 'dome' which are introducing contaminants (ibid). However, with unusually high winter temperatures, mid-latitude air can penetrate the central Arctic and as the Arctic front varies geographically, regions as low as 40 degrees North (Eurasia) might contribute as source regions at times (Norwegian Polar Institute, 2014). An exception is Greenland, as its high topography leads to a stronger influence of lower latitude air pollution (ibid). In the northern hemispheric summer, the poleward transport ceases and becomes more dynamic while low-level drizzling clouds lead to an augmented deposition rate of contaminants (ibid; Gogoi et al., 2015).

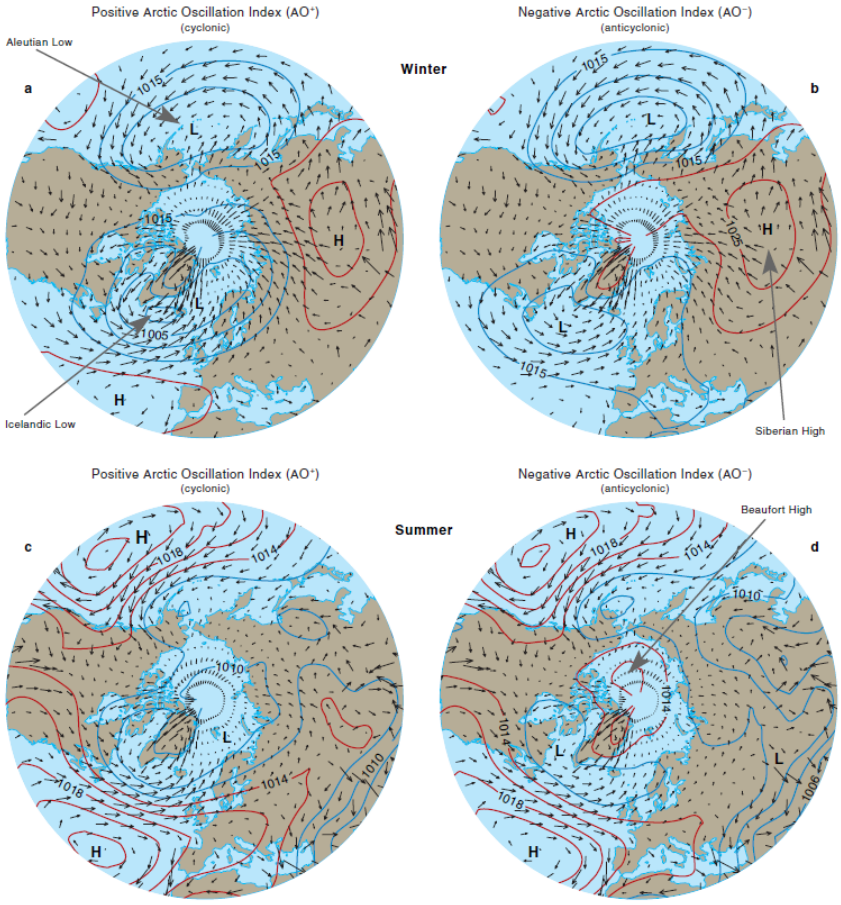

Figure 3. Atmospheric pressure fields and wind stream lines in the Northern Hemisphere: a) strong AO+ conditions in winter; b) strong AO– conditions in winter; c) strong AO+ conditions in summer; and d) strong AO– conditions in summer (AMAP, 2005).

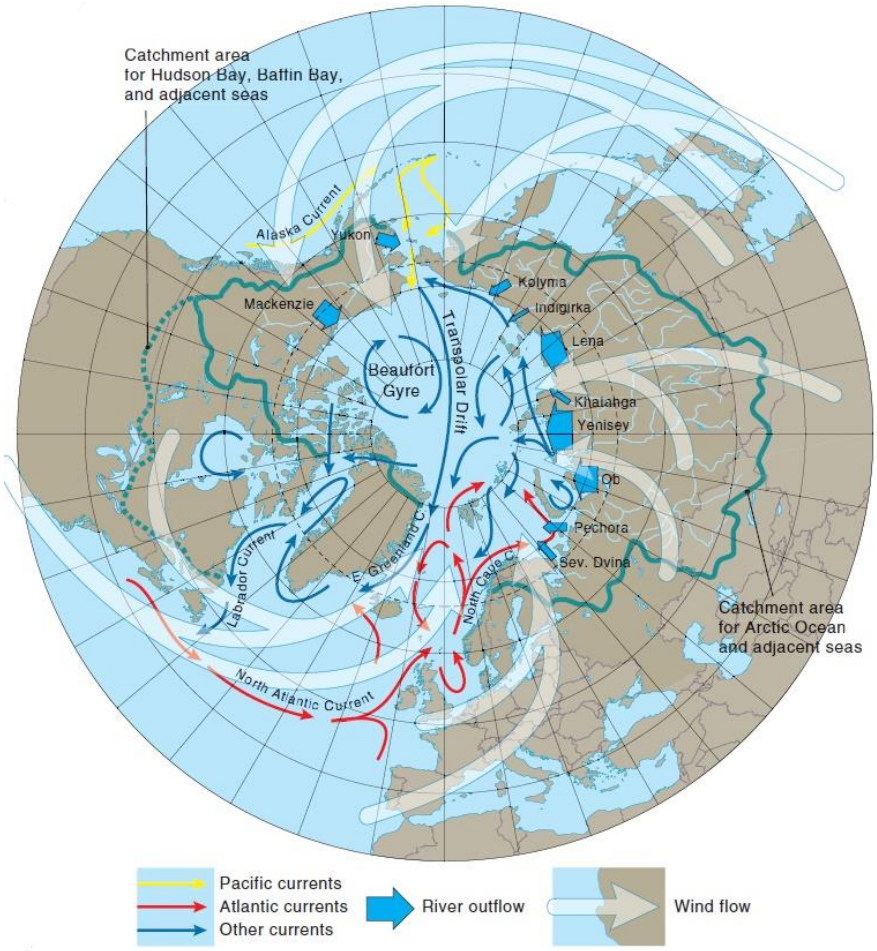

Figure 4. The major physical pathways (wind, rivers and ocean currents) that transport contaminants to the Arctic (AMAP, 2005).

The climatic conditions of the northern regions, especially the cold temperatures and the large-scale atmospheric wind pattern, turn this area into a sink for global emissions. However, the long-range transport of particles is further complemented by emission from local sources (AMAP, 2009). The Arctic and especially the sub-arctic hosts a substantial number of major population centres and large industrial and extraction sites, many of which are growing in numbers and size (Korosi et al. 2016; Hustrich 2008). Alaska's Red Dog mine, the world's largest zinc mine, gas flaring in western Siberia (Evangeliou et al., 2018), Norilsk and Monchegorsk, the centres of metallurgy in Russia (Revich, 1995), the Tibbitt to Contwoyto winter road in Northwest Territories in Canada (Korosi et al. 2016) or the usage of wood stoves in northern Scandinavia (Solbakken, 2017) are only some examples for local anthropogenic contamination sources in the region.

2.2 Deposition of Atmospheric Particulate Matter on Snow

Since precipitation in the polar regions is mostly solid during the winter months, the removal of particles from the atmosphere by snow can be an important deposition mechanism at these latitudes (Kyrö et al., 2009). Wet deposition comprises both in-cloud removal of aerosols by ice nucleation as well as below-cloud scavenging ("washout") by hydrometeors such as snow, rain, cloud and fog droplets (APIS, 2016; Paramonov et al., 2011; Shrivastav, 2001). Multiple studies have shown that snow scavenging of aerosols by snow can be more efficient than scavenging by rain, which is why even a moderate snow fall can deposit a substantial number of particulates on the surface (Zhang et al., 2013). Dry deposition refers to aerosol deposition in the absence of precipitation. It can occur by gravitational settling, impaction, turbulent transfer and transfer by Brownian motion and is particularly important in high-latitudes during the dry winter months (Shrivastav, 2001). The particulate chemistry of the late winter snowpack is influenced by both types of deposition and is a first-order indicator of the composition of atmospheric PM during the snow season, despite other processes such as the diffusion of gases from the soil below (Thaillandier et al., 2006). This implies, that the deposition of PM varies during the snow season, as well as with geographical location and meteorological conditions (Paramonov et al., 2011). Once deposited, each element or chemical compound behaves differently in the snowpack depending on local climatic and snow conditions (Barcan & Sylina, 1995). Some volatile aerosols can be re-emitted from the snowpack into the atmosphere (e.g., NO_3^-), which can however be limited under very cold conditions (Norwegian Polar Institute, 2014). The release and transfer of chemical compounds from the snowpack into the surrounding hydrological and terrestrial ecosystems begins at the onset of spring freshnet and is partly controlled by rates of contaminant elution and the physiochemical properties of the snowpack during the melt period (Kepski et al., 2016; Korosi et al. 2016; Savinova et al. 1995).

2.3 Atmospheric particulate metals in northern regions

Primary natural sources of metal emissions to the global atmosphere include volcanic emissions, rock- and soil-derived dusts, and sea salt aerosols, while secondary metal-containing aerosols are formed by chemical reactions as well as the condensation of atmospheric gases and vapors onto a nucleus (Barbante et al., 2017; Halbach et al. 2017). Over the course of the last few centuries, human emissions of metals have significantly increased, often exceeding emissions from natural sources (Rauch & Pacyna, 2009). Possible anthropogenic sources of metal emissions are numerous and include the combustion of fossil fuels, waste incineration, mining and mineral processing as well as household and agricultural emissions (AMAP, 2005).

Metals that are commonly emitted to the atmosphere by coal combustion include Cr, Hg, Mn, Sb, Se, Sn, and Tl, while Ni, V, and Zn are more related to oil combustion (Pacyna & Pacyna, 2001; Vouk & Piver, 1983). Since the end of leaded gasoline use in the 1970-80s, the concentration of Pb in the atmosphere has decreased in many parts of the world. However, there are still important global emissions of other metals such as As, Cd, Cu, In, Zn as well as Hg, for example due to mining and metal smelting and refining. Also interesting in northern latitudes are chemicals used for de-icing aircrafts: Mn, Sb, and Tl (Rauch & Pacyna, 2009; Pacyna & Pacyna, 2001). The so-called toxic "heavy metals", which include As, Cd and Pb, as well as the bioaccumulative Hg, are further of particular concern for the health of Arctic ecosystems and humans living at these latitudes.

Snow and ice are valuable records for characterizing the chemical composition of the atmosphere, as the minerals trapped within them largely reflect the geochemical characteristics of the source region of the deposited particles, local or distant (Barbante et al., 2017; Tuohy, 2015). Through wet and dry deposition, elements attached to aerosols get removed from the atmosphere and deposited on the snow surface (Barbante et al., 2017). Thus, the elemental composition of snowpacks may change spatially and temporally, depending on atmospheric transport pattern, local deposition mechanisms, and emission source changes (Douglas & Sturm, 2004). Another factor adding to the accumulation of trace and major metals in northern regions is the impedance of re-conversion of particles into a gaseous form after deposition under cold climate conditions (Dinis & Fiurza, 2010). This phenomenon has inter alia been observed for mercury (Hg) and decreases a re-distribution of contaminants once precipitated (ibid). While seasonal snow holds information from one winter, multi-year snow as well as firn and ice provide archives of the atmospheric chemical composition of decades and centuries (Hur et al., 2007).

To assess the availability, concentrations, and effects of potentially hazardous metals in the Arctic, the Arctic Council issued three reports compiling information from major studies containing observational as well as model data available up to 1998, 2002, and 2011. The first two AMAP reports focused on three trace metals which can already be toxic to biota and fauna at concentrations just above background levels: cadmium (Cd), mercury (Hg), and lead (Pb) (AMAP 2005; AMAP, 1997). Other elements under investigation were: arsenic (As), zinc (Zn), copper (Cu), manganese (Mn), vanadium (V), and nickel (Ni) (ibid.). (AMAP, 2005). The 2002 report found that "[…] anthropogenic emissions both in and outside the Arctic account for more than 50% of the observed heavy metal concentrations in the

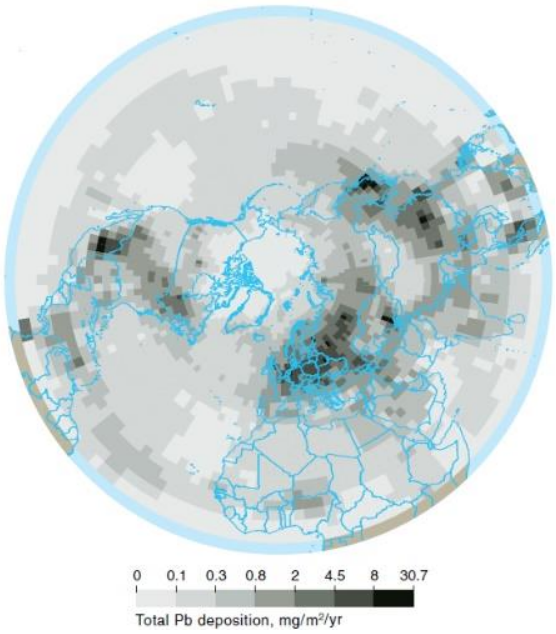

Figure 5. Total annual deposition of lead to the Arctic in 1990, as calculated by the MSC-E Hemispheric Model (Meteorological Synthesising Centre, Moscow) (AMAP, 2005).

Arctic" (Halbach et al., 2017 adapted from AMAP, 2005). The third AMAP report converged Hg only and emphasized the risks to Arctic ecosystems and humans, as levels of this element are still increasing in some regions (AMAP, 2011). Data included in the reports was derived from measurements of a variety of different ecosystem compartments: the atmosphere, snow and ice, soils, waterbodies, and flora and fauna. Modeling efforts were specifically focused on atmospheric distribution of metal concentrations as well as their deposition across the Arctic (e.g. Fig. 5, deposition of lead).

In general, levels of metals found in water bodies and soils in the Arctic decreased over the last decades. However, compared to global background levels, atmospheric concentrations of metals are still high near anthropogenic point sources such as mines, smelters and locations of oil and gas extraction (AMAP, 2005). Examples of contaminated environments with elevated metal concentrations are the Pasvik watercourse in the border area between Finland, Norway and Russia, which is strongly affected my nearby smelters (Amundsen et al., 2011), as well as snow in the proximity of the 'Severonikel' industrial complex in northwest Russia (Kashulina et al., 2014).

During spring thaw, particulate metals deposited from the atmosphere into the winter snowpack can be transferred to adjacent water bodies in a matter of days to weeks, where they may become available to aquatic biota, such as fish and waterfowl. These important subsistence foods, as well as larger apex predators such as bears, whales and seals, have been shown to be the major pathway of human uptake of metals in the Arctic, especially affecting the traditional diets of many native groups (AMAP, 2005). An important component in understanding this uptake is the process of bioaccumulation, through which even trace amount of metals can build up in both human and animal tissue over time, as well as biomagnification, the increase in concentration of a pollutant as it moves to higher trophic levels of a food chain or food web (Van der Hoop, 2013; Datz and Perry, 2012). The most susceptible and vulnerable group of northern societies are unborn and new-born babies, who

are at risk of exposure mainly through their mother's diets (Bose-O'Reilly et al. 2010).

In general, both environmental and health effects of metals depend upon on their mobility through environmental compartments (e.g., solubility in water, volatility in air), the pathways through which the metals reach the human body, and the level and time of exposure to the respective contaminant (AMAP, 1998). Yet, the degree of concern for ecosystems and humans varies strongly with each metal. While some are clearly toxic, others are essential micronutrients to the human body but nevertheless toxic in excess. Of specific concern are As, Cd, Pb, Hg. These metals, once deposited, can form harmful organic complexes like organolead or methylmercury in the environment, which may cause neurological damage, even at low concentrations (Dinis & Fiurza, 2010). Metals such as Cu, Cr, Ni, and Zn, on the other hand, are essential micronutrients for many living organisms, becoming toxic only in excess (AMAP, 1998).

2.4 Carbonaceous aerosols in northern regions

A large fraction of atmospheric particulate matter consists in carbonaceous (i.e., carbon-rich) particles, hereafter abbreviated "CP". These are closely monitored by the air pollution, respiratory health and climate research communities (Petzold et al., 2013). Atmospheric CP strongly absorb visible and near-ultraviolet light, which leads to atmospheric warming (Bond et al., 2013). Furthermore, when deposited, these aerosols lower the albedo of the otherwise highly reflective snow cover (Doherty et al., 2010). This change in the surface energy budget can lead to earlier snowmelt and snow cover retreat, creating a positive snow-albedo feedback that enhances surface atmospheric warming in the springtime. Next to rising global air temperatures caused by the enhanced greenhouse effect, CPs are considered one of the main drivers for accelerating snow cover decline in the Arctic (Dou & Xiao, 2016).

To account for the wide compositional variety of CP, researchers have developed a multitude of instruments to quantify and/or characterize them (Lack et al., 2013). This can be done based on the chemical composition, optical properties, sources, and morphological characteristics of CP. Definitions and terminology for CP vary with the field of study and analytical techniques (Hegg et al., 2009). A full discussion can be found in Lack et al., 2013, Petzold et al. 2013, or Andreae & Gelencsér, 2006. The generic expression black carbon (BC) is broadly used to describe those types of CP that strongly absorb light (Lack et al., 2013; Petzold et al., 2013). The expression thus refers to both their optical and chemical properties. The main source of BC is the incomplete combustion of fossil fuels or biomass (Hegg et al., 2009).

In this work, three different operationally-defined expressions will be used to characterize CP filtered from melted snow samples, depending on the analytical method used: *elemental carbon* (EC), *organic carbon* (OC), *equivalent black carbon* (BCe), or *effective black carbon* (eBC). Briefly, EC (often used interchangeably with BC) and OC are the refractory and volatile fractions of CP, respectively, quantified using the Thermal-Optical Transmittance (TOT) method (Petzold et al., 2013). Their sum is called total carbon (TC). BCe is measured by analytical methods based on light absorption. For the present study, this includes the Particle Soot Absorption Photometer (PSAP; Sharma et al., 2002). The Light Absorption Heating Method, a thermal method, quantifies CP in eBC (LAHM; Schmitt, 2019). In the latter two cases, the estimated carbon content might not be BC only, but it is reported as the equivalent/ effective quantity of BC that would have the same light absorbance as measured in the sample (Petzold et al., 2013).

There are several global BC models, that give insight into atmospheric BC concentrations in the Arctic. As an example, figure 6 shows the average values of surface concentration of BC derived from averaging the output of 17 models provided by an aerosol model intercomparison group known as 'AeroCom' (Koch et al., 2009). It shows that the atmospheric BC concentrations in the western and central Arctic and subarctic (Alaska, Canada, Greenland) are relatively low with atmospheric BC ranging from approximately 10-25 ng/m^3 in north-eastern Canada and Greenland to up to 100 ng/m^3 in Alaska and large parts of Canada. Except for the European High-Arctic (Svalbard; 25-100 ng/m^3), the European Arctic and subarctic experience high BC surface values of up to 500 ng/m^{3,} according to the model mean. Yet, the study by Koch et al. (2009) found that these models tend to underestimate BC in the Arctic region.

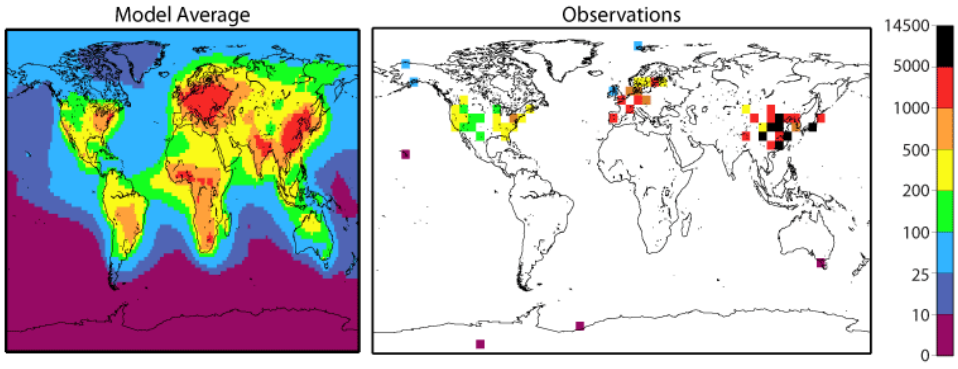

Figure 6. Surface concentration of black carbon for average of AeroCom models (left) and observations (right). Units of the scale are ng/m3 (Koch, 2009).

BC counts as a 'short-lived climate pollutant' (SLCP) meaning that these particles remain airborne from a few days to up to a decade, unlike CO_2, which can last for centuries (Schoolmeester et al., 2019). Thus, close emission sources of BC have the greatest potential to impact the Arctic and the subarctic. Comparing the map of global SLCP emission hotspots (Fig. A.1) can therefore explain the above description of the modeled atmospheric BC levels. Both biomass burning and industrial emissions in the mid-latitudes of Asia, North America and Europe are driving BC levels. However, the level of emission is highest in Europe and China, which leads to higher contamination levels in the European and Russian high-latitudes.

Efforts to compile information from field measurements were made in the mid-80s (Clarke & Noone, 1985) as well as in recent years (Doherty et al., 2010; Dou & Xiao, 2016). A first survey of CPs in Arctic snow has been undertaken by Clarke and Noone in 1983-1984 (Clarke and Noone, 1985). The two researchers collected 60 samples in the western circumpolar north in order to give a better understanding of the spatial distribution as well as the properties of CP in snow. Several other studies followed, with extensive sampling campaigns during 2005 -2009, which also included taking measurements in the Russian Arctic and subarctic region and the Arctic Ocean (Doherty et al., 2010). Overall, more than 1600 samples were taken, 1200 of which were included in the paper by Doherty et al. (2010) (Fig. 7a)). A follow up has been published by Dou and Xiao in 2016, which included additional measurements from Scandinavia and the European Arctic as well as the Canadian Basin and the Arctic Ocean.

Most of the over 1200 data points included in the dataset were collected in remote areas with as little human influence as possible (Forsström et al., 2013; Doherty et al., 2010). An exception was Russia, where a significant portion of the samples could only be taken in areas close to human settlements that were suspected to experience anthropogenic influence (Doherty et al., 2010). Despite the Russian snow sampling locations, the large-scale trend of CP in the snow in remote areas in the high latitudes followed model findings which suggest that the concentration of BC in snow is largely caused by long-range atmospheric transport of particles from lower latitudes (Jiao et al., 2014). According to Dou and Xiao (2016), BC in snow indeed decreases significantly with higher latitudes due to the increasing distance to human activity areas. According to their study, the mean BC concentrations north of 65°N were 13.6 ng/g (Fig. 7b).

Dou & Xiao (2016) clustered the samples from the previously mentioned field campaigns into geographic groups and compared their mean CP values, which showed, that general spatial patterns could be established: With mean BC (terminology changes between the different studies, however Dou & Xiao, 2016 chose to use the term 'BC') values of 33.7 ng/g and 21.4 ng/g, Western and Eastern Russia exhibited the highest mean values, followed by the Canadian and Alaska Arctic

region with mean EC values of 7.9 ng/g. The lowest concentrations were found in snowpacks in the Arctic Ocean (~4.5 ng/g), Western and Eastern Svalbard (~2.5 ng/g and ~7 ng/g), and Greenland (~3.8 ng/g) (Dou & Xiao, 2016). The studies these values are based on measured 'BC' and 'EC' with different instruments (Doherty et al., 2010: ISSW integrating-sandwich spectrophotometer; Forsström et al., 2013: TOT thermal-optical transmittance) and used different sampling techniques such as surface or bulk sampling. For site specific observation results see Dou et al., 2012, Forsström et al., 2013; and Doherty et al. 2010.

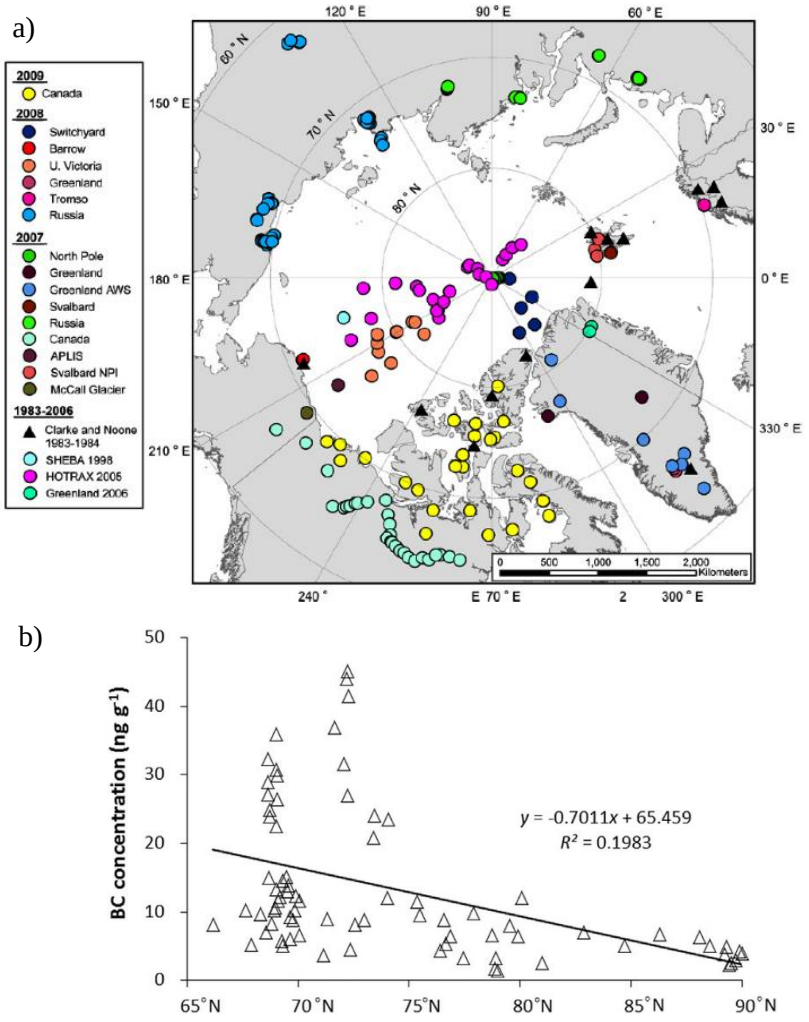

Figure 7. a) All snow-sampling locations used in the paper by Doherty et al. 2010. Colours indicate the different field campaigns on which snow was sampled. b) The variation of BC concentration in snow and ice in spring with latitude. The BC values are derived from the same field campaigns as described in Doherty et al., 2010 (a) (Dou & Xiao, 2016).

As can be seen in figure 7a, published data on snowpacks in the Scandinavian Arctic and subarctic regions are rather sparse. Clarke and Noone (1985) published the first values taken in Abisko, and Forsström et al. (2013) reported measurements from Abisko and Storglaciären, a glacier by Tarfala and the area around Tarfala in Northern Sweden which is at a similar latitude as Kiruna and about 60 km west from the city. The two snow surface sampling campaigns from Storglaciären/ Tarfala in the latter study were carried out in July 2008 (1), and from December 2008 to April 2009 (2) with nine samples taken at three subsites during the first and 15 samples taken at six subsites during the second campaign. The median EC concentration and the 25% to 75% Percentile of campaign 1) were: EC: 42.9 ng/g (range: 42.5–60.5 ng/g) (lat: 67.93) and of campaign 2) 14.5 ng/g (range: 4.0–32.5 ng/g) (lat: 67.91). The two sample locations were reported to have been affected by pollution from local sources. The two campaigns in Abisko were carried out from January to April 2008 with 19 samples taken at 15 forested subsites and the second campaign was undertaken during November 2008 to April 2009: The median EC concentration for the first campaign in Abisko was reported as 51.4 ng/g (range: 27.6–90.7 ng/g) (lat: 68.35) and as 32.2 ng/g (range: 17.5–41.8 ng/g) (lat: 68.35) from the second campaign.

3 Terminology

3.1 Environmental Contamination and Pollution

The terms ‘environmental contamination’ and ‘environmental pollution’ are often used interchangeably. Contamination, however, defines the “presence of a substance [or energy] where it should not be or at concentrations above background” (Reinardy, 2018 after Chapman, 2007, p.492). Pollution, on the other hand, is a result of contamination (Reinardy, 2018). Chapman (2007, p.492) defines pollution as “contamination that causes adverse biological effects in the natural environment” and Reinardy (2018) adds, that the contamination could be either by natural or artificial means. Thus, pollutants are by definition contaminants, but not all contaminants become pollutants (Chapman, 2007). Differentiating the two terms is of importance to this study, as the exceedance of certain elements above background levels can be harmful to people and the environment. In this context, Arctic contamination presents a risk to humans, animals and ecosystems depending on the bioavailability of specific elements to organisms, the reactions of these elements within the environmental compartment they occupy, and especially the exposure of organisms to the respective contaminant (Chemsec, 2016).

3.2 Trace or ‘Heavy’ Metals

The International Union of Pure and Applied Chemistry (IUPAC) has found no less than 38 definitions for ‘heavy metals’, many of which are contradictory (Duffus, 2002). Ranging from “metals with an atomic weight greater than sodium that form soaps on reaction with fatty acids” to “a metal of high specific gravity; esp: a metal having a specific gravity of 5.0 or over” (Hawkes, 1997, p.1374), these definitions use a variety of criteria such as atomic weight or numbers, density, chemical behaviour and properties (ibid). A common feature is the association of ‘heavy metals’

with toxicity and environmental pollution (Duffus, 2002). As Hodson (2004, p.342) however rightly points out, “toxicity is a function of the chemical properties of the element/compound and the biological properties of the organism at risk”, which defines toxicity as a function of the dose rather than being an inherent criterion of a specific element. Hence, to avoid any misconceptions about the term, this report will henceforth refer to the set of metals under investigation as trace elements/ metals or analytes, which, given their abundance, could reach pollution levels and subsequently inflict harmful consequences for ecosystems and people living therein.

4 Study Area

The snowpacks of two regions were under investigation: Northern Sweden and the Interior of Alaska, USA (Fig. 8 and 13). The characteristics of these two regions that are of particular relevance to the study are presented in the following sections.

4.1 Northern Sweden

4.1.1 Climate

Figure 8: Map of Sweden with sample region marked with a black box.

The snow samples for this thesis were collected in Swedish Lapland, Norrbotten, and Västerbotten, between latitudes 63° and 68° N (region framed in figure 8). Four of the eleven sample locations were situated above the Arctic circle. The climate of this part of Sweden is defined as sub-arctic or arctic (ET = tundra climate according to the Köppen Geiger classification).

One important factor influencing the regional climate is the relative position of the Polar Front, which determines whether the dominant air masses originate from the mid-latitudes or the Arctic (CMMAP, N.d). A second factor is the region's topography (Fig. 9a). From west to east, the surface elevation drops from ~2500 m. a.s.l in the Scandinavian Mountains (Scandes) down to the northeast coast of the Gulf of Bothnia. The study region lies in the lee of the mountains, which limits precipitation rates as westerly winds force moist air from the Atlantic to rise, creating orographic precipitation over the western side of the Scandes (Fig. 9b). Hence, only the western regions of Swedish Lapland profit from these orographic rain- and snow falls, resulting in cumulative precipitation >

1900 mm a-1. Regional precipitation patterns are otherwise variable, and sudden, high precipitation events can accompany the passage of low-pressure systems (SCCV, 2007). A third major factor is the heat supplied by the North Atlantic Current, which results in relatively mild temperatures across northern Fennoscandia compared to other regions at the same latitudes (Fig. 9c) (Palter, 2015). Average annual temperatures are higher at the coast (~4°C) than in the mountains (~-3°C) (Fig. 9c), ensuring a lasting snow cover in higher altitudes throughout the winter (SMHI, 2019c).

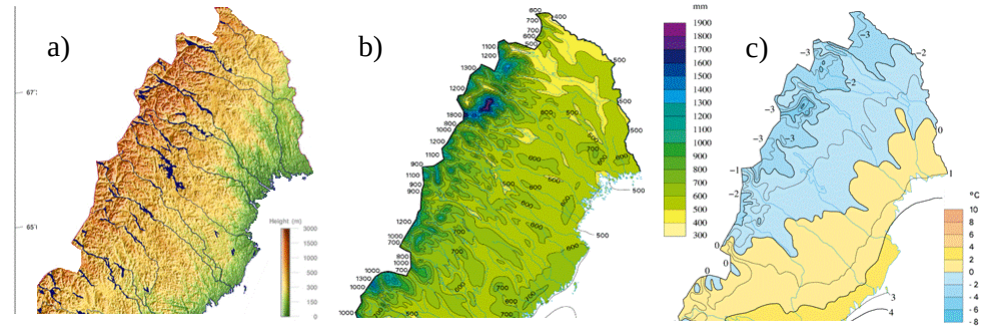

Figure 9. Thematic maps of Northern Sweden. a) Topography (GinkoMap project, Nd.), b) annual average precipitation for 1961-1990 (SMHI, 2019b) c) normal annual average temperature for 1961-1990 (SMHI, 2019c).

4.1.2 Snow Conditions

Northern Sweden is entirely covered with snow for almost six months of the year (Fig. 10a), however the depth and duration of snow cover vary across the region depending on factors such as local temperature, topography and predominant winds (Sandström, Nd.).

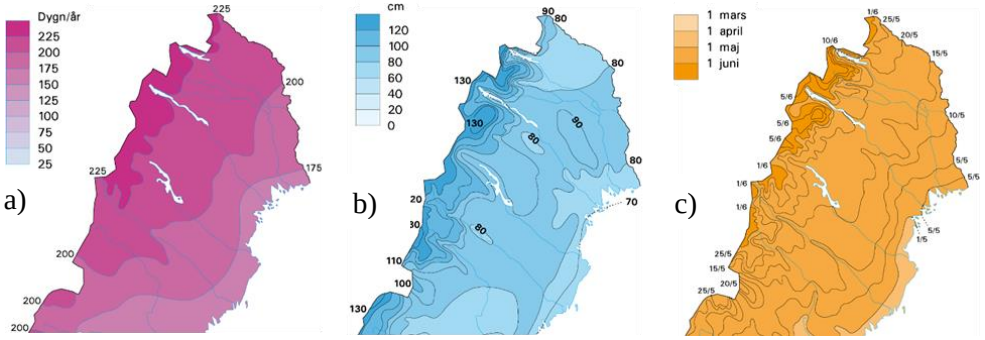

Figure 10. Climate maps illustrating a) mean for the number of days with snow cover per year for 1961-1990 (SMHI, 2017) b) mean of the largest snow depth during the winter for 1961-1990 (SMHI, 2017a) c): mean for the last day with snow cover for 1961-1990 (SMHI, 2017 b).

Both snow cover depth and duration decrease towards the south-east and average 175 days per year and 70 cm at the Bothnian coast, respectively (SMHI, 2017). Snow cover can persist until the beginning of June in the Scandes, but only until late April at the coast (Fig. 10c). The snow cover period in most of Sweden has considerably shortened within the last decades, but this trend is not yet apparent in the study region (SMHI, 2018). In the 2016-17 winter, maximum snow depth for most of Northern Sweden were recorded on the last day of March (Fig. 11a). The snow samples obtained for this study were collected between 2-9 April 2017. As figure 11b shows, snowpack depths on these days were only slightly less than the late March maxima.

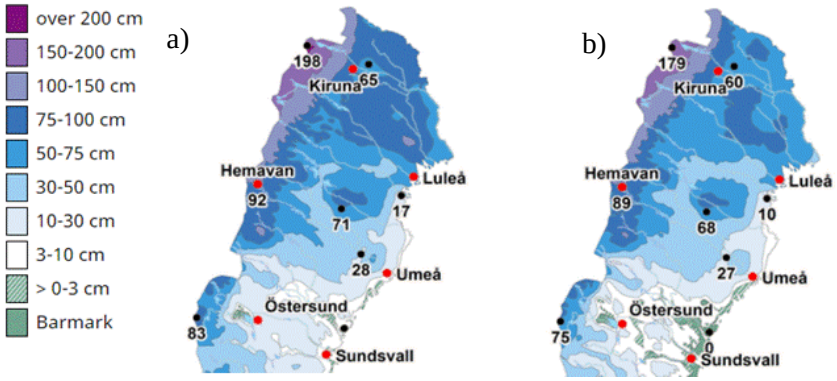

Figure 11. Snow depth in Northern Sweden a) on 31.03.2017 b) on 06.04.2017 (SMHI, 2019d).

4.1.3 Surficial Materials and Soil Chemistry

Sweden has been subject to multiple periods of glaciation and deglaciation, and the most commonly found soil types are those developed from till, covering 75 % of the landscape (Peterson, 2016). Topsoils in the study area are predominantly alpine podzols and lithosols, and in Lapland consist mostly in orthic (gleyic and humic) podzols (Troedsson & Wiberg 1986). The chemical composition of mineral soils across Sweden has been mapped by the Department of Soil and Environment and the Swedish Environmental Protection Agency (Stendahl, 2019). In this study, these maps were used to extract data on major and minor metal concentrations in soil at a depth of 50 cm, near the snow sampling locations.

4.1.4 Pollution Sources: Local and Global

Air quality in Northern Sweden is high compared to most of Europe, with generally low levels of ambient particulate matter (EU daily limit value: PM_{10} – 50 µg/m^3; $PM_{2.5}$ – 50 µg/m^3 annual limit: PM_{10} – 40 µg/m^3; $PM_{2.5}$ – 25 µg/m^3) (EEA, 2018;

Hak et al., 2009). Modelled annual background $PM_{2.5}$ and PM_{10} levels for the last years were, on average, < 5 µg/m^3 across the study region, but they increase towards the south with the highest concentrations found around Umeå, where they reach 6-8 µg/m^3 for $PM_{2.5}$ and ~10 µg/m^3 for PM_{10} (Willers et al., 2013; Hak et al., 2009). Potential local sources of contaminants include particulate emissions from oil and gas combustion, or from firewood used for residential heating (e.g., Krecl et al., 2008), especially around main population centres. Several large mines can also contribute PM emissions from heavy vehicle traffic as well as aeolian dispersion of fine mineral particles from exposed soil and bedrock (e.g., waste rock piles, tailings). The Kiruna iron (Fe) mine in northern Lapland is the world's largest underground Fe-ore mine. Aitik, just 20 km south of Gällivare, is Europe's largest open-pit copper (Cu) mine as well as the country's largest gold (Au) producer, and five large Au and base metal mines are an important economic driver for Västerbotten (Fig. 12) (SGU, 2018).

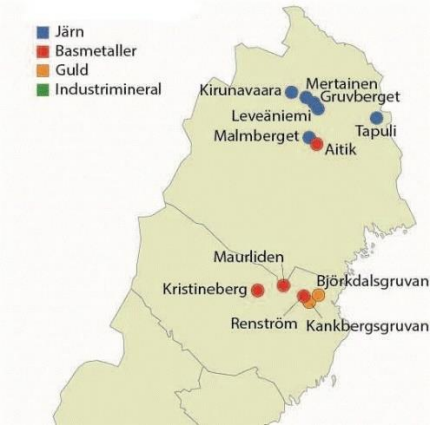

Figure 12. Mines in Northern Sweden in 2018. Järn = Fe, basmetaller = base metals, guld = gold, industrimineral = industrial minerals (SGU, 2018).

Apart from local contamination sources, the snow cover in Northern Sweden may also collect aerosols delivered by long-range atmospheric transport from distant sources. The widespread acidification of forests and lakes in the 1960s-70s made it clear that Sweden is exposed to contaminants introduced to the region by air masses moving across industrial regions elsewhere in Europe or beyond (Maas & Grennfelt/ UNECE, 2016). A study conducted by the European Environmental Agency (EEA) in 2013 names Germany, Poland, Denmark, Great Britain and Norway as the five highest foreign emitter countries in terms of primary and secondary $PM_{2.5}$ emissions affecting Sweden (EEA, 2013).

4.2 Interior Alaska

4.2.1 Climate

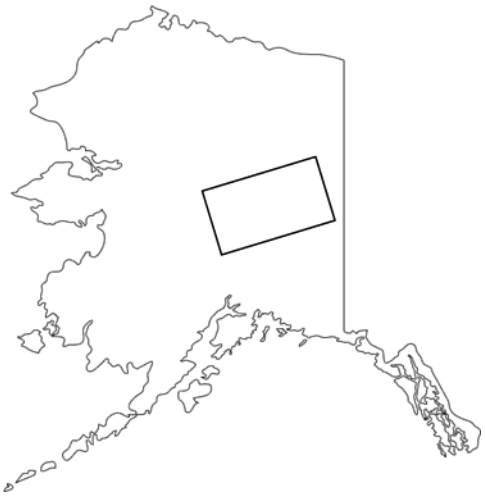

Figure 13. Map of Alaska with sample region marked with a black box.

Snow samples used in this study were obtained in Interior Alaska, which is commonly defined as the region between the Alaska Range to the south, the Brooks Range to the north, the Canadian border to the east, and the southwestern flats to the west (ADF&G, N.d.; Shulski & Wendler, 2007). The study area is located in the eastern part of Interior Alaska (region framed in figure 13), and all samples were collected between latitudes 63°N and 65°N, below the Arctic Circle. The dominant feature of Interior Alaska's climate is its continentality, owing to its remoteness from moderating coastal influences. Large interseasonal temperature variations (-62° to 38°C), low humidity, and low and irregular precipitation rates define the region (Shulski & Wendler, 2007). Temperatures in winter can drop well below -40°C, especially in valleys and depressions, although long periods of extremely cold temperatures have become less prevalent over the last decades (Stuefer, 2019). The relationship between temperature and latitude (Fig. 14) is more expressed in winter than in summer.

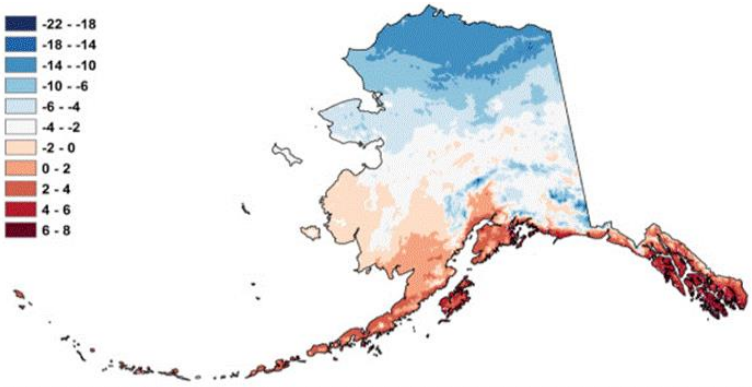

Figure 14. Mean Annual Temperature in Alaska (°C) (Walsh/ AK CASC, 2018).

The main climate control during the winter is a prevailing high-pressure system. This changes in summer, allowing warm, moist air from lower latitudes to come into the region (Shulski & Wendler, 2007). Prevailing winds during the cold season months (Sept.-May) are from the north, switching to southerly winds in the summer months (June-Aug.). Due to the high-pressure system in winter, surface wind speeds are usually low, which can lead to strong temperature inversions in certain locations such as Fairbanks. Occasionally, low-pressure systems track through Interior Alaska during winter months, often associated with snowfall. Anticyclones with surface pressures ≥ 1030 mb have also been observed to move into as well as form in the Interior, which oftentimes leads to extremely low temperatures (ibid).

Most of the annual precipitation in Interior Alaska falls during the summer months as rain, except for the high mountain ranges, where solid precipitation predominates (Fig. 15; Shulski & Wendler, 2009). Within the study area, mean annual precipitation varies from 200 mm in low-lying areas such as the Tanana-Kuskokwim Lowlands (~200-900 m.a.s.l.), to 700 mm in the foothills of the Alaska range (> 900 m.a.s.l.) (Fig. 16).

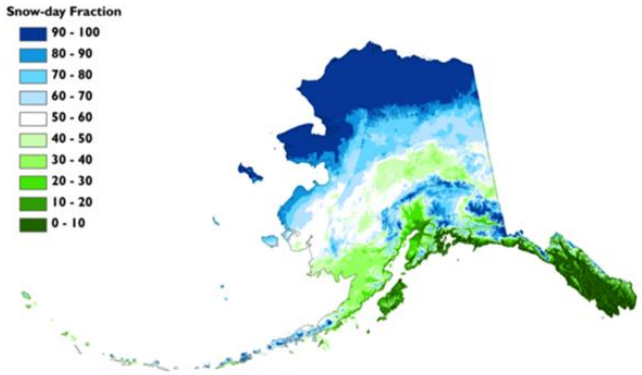

Figure 15. Downscaled projections of rain/snow partitioning for Alaska shown as Snow-day Fraction (%). Blue shades indicate high snow to precipitation ratio, green shades indicate less solid precipitation (McAfee, 2013).

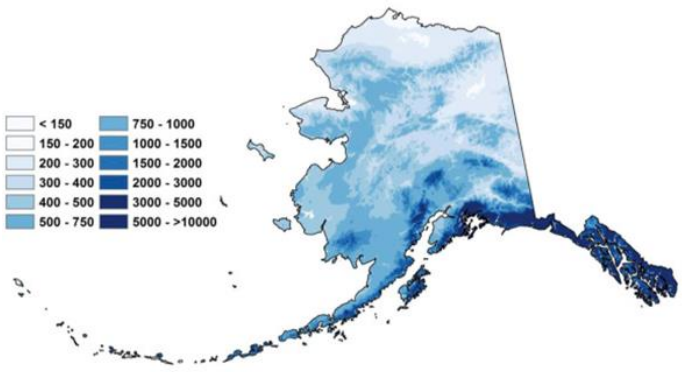

Figure 16. Mean Annual Precipitation in Alaska (mm) (Walsh et al./ AK CASC, 2018).

4.2.2 Surficial Materials and Soil Geochemistry

The topsoils of eastern Interior Alaska are dominated by gelisols (turbels) and inceptisols (aquepts, gelepts, and cryepts). Gelisols are soils that are frozen for a part of the year and contain permafrost near the surface. Turbels occur mostly in places that receive enough solar radiation for the top layer to thaw in the summer months, or in areas that have been subject to forest fires or land clearing (USDA/NRCS, N.d.). Inceptisols are very poorly developed soils mostly situated in wet areas with a deeper active layer than Gelisols or no permafrost at all (USDA, 1999). Soils of the Tanana series, which are aquiturbels developed from loess or alluvium in permafrost areas, are prevalent in the interior of Alaska (Mulligan& Cole, Nd.). Chemical composition maps of the topsoils in Alaska have been compiled by the U.S. Geological Survey (USGS) based on soil and sediment measurements taken since the 1960s by the USGS, the National Uranium Resource Evaluation program, and the Alaska Division of Geological & Geophysical Surveys geochemical databases (Lee et al., 2016). In this work, the USGS maps were used to extract information on metal concentrations in soils in proximity of the snow sampling locations.

4.2.3 Snow Conditions

The duration of snow cover across the study region varies considerably with altitude. Low-lying areas such as the Tanana-Kuskokwim Lowlands experience 170-210 days of snow cover every year while in higher areas such as the Yukon-Tanana Uplands and the Steese National Recreation Area (SNRA) it may last 210-260 days, or 250-290 days near the Alaska Range (Lindsay et al., 2015; data for 2001-2013). This pattern is mirrored by mean annual snow water equivalent (SWE; Fig. 17), which decreases from >40 cm in the foothills of the Alaska Range to >10 cm in the Tanana-Kuskokwim Lowlands. The last day of snow cover in Interior Alaska also strongly varies with altitude (Fig. 18). The snow may disappear in early April in the Yukon-Tanana flats but can persist until the beginning of June in parts of the Yukon-Tanana Uplands and the foothills of the Alaska range. For the winter 2017-18, when the snow samples for this study were taken, the study region experienced above-average winter snow accumulation. On May 7, 2018 (start of the sampling period), the snow now depth across the study region was ~15cm greater than to the average for 1998-2012 time period. The contributing factors were both colder than average winter and spring air temperatures, and above-average winter precipitation (Brown & Luojus, 2018).

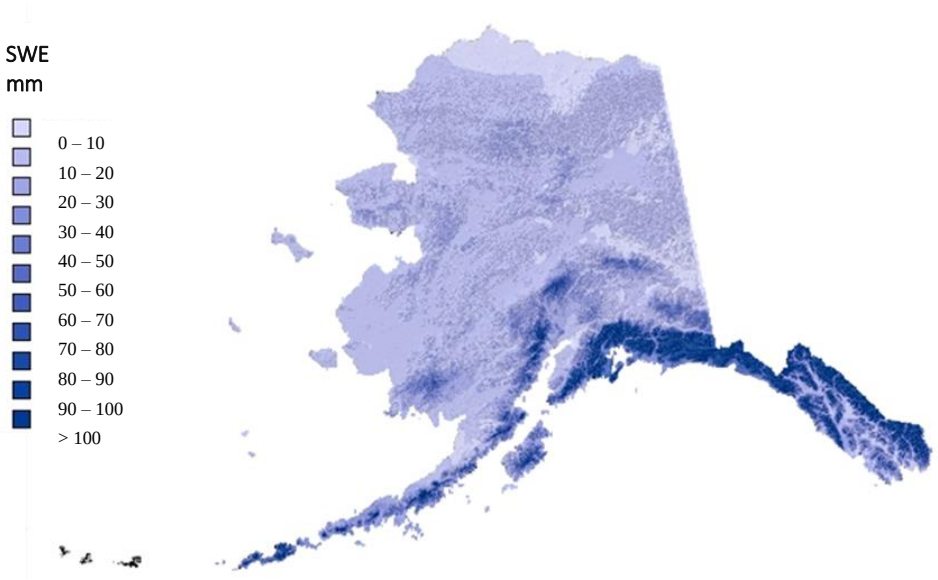

Figure 17. Snow water equivalent in Alaska (mm) (topography: ArcticDEM Release7, PGC, 2018; ArcGIS 10.6.1, SWE data: NSIDC, 2019)

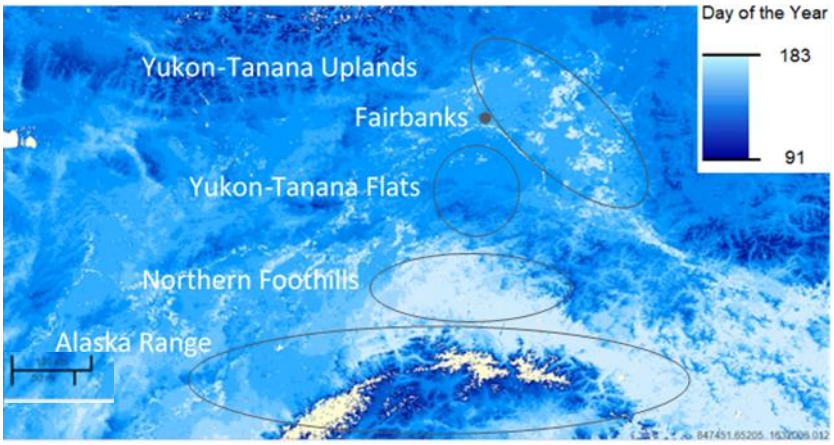

Figure 18. Last day of spring snow cover Interior Alaska 2016 with schematic delineation of the large-scale geographic regions. Data based on the MODIS daily snow cover fraction product (MOD-SCAG), 500-m resolution. The annual last day of spring snow for each pixel was identified by day of the year ranging from 91 (April 1) to 183 (July 2) (NASA/ ABoVE, 2017).

4.2.4 Pollution Sources: Global and Local

Just as in Northern Sweden, expected local contaminant sources in the eastern part of Interior Alaska include releases from oil and gasoline combustion. In particular residential heating, transportation, and industrial activities lead to drastic increases

of concentrations of air contaminants close to population centres and roads (Simpson, 2019). Measuring stations for $PM_{2.5}$ and PM_{10} are relatively sparse in Alaska and confined to the population centres (Simpson, 2018). Hence, modelling efforts are strongly focused on the bigger cities in the State, such as Fairbanks (ibid). In general, however, both $PM_{2.5}$ and PM_{10} concentration levels can be expected to be rather low in the remote areas of the state, due to the lack of local pollution sources. Two global modelling efforts show Alaska with relatively low annual mean annual background values of below 10 µg/m^3 for $PM_{2.5}$, with the exception of eastern Interior Alaska (Fairbanks) with levels of up to 15 – 25 µg/m^3 (WHO, 2016; Lary et al. 2014). Yet, results from measuring stations in and around Fairbanks continuously exceed air quality standards by a large margin (e.g. daily average $PM_{2.5}$ concentration 170 µg/m^3 in December 2012) (DEC, 2019; Rozell, 2018). This is in part due to the cold temperatures, coupled with a strong temperature inversion and low winds, which trap particles released mainly by traffic and wood burning in the city in winter (ibid).

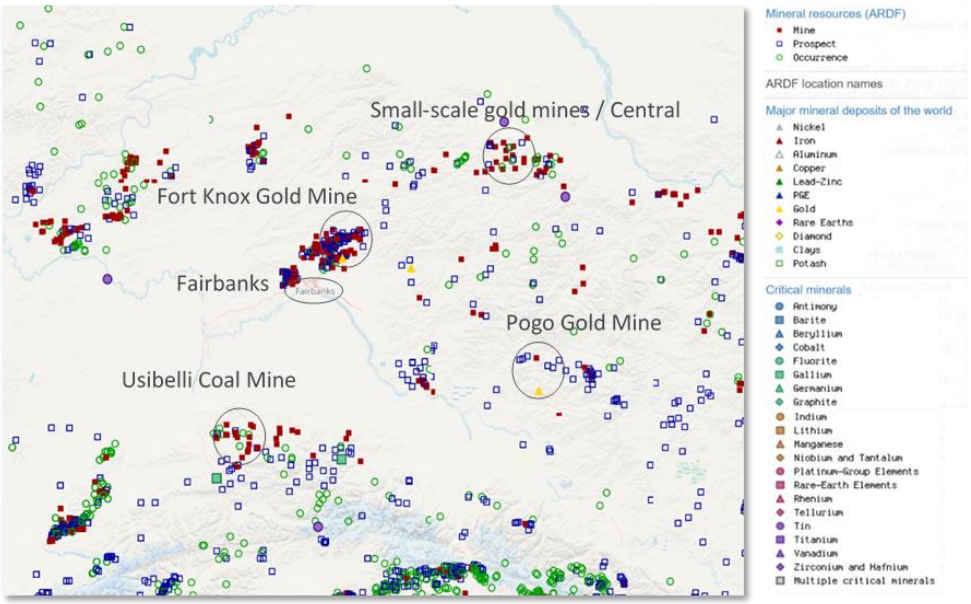

Figure 19. Mines and Mineral Deposits in Interior Alaska (USGS, 2018)

Similarly to Sweden, several large mines contribute to PM levels through heavy vehicle traffic emissions and aeolian deflation and dispersion of fine mineral matter of exposed soil and bedrock. The open pit, truck-and-shovel operation Fort Knox gold mine is located about 45 kilometres north-east of Fairbanks. The Usibelli coal mine just 10 kilometres east of Healy in the Northern Foothills of the Alaska Range is the only operational coal mine in Alaska and transports coal on open train cars

through the Interior. The underground cut-and-fill operation Pogo mine is a regional employer for the communities around Delta Junction about 120 kilometres south-east of Fairbanks (Fig. 19) (Usibelli Coal Mine, 2015; ADNR, 2016; USGS, 2018; ADNR, 2019). As of 2018, Alaska had six large operating mines with several large projects in the permitting process and hundreds of smaller-scale mines in operation (McDowell Group, 2018).

Apart from local emission sources, a study by Glenn E. Shaw found that (Interior) Alaska "is affected by two highly contrasting air mass types: a maritime northern Pacific system lying to the south, and an Arctic strongly polar air mass system to the north" (Shaw, 1988, p.2239). According to Shaw (1988), these two tropospheric air mass systems, which are large, semi-global in scope, have a very different aerosol chemistry. These systems change 'pattern' and position depending on the displacement of the Polar Front. When the latter is displaced northward and strong winds prevail, Interior Alaska (measuring station was located close to the Poker Flat Rocket Range just north of Fairbanks) is covered by Pacific air. This air mass is dominated by 'marine' air chemistry, characterized by enrichments in Cl, Se and Zn (ibid). In the opposite situation, Arctic-extruding cold air can bring high concentrations of "pollution-derived elements from industrial regions in Eurasia, characterized by enriched Cr, non-crustal Mn, As, Se and Br" (ibid). In summer, the chemistry of aerosols has different characteristics, being dominated by elements found in minerals, such as Al, Sm and La. He found, that a similar signature can be measured in the winter months when the air is relatively calm. Shaw (1988) interprets this as natural, local aerosols having the predominant impact when meteorological conditions are quiescent or when clouds in the summer remove long-distance aerosols from the air.

5 Materials and Methods

The overall aim of snow sample collection was to obtain two comparable datasets from highly heterogeneous sample locations in the two northern countries for the purpose of analysing the chemical composition and content of carbonaceous particles in the snow. The snow sampling and filtration methods have therefore been undertaken according to a protocol developed for snow sample analyses in Arctic regions (Gallet et al. 2018). The analysis of the filters comprised five different methods. One analysis was carried out by the author of this study while the remaining four were carried out at different laboratories in Stockholm, Sweden, Venice, Italy and Colorado, the United States.

5.1 Site Description

The snow samples analysed in this study were collected during two separate field campaigns; one in spring 2017 in Northern Sweden, and one in spring 2018 in Interior Alaska. The sampling locations were chosen so as to include urban, suburban, rural and remote settings exposed to different mixtures of airborne particulate matter emissions from local and/or distant sources.

5.1.1 Northern Sweden

Sampling in Northern Sweden took place from the 2nd to the 9th of April 2017, shortly after snow accumulation reached its maximum in the region. Sampling was carried out by Madeleine Syk, Joakim Vollmer, and Christian Zdnanowicz (Vollmer and Syk, 2017). The samples were taken in the proximity to specific pollution point sources (e.g., power plant) as well as in rural and remote areas (Fig. 20). Wherever possible, snow sampling was conducted downwind relative to any nearby settled areas, as determined from meteorological data obtained from the Swedish Meteorological and Hydrological Institute (SMHI).

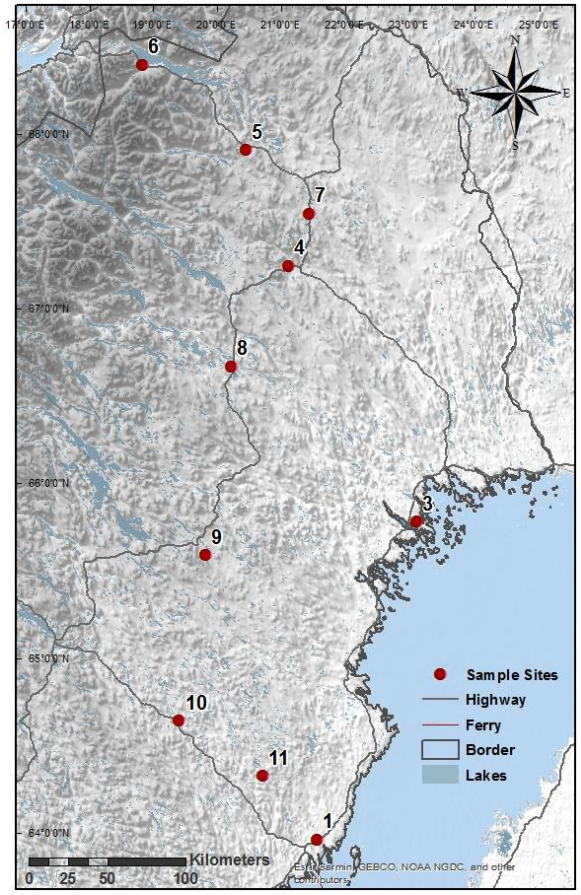

NR	SITE	SAMPLEID
1	Umeå	UM01, UM02
3	Luleå	LU01
4	Gällivare	GA01
5	Kiruna	KR01
6	Abisko	AB01
7	Puoltikasvaara	PU01
8	Jokkmokk	JK01
9	Arvidsjaur	AR01
10	Lycksele	LY01
11	Svartberget	SV01

Figure 20. Sample sites with sample-IDs in Northern Sweden (topography: ArcticDEM Release7, PGC, 2018; ArcGIS 10.6.1).

The first two samples (S(1): Umeå1 (UM01) and S(2): Umeå2 (UM02)) were collected close to the city of Umeå, sample 3 (S(3): LU), close to Luleå on April 3rd 2017. The first of the two sampling sites was in a clearing about 400m east of the chimney stack of the Dåva biofuel power plant, and about 20 m from its access road (Fig. 21). The Dåva waste recycling depot was located about 900 m north of the site. The average total snow depth at this site was 49 cm and the snowpack had been affected by some melting. The second sampling location was situated in a forest clearing about 600 m east of the power plant. The snowpack there was the thinnest of all Swedish sites (37 cm) and there were some snow scooter tracks nearby. The next sample (LU01) (3) was taken on the same day in a public park, 40 to 50 m from houses, in a suburban residential area at the northern city limit of Luleå. The snow-pack there was 69 cm deep. Some snow scooter tracks were also observed nearby.

Figure 21. Snow sampling in Umeå (UM01) ~400m from Dåva waste recycling depot (Zdanowicz, 2019).

On April 4th, two snow samples were taken close to the towns of Gällivare (S(4): GA01) and Kiruna in Lapland (S(5): KI01). The snowpit near Gällivare was dug in a forest clearing off a secondary road ~3 km to the northeast of the town itself, and ~3.5 km southeast of the Malmberget open-pit Fe ore mine. The airport was ~3 km southeast of the site and an open sand and gravel quarry was located ~2.5 km to the northeast. The snowpack at this site was relatively deep (99 cm), with an average temperature of -3.4°C. The next sample (KR01) was taken in a public ski trail area dominated by scattered birch trees, at the southern periphery of the city of Kiruna. The nearest homes were ~60 m to the east. The sample site was located ~1.3 km to the west of the nearest parts of the tailings of the Kiruna open-pit Fe ore mine, these tailings stretching another ~3.5 km to both the north and the south of this point. The surface of the 66 cm deep snow pack (~ -2.5°C) showed signs of windblown dust from the mine tailings. Recent snow scooter tracks were also seen.

On April 5th, a snow sample (AB01) was collected near Abisko in northern Lapland (S(6)). The sampling site (73 cm deep, ~ -0.6°C) was located in a remote forest of dwarf birches. Except for a ski station ~1 km to the southeast and the Abisko research station and its supporting buildings ~2.5 km to the southeast, the region is mainly dominated by rolling hills with a sparse tundra vegetation cover. The nearest road and railroad were about 500 m away.

The following day, April 6th, three samples were collected near the communities of Puoltikasvaara (S(7)), Jokkmokk (S(8)), and Arvidsjaur (S(9)), the latter being at the same latitude as Luleå, but further inland. All sampled snowpacks were of the same approximate depth (65-70 cm). Sample 7 PU01 was collected in a rural setting on a meadow at the southern edge of the village of Puoltikasvaara, just north of the shore of lake Puoltika (Puoltikasjärvi). A boathouse was close by as well as a small

road at ~20 m distance. Sample JK01 (S(8)) was taken in an open forest of pine and birch trees in a reindeer pen ~2 km west of the town of Jokkmokk. A small road and an aggregation of approximately 10 houses laid 200 m south of the sampling site. The snow pit was 68 cm deep and nearly isothermal (-0.4°C), and hence possibly affected by melt. The snow sample near Arvidsjaur (AR01) was taken in a clearing between pine trees at the edge of a right-of-way clearing of a power line. The site was ~150 m east of a highway and ~ 9.5 km southeast of the village. The site was located ~4 km east of a road safety test track and ~8 km west of the local airport. Snow scooter tracks were also seen close to this location.

On the last day, April 7th, snow samples were obtained from sites at Lycksele (S(10): LY01) and in the Svartberget forest (SV01) north of Vindeln (S(11)) , ~120 and 50 km north-west of Umeå, respectively. The snowpit in Lycksele (64 cm deep, -1.1°C) was dug in a clearing among birch trees, at the edge of the right-of-way of a power line that runs along the eastern limit of Lycksele. Close by were a scooter and a reindeer trail as well as a small road, ~30 m to the north. The last sample (S(11) V01) was taken in a clearing within the forested reserve that surrounds the Svartberget Field Research Station, located ~7 km north of Vindeln.

5.1.2 Interior Alaska

Logistical complications prevented sampling before the beginning of May in Alaska. As snow melt had already set in in parts of the State, scouting for sampling locations in the Interior had to be adjusted accordingly. This implied choosing locations in somewhat higher elevations. The aim was to get high enough to sample intact snowpacks but not being above an altitude of 1000 meters to stay consistent with the site locations of the Swedish dataset. Moreover, the road network only allowed for certain regions to be sampled without losing too much time accessing the various locations. Another factor that was considered was to sample in both remote areas and urban settings, as well as locations that were assumed to be affected by local pollution sources such as mines. The eventual sample sites are displayed in figure 21 below. Despite the effort to find intact snowpacks, some measurements were taken from snowpacks which had already been affected by snowmelt. The aim to represent varied locations made it necessary to compromise and to sample in lower-lying areas as well (e.g. Fairbanks, Central, Railroad by Healy). The fact that snowmelt had already affected some of the sample sites could have influenced both the chemical composition and to a lesser extent the content of CP of the respective snowpack. In general, measurements were preferentially taken downwind of local emission sources. Wind directions for the Alaskan sites have mainly been provided by the Western Regional Climate Center and the Alaska Climate Research Center (WRCC, 2019; ACRC, 2019).

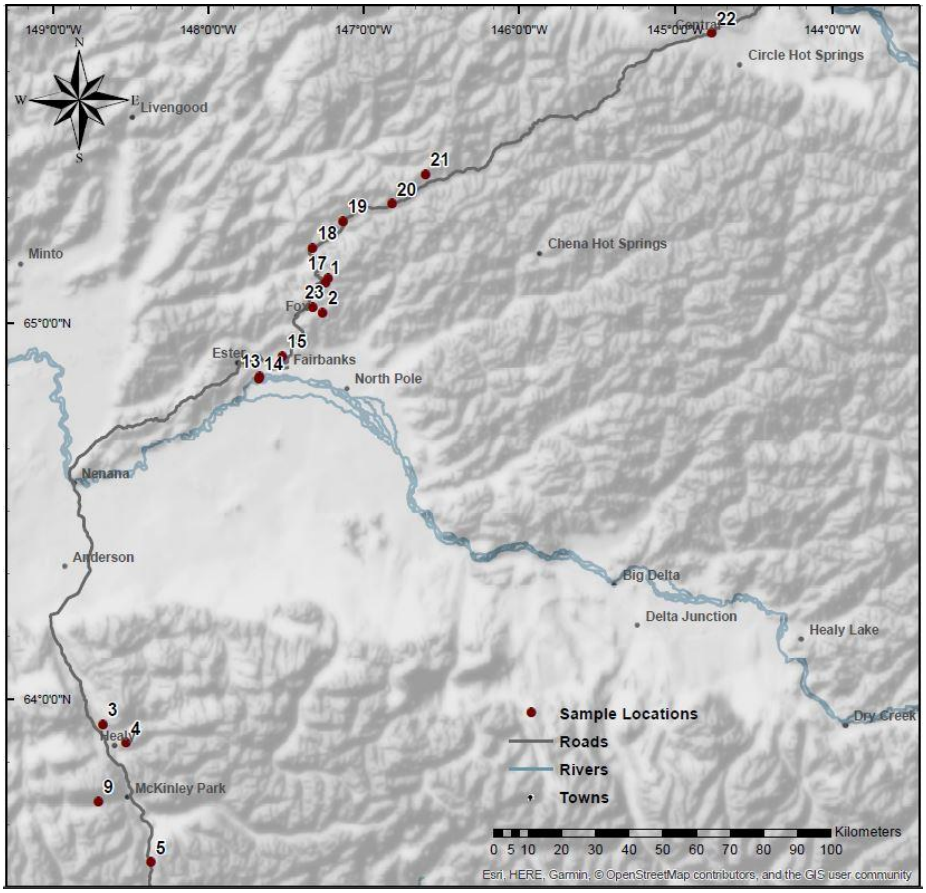

NR	SITE	SAMPLEID
1	Cleary Summit	A1 CS
2	Dark Hollow Drive	A2 DHD
3	Railroad	A3 RR
4	Healy Spur Road	A4 HSR
5	George Parks Highway	A5 GPH 0
		A8 GPH IV
9	Denali Park Road	A9 DPR 0
		A12 DPR III
13	Fairbanks Airport	A13 AIR
14	Lake by Fairbanks Airport	A14 AIR_L
15	Johansen Expressway	A15 JOH
16	Johansen Expressway Melt	A16 JOH_M
17	Skiland	A17 SKI
18	Poker Flat	A18 PF
19	Dog Kennel	A19 DK
20	Davidson Ditch	A20 DD
21	US Creek Road	A21 USCR
22	Central Airport	A22 AIR_C
23	NOAA Satellite Facility	A23 NOAA

Figure 22. Sample sites with sample-IDs in Interior Alaska (topography: ArcticDEM Release7, PGC, 2018; ArcGIS 10.6.1).

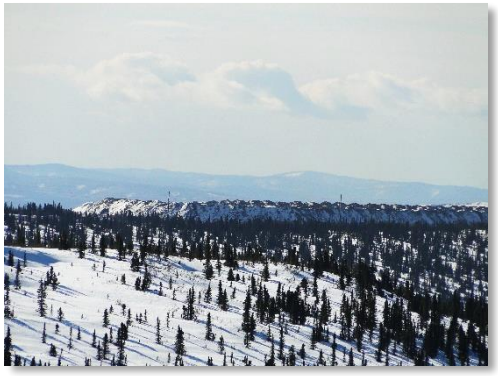

Figure 23. Cleary Summit in sight of the Fort Knox gold mine

Sampling in Alaska was carried out on five days between the 5th and 15th of May 2018. The two samples taken on May 5th (Sample[1]: Cleary Summit (CS); S[2]: Dark Hollow Drive (DH)) were chosen as they were located close to the Fort Knox gold mine just north of Fairbanks (Fig. 23). The sky was clear with intermittent cloud cover and temperatures were well below freezing in the morning, climbing to +1°C in the afternoon at a height of two meters above the ground and a location exposed to the sun. The sample on Cleary Summit was taken at a location approximately four kilometres northwest and downwind of the outskirts of Fort Knox. The snow pit was dug on a hill (~720 m.a.s.l.) facing the north-western site of the mine with a direct line of sight to the mine. A dirt road leading to the mine and frequently used by trucks coming in and out of the mine was approximately 300 meters from the sample location. The surrounding vegetation was sparse, consisting only of some small, unfrequently distributed brushes on a thin layer of soil with bare bedrock and boulders near. The snowpack was rather thin (41cm) and the top two centimetres showed signs of sintering through melt. The second sample was taken in a clearing about four kilometres southwest of the mine (~500 m.a.s.l.). The site was directly facing the mine with only a small hill interfering. Yet, at this location medium-sized trees were intercepting winds from any directions other than south-west. The snowpack was deeper at this site (~75cm) and slightly colder (-0.35°C) with no signs of melting.

Figure 24. Healy coal power plant.

The next day (May 6th), sampling was carried out further down south in the foothills of the Alaska Range following the Parks Highway. Temperatures were colder overnight and stayed below freezing (~ -7 to -3°C) especially in the higher altitudes. The first sample of the day (S[3]: Railroad (RR)) was taken on a frozen lake just 15 meters from the railroad track leading from Anchorage to Fairbanks. On this part of the train tracks, trains with open cars pass by several times a

week to transport coal to Fairbanks from the Usibelli coal mine just northeast of Healy. The location is approximately five kilometres downwind from the eastern side of the coal mine and ten kilometres from the local coal power plant at an altitude of 360 m.a.s.l. (Fig. 24). The snowpack was heavily affected by snowmelt. No vegetation was intercepting the railroad tracks and the snowpack. The fourth sample (S[4]: Healy Spur Road (HSP)) was collected further to the south, approximately five meters from the dirt road leading to the Usibelli mine at an elevation of 600 m.a.s.l. The location was approximately four kilometres south of the mine and two and a half kilometres east of the coal power plant, separated by a small ridgeline. The surrounding vegetation was dominated by low, thick brush and some of the surrounding, rather sandy soil (mainly along the road) was exposed. The snow at this site was also affected by snowmelt, though not as strongly as at S[3]. The next four samples (S[5], S[6], S[7], S[8]: George Parks Highway (GPH)) were taken just before the village of Carlo. Wedged in-between the eastern and western Alaska Range, the highway finds its way through the range on lower elevations but the altitude at this southernmost sample site was still about 750 m.a.s.l. The samples were taken in a perpendicular line from the road, with the first sample (S[5]: GPH 0) taken about a meter from the road, the second sample (S[6], GPH 1) approximately 5 meters from the road, S[7] (GPH 2) was taken about 10 meters from the road, and S[8] approximately 15 meters from the road. It was snowing heavily during the sampling and wind speeds very relatively high. Tall spruce trees and low brush dominated the surrounding vegetation under the powerline that was leading away from the road. The last set of samples that day was taken in Denali National Park along the Park Road about 20 kilometres south of Healy (S[9], S[10], S[11], S[12]: Denali Park Road (DPR)). The park road had just re-opened after the winter months during which the road is closed for private vehicles and the park busses. Hence, the surrounding snowpack is a representation of the last and first tourist traffic in early September and May, usage of the road by park staff and scientists during winter, as well as long-range aerosol transport. Samples were taken after driving for about 9 kilometres into the park at a site where the snowpack was around 150 cm deep. The weather was a mix of sun, cloudy sky and snow flurries and temperatures were measured to be -3°C at around 4pm. The altitude at the sampling site was approximately 870 m.a.s.l. and the snowpack showed almost no signs of previous melt. The vegetation was dominated by sparsely vegetated with intermittent stands of spruce and shrubs. Just as along the George Parks Highway, samples were taken directly next to the road, as well as at a distance of five meters, ten meters and fifteen meters.

In order to obtain samples with a presumably very different chemical composition, snow was collected at both the airport as well as at a snow-dump in the median of a major road in Fairbanks on May 9th. The temperature in the morning registered

at 4°C and climbed to 13°C in the afternoon under a cloud-free sky. The first two samples (S[13], S[14]: Airport and Airport Lake (AIR, AIRLA)) were taken at the airport in Fairbanks. Sample 13 was obtained from a snow dump from runway clearing, while the second sample (S[14]) has been obtained from a small, half-frozen lake which was the result of snow melt from the runway topped with approximately 20 cm of snow on the frozen part. The second sample location in Fairbanks was the largest snow-dump in town in-between the east- and westbound lanes of the Johansen Expressway (S[15], S[16]: Johansen and Johansen-Melt (JOH, JOH-M)). The collected snow at this site comes from clearings of all parts of the eastern-side of town. The snow-pile is about ten metres high and was subject to melt. Sample 15 was collected from a thin stretch of about two meters in length along one of its sides. As meltwater was running off this pile, sample 16 was extracted from the slowly forming melt-puddle (S[16]).

On sample day four (May 12th) snow was collected along the Steese Highway, which leads into the Yukon-Tanana Uplands northeast of Fairbanks. The weather on this day was sunny with some intermittent clouds and temperatures just below freezing in the lower altitudes dropping to approximately -5°C in higher terrain. The first sample of the day (S[17]: Skiland (SL)) was taken on the north-facing ski-slope of the local ski-resort under the ski lift. The slope is located about five kilometres from the Fort Knox gold-mine in close proximity to the Cleary Summit sample location (S[1]). The snowpack was affected by melt and was packed from grooming and skiers and snowboarders. The second sample of the day (S[18]: Poker Flat (PF)) was taken on a clearing next to the Poker Flat rocket launching station (~210 m.a.s.l.). The snowpack was affected by melt and surrounded by small birch and spruce trees. Sample [19] (Dog Kennel (DK)) was collected on the hills on one side of a valley at the bottom of which lies the Steese highway. The site was located about a hundred metres off the road behind a dog-kennel which is surrounded by mainly birch trees (~300 m.a.s.l.). The owners of the kennel live in a small cabin on their property and use a wood-fired stove as their main source of heat in the house. The snowpack at this location was relatively thin and showed meltforms. The next stop was made at a section of the Davidson Ditch (S[20]: DD), an old channel- and pipeline system which was used to funnel water from the Chatanika river to placer mines in Fox. Notched between small hills and a forest that likely burned about 20 years ago based on the newly grown birch trees, was a section of the rusty steel pipeline from 1929. The samples were taken underneath the pipeline. As the site is located at about 400 m.a.s.l., however, the snowpack was affected by melt already. Sample [21] was taken at a higher altitude (~820 m.a.s.l.) on a plateau overlooking a part of the White Mountains to the north, which was accessed by branching off the Steese and following U.S. Creek Road for about 18 kilometres uphill (Fig. 25). The dirt road had just been cleared a day before, so other than snow machiners no

other traffic had been going through all winter. Many of the surrounding trees and most of the trees on neighbouring hills had burned in a wildfire some years before. Only the top two centimetres showed some melt forms, and some harder layers within the snowpack were signs of wind compaction due to higher windspeed. The last sample of the day was taken at the airport in Central (Sample [22]), a small village of about 90 people, which hosts one of the checkpoints for the Yukon Quest sled dog race. The landing-strip, from which the sample was taken, had been exposed to the sun and with an altitude of 290 m.a.s.l., and therefore this snowpack was also affected by melt.

Figure 25. Sample location A21 along the US Creek Road.

The last sample in Alaska was taken two days later on May 15th. With special permission from NOAA, snow was sampled on the property of the Fairbanks Command and Data Acquisition Station, a satellite data receiving station 15 kilometres north of Fairbanks. The site was located on a hill between the sampling sites at Cleary Summit and Dark Hollow Drive and in the main wind direction downhill of the Fort Know gold mine at an altitude of approximately 400 meters. The samples collected at Skiland and these three locations hence form a semi-circle around the mine downwind of the most common wind-directions. The snow showed signs of melt but surrounding shrubs had cast their shadows over the snow and kept it from melting too much.

5.2 Snow Sampling

The Alaskan samples were collected by the author of the present document. Both parties followed a standard protocol for snow sampling developed by the Svalbard Science Forum (SSF), which was designed to ensure comparability of snow sampling results (Gallet et al., 2018). The focus of the snow collection was to investigate the BC aerosol content while following a protocol that would additionally allow for a chemical analysis of the snow filters (Syk & Vollmer, 2017). The two field campaigns were designed to obtain measurements prior to the onset of snow melt in spring, which coincides with the maximum snowpack depth and particle loading. Nonetheless, the Swedish field campaign in 2017 took place just days after the maximum snow depth was recorded for most parts of Northern Sweden. Snow melt in Interior Alaska in 2018 had begun especially in the lower-altitude sample locations. However, due to an unusually high snowpack and long-lasting low temperatures, only about one third of the chosen snowpack locations were affected by snowmelt.

At each snow pit site, metadata including GPS coordinates, the meteorological conditions and any possible influencing factors of the surroundings of the snow pack (open water, trees, etc.), were recorded as fieldnotes and photographs, before approximately 1m² snow pits were dug to the bottom of the seasonal snowpacks. At each site, both snow physical observations were recorded before the actual snow samples were taken. Obtaining snow physical observations included measuring the temperature profile (precision of ±0.01°C), determining the snow stratigraphy, and defining the snow grain size and shape as well as the snow density (100cm^3 or a 250cm^3 sampler; precision of ±1 g) in different depths where possible. The snow sampling of the Alaska samples was carried out wearing non-particulating coverall suits and disposable plastic gloves. The snow collection was carried out using plastic spatulas, which were 'sterilized' before usage by pulling them through the snowpack close to the snow pit. To obtain samples representing the entire snowpack, a column from the top to the bottom of the snowpack was dug and the snow collected in sterile Whirl-Pak bags. Care was taken not to include soil material in the sample. Each sample was then weighed on a digital scale with a precision of ±1 mg and stored inside insulated cooler boxes, which maintained them at sub-zero temperatures until they were ready to be processed. (Sampling description can also be found in Syk & Vollmer, 2017.)

5.3 Filtration Procedure and Filter Handling

Two different filtration kits were used to collect impurities from snow meltwater. A suction-based filtration set-up with a handheld vacuum pump used filters with a diameter of 50 mm (section 5.3.1) and a pressure-based filtration set-up based on a

syringe with attached filter-holder produced 25 mm filters (section 5.3.2). The Swedish snow samples were processed at the research stations at Abisko and Svartberget, which are part of the Swedish Infrastructure for Ecosystem Science (SITES) network. The Alaskan samples were handled at atmospheric science lab at the University of Alaska Fairbanks.

5.3.1 Vacuum pump filtration set-up (50 mm filters)

Figure 26. Vacuum pump filtration set-up with 50 mm tissuquartz filters and filters after snow meltwater filtration.

After carefully melting the snow samples in a microwave oven, the meltwater from each ziploc-bag was pre-filtered through a cleaned tea strainer to remove macroparticles. The pre-filtered water was then quickly filtered using a filtration kit as shown in figure 26 to minimize the adhesion of particles to the surface of the Ziploc bag. The filtration set was thoroughly cleaned and sterilized with methanol and distilled water before and in-between usage. Suction was created using a hand-operated vacuum-pump (1), which forced meltwater from a borosilicate glass beaker (2) through a 50 mm tissuquartz filter (3), which was placed on a glass funnel (base with frit support) (4), which in turn was attached to a vacuum filtering flask (capacity: 1L) (5) to collect the filtered water.

The filters used for this filtration method are ultra-pure quartz microfiber filters (Munktell Ahlstrom micro-quartz filters, MK 360, 0.3 µm) with a diameter of 50 mm (Fig. 26). Before usage, the filters were baked in a furnace for 48 hours at 800°C to get rid of any organic residues. The surface area of the filter which is exposed to the meltwater is approximately 700 mm^2 (= a circle with a diameter of 30 mm).

After filtration of the snow meltwater, the filters were dried in an oven at 50°C for 24 hours and then kept stored in sterile petri dishes (Zdanowicz, 2018).

5.3.2 Syringe filtration set-up (25 mm filters)

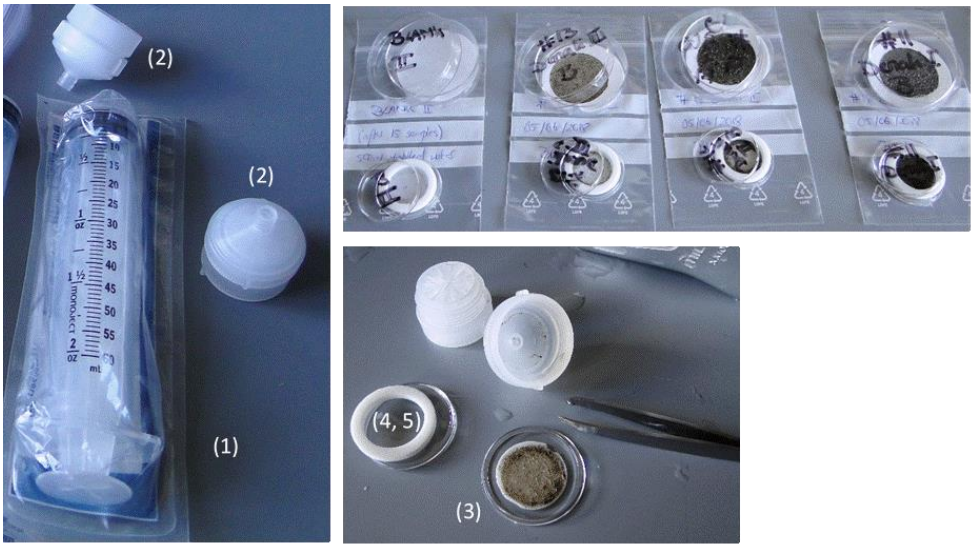

Figure 27. Syringe filtration set-up with 25 mm tissuquartz filters and filters after snow meltwater filtration.

The meltwater from the Alaska samples was additionally filtered with a different method, using a pressure-based syringe filtration set (Fig. 27). This filtration kit has been designed so as to be easily usable in field camp conditions. The water is thereby drawn into a sterile-one-time-use 60 mL syringe (1), which has a filter holder attached at its outlet (2), and slowly pumped through a 25 mm tissuquartz membrane fibre filter (0.7 µm, Pallflex Tissuquartz, 2500QAT-UP) (3). The amount of meltwater was carefully tracked, but due to high particle loading in the meltwater, the recommended benchmark amount of about 600 mL of total snow meltwater for filtration (Schmitt et al., 2015) was almost never reached as the filters clogged up quickly. The 25 mm filters were then carefully removed from filter holders and placed into plastic petri dishes (4) and held in place with a thin foam ring (5). Tissuquartz filers have commonly been used to collect carbonaceous particles of meltwater from snow samples (Chai et al. 2012). However, a study by Carl Schmitt et al. (2015) found that these types of filters do not efficiently collect particles which are smaller than 0.6 microns and it is unclear what portion of the particles is being missed. As CP in the atmosphere tent to be relatively small (<0.6 µm), a large fraction of particles dispersed in air might not be caught on the filters. Thus, the content of CP derived from the analysis of these filters is likely to be an underestimate of

the true content in the snowpack. Yet, a follow-up study by the group of researchers determined, that the concentration of particles on 0.22-micron filters after filtration through tissuquartz filters only showed an average 5 percent higher effective black carbon (eBC) content than the tissuquartz filters, which might be due to the effect that larger particles have a greater influence on the energy absorption of the filter than smaller particles. A factor which has been found to decrease the effective pore size of the filters are dust particles (it is getting harder to push water through the filter the with particle load), which might lead to smaller-size fractions being caught.

5.4 Laboratory Analysis

5.4.1 Methods for the detection of carbonaceous particles

Thermal-Optical Transmittance Method (TOT)
In addition to determining the mass of TC (total carbon), the thermal-optical reflectance and transmittance method (TOT) measures the mass of organic (OC) and elemental carbon (EC) in a sample (pers. communication, Wideqvist, 2018). The method exploits the difference in the volatilization temperature of OC and EC, the more refractory EC having a much higher degassing temperature than that of OC (Lack 2013; Karanasiou et al., 2015).

The determination of EC and OC in the snowmelt filters was performed the Department of Analytical Chemistry and Environmental Science (ACES) of Stockholm University using a Sunset Laboratory Thermal/Optical Carbon Analyzer, following the EUSAAR-2 heating protocol (Cavalli et al., 2010). Square-shaped, 1 cm^2 sections of each loaded filter were used for this analysis. The different carbon fractions on the filters are vaporized and analyzed in a series of gradual heating steps, detailed below (Fig. 28). The analyser is coupled with a laser diode (optical emitter) and a photo detector (optical receiver) to measure changes in the transmittance of light through the filter during the analysis.

The temperature in the oven is first increased from about 50°C to about 650°C and the filter is kept in a 100% nonoxidizing helium (He) atmosphere (Fig. 28). This leads to the decomposition and degassing of OC, while EC remains on the filter. The volatilized OC compounds are then oxidized to carbon dioxide (CO_2) by a catalyst. The CO_2 is reduced to methane (CH_4) in a methanator oven and quantified by a flame ionization detector (FID). However, not all OC compounds are degassed in the He stream: some OC (possibly as much as 30 %) is pyrolized or "charred" into EC that remains on the filter (Turpin et al., 2007). This leads to a gradual darkening of the filter deposit which is continuously monitored with a laser diode measuring the reflectance and transmittance of the filter. In the second heating step, ~2% O_2 is

injected into the combustion oven and the temperature is raised to 850°C. This leads to the oxidization of the remaining pyrolized OC as well as the EC to CO_2, which is then also reduced to CH_4 and measured by the FID. The reflectance of the filter slowly increases in this step, as degassing of the remaining light-absorbing carbon leads to a brightening of the surface. The carbon degassed after O_2 injection and up to a split point temperature of 1100°C is considered to be from pyrolyzed OC and is therefore counted as such. In the last step of the analysis, a known volume of CH_4 is introduced into the sample oven for internal calibration of the FID (Fig. 28), and the quantities of OC and EC are then calculated. Their sum is defined as total carbon (TC). Results are reported in terms of C mass loadings, in μg cm^2 of filter surface.

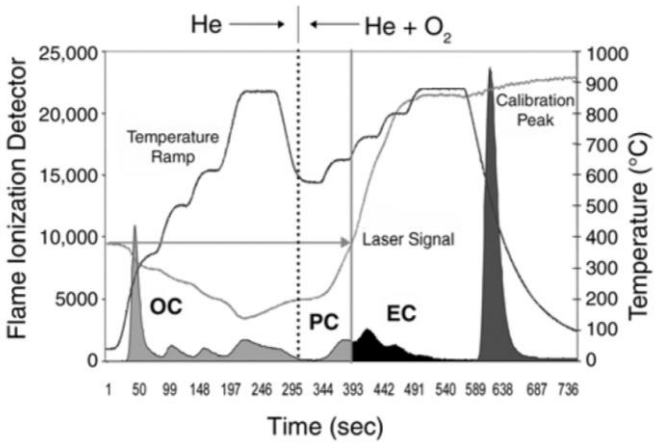

Figure 28. Example thermogram from analysis of OC and EC by thermaloptical transmittance in a Sunset Laboratory Carbon Analyzer (after Birch and Cary 1996) (in Turpin et al., 2007).

Particle Soot Absorption Photometer (PSAP)

The Particle Soot Absorption Photometer (PSAP) determines black carbon mass loadings based on the light absorption by aerosols on the filter material (Sharma et al., 2002; The University of Manchester, 2018). It therefore measures the attenuation of light by comparing the transmission of blank filters to the transmission of filters which have been used to filter snow meltwater. The natural logarithm of the ratio of these two intensities (I_0, I) defines the absorbance or optical depth of the particles and the filter material (ibid; NOAA, N.d.). The latter can be approximated to the carbon mass on the filter by dividing it by the specific absorption for BC at the respective wavelength of the instrument, the transmittance coefficient *K* (m^2 g^{-1}) (NOAA, N.d.; Minguillón, 2012) (equation (1), L_{BC}=BC loading). For this study, two different empirically determined transmittance coefficients K_1 and K_2 were applied. The reference material used to determine the two coefficients applied in this analysis were chimney soot as a proxy for residential heating emissions (K_1: 39.77) and NIST soot a standard used for diesel engine emissions (K_2: 34.42).

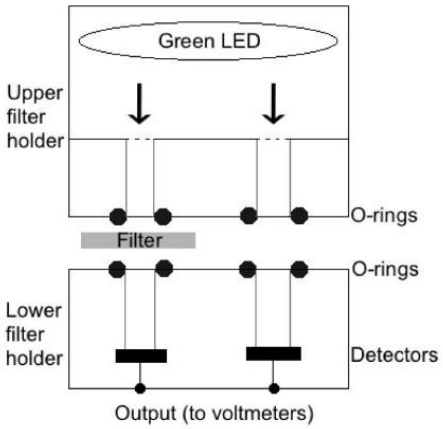

Figure 29. A schematic cross-section of the PSAP. While measuring, the upper and lower filter holders are clamped (Syk & Vollmer, 2018).

$$L_{BC} = \frac{\ln(\frac{I_0}{I})}{K} x\ 1000 \qquad (1)$$

Commonly, the measurements with a PSAP are made with a light source emitting at the 530 nm channel, which has been approximated to correlate with a K-value of 10 m^2 g^{-1} (Sharma et al., 2002; Minguillón, 2012). This value is often empirically determined utilizing a thermal LAP measuring technique. It can vary strongly depending on the chemical composition of constituents that are bound to or accompanying carbon particles (e.g. SO_4^2-, soil elements [Si, Al etc], organic carbon) as well as due to filter non-linearities (Sharma et al., 2002).

Hence, it is regarded as a correction factor which also accounts for scattering and absorption effects of the filter medium and the particles themselves (Bond et al., 1999). Using a correction factor introduces additional uncertainties to the method. For the calculation of mass loadings of BC-equivalents (BCe), NOAA (N.d.) estimated a total uncertainty of PSAP measurements of about 15%, while Springston (2018) evaluated that such corrections can account for up to 50% of the initial measurement for particles which have a high single-scattering albedo. Thus, results from optical measurements are oftentimes not understood as absolute values of light BC concentration but rather approximations of temporal trends and variations (NOAA, N.d.). As Dr. Springston (2018, p.15) at the ARM Climate Research Facility puts is: 'In sum, the PSAP measures what the PSAP measures.'

In this case, measurements were carried out at the Department of Analytical Chemistry and Environmental Science at Stockholm University using a green light emitting diode (LED) with a wavelength of 510 nm (oftentimes measurements are also made with three different wavelengths). The corresponding transmittance coefficients have been empirically determined for both chimney soot (K1: 39,77 m2 g-1) and NIST soot, a US standard for diesel engine emissions (K2: 34,42 m2 g-1). PSAP-instruments are oftentimes used to make continuous measurements of particles in suspension, which requires having a reference filter throughout the measurement. Diagram 29 shows a schema of a PSAP instrument, where the filter holder that would usually be used for a reference filter is empty. In this case, each filter has been measured twice, once in each filter holder, so as to have two independent values to account for possible light intensity fluctuations of the emitting LED diode.

The filters are held in by O-rings which sealed the filter from external light penetration.

Light Absorption Heating Method (LAHM)

The Light Absorption Heating Method (LAHM) instrument was recently developed by Carl Schmitt in response to the need to develop a low-cost method to measure the absorption ability of particles in snow (Schmitt, 2019). The method measures the infrared thermal emission of light-absorbing particles, which has been shown to correlate closely to the quantity of BC in a sample (Khan et al., 2017). The quantity measured by this method is called effective black carbon (eBC) and represents the BC mass that would absorb an equivalent amount of light as the actual particles in the sample (Schmitt et al., 2015 and Grenfell et al., 2011).

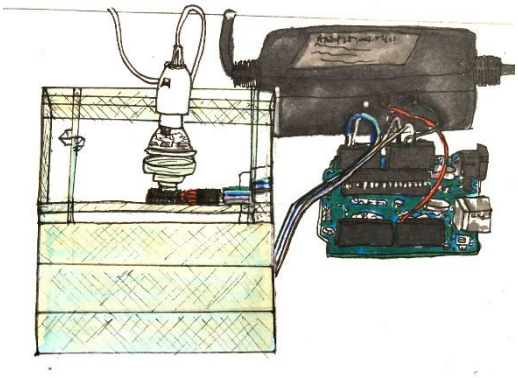

Figure 30. LAHM instrument set-up (Schmitt, 2019).

The particle-loaded filter is placed on a plexiglass base, which provides a thermally stable background, so the plexiglass has a negligible effect on the measurements (Fig. 30). A laboratory grade light source (Cole-Parmer Fiber-Lite Fiber Optical Illuminator model 9745-00) directs high level visible light (wavelength: 300-800 nm) at an approximate angle of 45° on the filter material through a fibre optic light pipe, which reduces the effects of multiple reflections. An infrared (IF) thermometer (Omega OS1327D) monitors the temperature increase of the sample filter with a time resolution of one second.

The measurement routine includes five cycles and starts with an initial 10 s exposure of the filters by the light source. The average temperature during these first ten seconds serves as a normalization step for the subsequent measurements. The light source is then turned on again for an additional 30 s and the IR thermometer starts to record the temperature but keeps recording for an additional 20 s after the light has been extinguished (the procedure which is described here is based on the previous LAHM instrument set-up, hence the procedure of the current instrument might deviate slightly from this description; the underlying principle is the same however). The analyses are calibrated using a clean filter as well as a filter through which water with a known concentration of a BC standard has been passed. The estimated uncertainty of the measured eBC mass is about 10%. However, the latter can vary greatly as measurements with light absorption methods on filters are especially prone to measurement artifacts caused inter alia by filter over- or

underloading, optical interactions between the particles and the filters and their changes in morphology while filtration (Moosmüller et al., 2009).

5.4.2 Methods to for the detection of trace elements

Energy Dispersive X-Ray Fluorescence (EDXRF)

Energy dispersive X-Ray Fluorescence (EDXRF) spectroscopy is a non-destructive analytical method used to determine the chemical composition of a sample (Petiot 2018, Vanasupa, 2015). The method is based off the phenomenon that elements, when stimulated with an accelerated electron-, ion-, or photon source, emit characteristic fluorescent radiation spectra (Petiot, 2018; Fiola, 2017). Typically, a primary high-energy X-ray photon beam (up to 125 keV) is directed on a sample material. The photon bombardment overcomes the binding energy of electrons and displaces them from the inner shells of the composing atoms. Electrons from higher energy levels/ shells then fill the resulting voids, emitting secondary (fluorescent) X-ray radiations in the process. The resulting fluorescence spectrum is characteristic of the elemental composition of the material in the sample (Petiot, 2018; Vanasupa, 2015; Fischer, N.d.) (Fig. 31c). The measured energy of the emitted X-ray depends on several factors: the energy of the incoming primary beam as well as the thickness, density and composition of the material (Petiot 2018; Brouwer, 2010). In the context of this thesis, the EDXRF method was used to test the feasibility of quantifying elements associated with dust particles (mineral or technogenic) by XRF measurements performed directly on the snowmelt filters. The measurements were made at the Department of Earth Sciences of Uppsala University using a portable XRF analyser (pXRF; Bruker Tracer 5i, Fig. 31a,b).

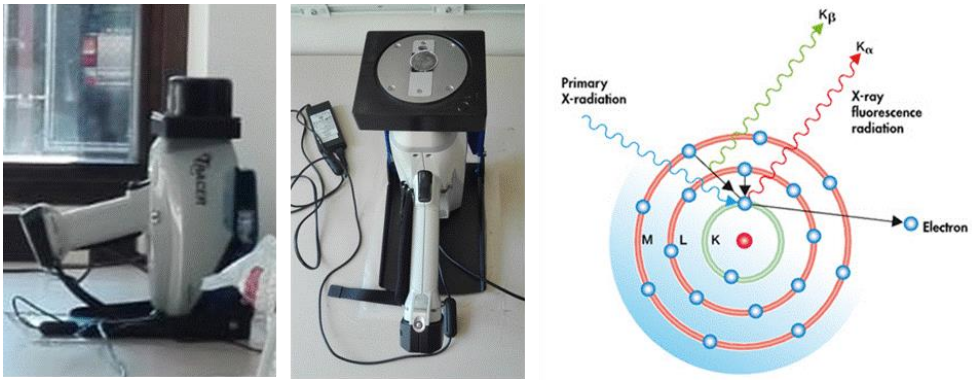

Figure 31. Measurement set-up of the pXRF instrument Tracer 5i from Bruker (a). The 25 mm filter b) has been placed on the collimator and been adequately covered to prevent radiation to escape. c) schematic of the atomic model for the X-Ray Fluorescence analysis method (Fisher, N.d.).

The Tracer 5i pXRF unit allows the detection of elements ranging from sodium (Na) to uranium (U) from ppm to ppb levels, depending on the matrix composition. The instrument is equipped with a Rh thin window X-ray tube, 3- and 8mm collimators, automated beam filters and manual insertion filters (thin metal foils to modify the spectrum of the incoming radiation), and a proprietary 40 mm^2 Si drift detector (SDD) (Fiola, 2017; user manual of Tracer 5i, Bruker 2018). The instrument also comes with two built-in calibrations settings, GeoMining and GeoExoploration, which use measurements in three phases (30 kV, 50 kV, 15 kV). The GeoMining calibration setting has a higher accuracy for minor and major elements, whereas GeoExploration is optimized to yield high accuracies for trace elements (Tim Heek. Bruker, pers. comm., 2018). Both calibrations were tested in this study.

The optimal irradiation/measurement time is dependent on the number of elements which are to be determined as well as the desired accuracy. Here, a measurement time of 180 s was used, with a 60 s step for each of the three measuring phases. The three phases vary in energy levels with phase one measuring with 30kV, phase 2 with 50 kV and phase 3 with 15 kV (Heek, 2018). Each sample filter was measured at multiple points to estimate the variability of results arising from the uneven loading of particles over the filter surface. The 25 mm filters from Alaska were measured at two points and the 50 mm filters at five points. The 50 mm filters from Sweden were measured at 3 points. As for each snowpit in Sweden two or more half-filters were produced (e.g. AB01A+B and AB01C+D), a second technique, to stack the two filters while measuring, has been tried for the Sweden filters (Fig. 31).

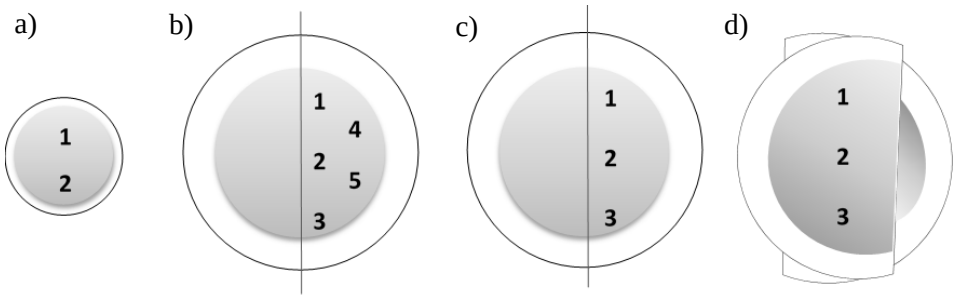

Figure 32. Schematic display of a) 25 mm filter and the two pXRF measurement points, b) 50 mm filter and the five pXRF measurement points as done for the Alaska samples, c) 50 mm filter and the three pXRF measurement points as carried out for the Sweden samples, and d) two 50 mm filter halves stacked on top of each other as done in for the second pXRF measurements of the Swedish filters.

Inductively Coupled Plasma Mass Spectrometry (ICP-MS)

In order to validate the experimental pXRF results against those obtained by a more conventional, well-established analytical method, the concentration of major, minor and trace elements on the sample filters were determined by Inductively Coupled

Plasma Mass Spectrometry (ICP-MS). These analyses were performed at the Institute for the Dynamics of Environmental Processes of Ca' Foscari University in Venice, Italy, on an Agilent 7500I inductively coupled plasma quadrupole mass spectrometer (ICP-QP-MS). The first step was to digest the quartz filters inside teflon vessels with 6 mL HNO_3, 3 mL H_2O_2, and 1 mL HF (UPA grades, Romil, Cambridge, UK). The digestion was carried out in an Ethos1 Advanced Microwave Digestion Labstation (Milestone Srl, Sorisole, Italy) (Morabito et al., 2014; Gregoris et al. 2015). The microwave digestion temperature was set to 190°C for 15 min. The digested samples as well as digested blank (unexposed) filters were then diluted with ultrapure water (~30mL). Between sample digestions, the teflon vessels were cleaned with a solution of 10 mL HNO_3 (Romil Suprapur grade) and 1mL HF (Romil UPA grade) heated to 160°C over 20 min.

The diluted solution obtained from the digestion step was then pumped into the inlet system of the ICP-QP-MS. There, it is nebulized to a fine aerosol and introduced into the Ar plasma chamber. The resulting positively singly-charged ions are then accelerated into the vacuum system of the mass spectrometer. The paths of ions are magnetically deflected according to their mass-to-charge ratio (m/z) and the ions captured in faraday cups. The instrument measures the concentrations of element by their specific m/z ratios with an electron multiplier detector (Wolf, 2005; PerkinElmer Inc., 2011; Clark, 2015). The signals are calibrated against those obtained from a multi-element standard solution. The latter was prepared by digestion of a few mg of certified aerosol reference material NIST 1684a (Urban Particulate Matter) obtained from the National Institute of Standards and Technology (USA).

In this study, the following elements were measured: Al, Ba, Ca, Fe (^{56}Fe and ^{57}Fe), K, Mg, Mn, Na, Cd, Co, Cr, Cu, Ni, Pb, Sr, V and Zn. The limits of detection (LOD) for each measured element were set to the mean concentration obtained on blank filters, plus three standard deviations. Recovery rates were evaluated for some elements using the standard reference material (NIST 1648a) and were: V (114 %), Cr (81 %), Fe (121 %), Co (117 %), Ni (121 %), Cu (103 %), Zn (84 %), As (100 %), Cd (92 %), Sb (72 %) and Pb (112 %).

5.5 Statistical and Graphical Analysis

The statistical analysis and graphical processing was carried out using the statistical software Matlab R2018a as well as RStudio Version 1.1.456 and R Version 3.3.3. The Microsoft Office 365 ProPlus Excel Version 1808 was additionally used to carry out calculations and data analysis. Results, which were rated to be highly uncertain due to measurement errors and irregularities or instrument limits, were omitted as advised by the respective laboratory (marked in italic in the provided data

sheets). Due to the small sample sizes, the choice of statistical methods was rather limited. Making maps for the graphical presentation of the sampling sites was performed using ArcMap 10.3.

6 Results and Discussion

6.1 Analysis of Carbon Particles

This section presents results of three different analytical methods that were used to measure and characterize airborne carbon particles (CP) deposited in seasonal snow. To this end, the data from the two arctic/subarctic snowpacks in Northern Sweden and Interior Alaska were analysed with a Particle Soot Absorption Photometer (PSAP), the Thermal-Optical Transmittance (TOT) method, and the Light Absorption-Heating method (LAHM). One aim was to assess the results of the three measuring techniques through comparison among the methods. A second aim was to quantify differences in snow-deposited CP between the two high-latitude regions according to both their intensities and the types of emissions. Lastly, the levels of CP in both regions were compared to other high-latitude regions to understand how the snowpacks in Northern Sweden and Interior Alaska rank with regard of other Arctic/ subarctic regions. Due to a lack of a uniform filter type across all methods, the comparisons and analytical methods were necessarily chosen according to the shared set of filters analysed with the respective methods. Table 1 gives a brief overview of the methods used for the different sets of filters. TOT was chosen to be the method of reference for all three questions, as this was the only analytical technique used on both 50 mm filter sets, Alaska (AK) and Sweden (SW). In this regard, the measurements of the SW50 filters with the PSAP could be compared to the results of the SW50 filter analysed with the TOT and the small AK25 filters used for the LAHM measurements be compared to the AK50 filter results from the TOT measurements. As the TOT method reports the results as computed from both the transmission (Trans/FID) as well as the reflectance signal (Refl/FID) the average of both has been utilized in the analysis.

Table 1. Sets of tissuquartz filters measured by the TOT, PSAP, and LAHM method. AK25: 25 mm filters filtered with meltwater from Alaskan sites. AK50: 50 mm filters filtered with meltwater from Alaskan sites. SW50: 50 mm filters filtered with meltwater from Swedish sites.

FILTER SET/METHOD	TOT	PSAP	LAHM
AK25	-	-	X
AK50	X	-	-
SW50	X	X	-

6.1.1 Method comparison: TOT vs PSAP and TOT vs LAHM

This section establishes how the EC concentration of a sample measured by the thermal-optical TOT method compares to the black carbon equivalent (BCe) concentration determined by the optical PSAP method as well as the effective black carbon (eBC) concentration derived from measuring filters with the LAHM method. To do so, a Reduced Major Axis (RMA) model was fitted to the data (Fig. 33; Fig. 34). The RMA is the model fitting method preferentially used when uncertainties exist regarding which of the two variables presents the dependent or independent variable. Compared to the least-square regression LSR, the RMA handles errors in both the x and y axis well (Harper, 2014). For every plot the Pearson's correlation coefficient R as well as the coefficient of determination R^2 were determined. The two coefficients help to a) establish whether a co-relationship or an association between the methods exists and to establish how strong this relationship is (R) and b) assess in how much the variance between the variables is accounted for by the relationship.

Table 2. Pearson's product-moment correlation coefficient R and coefficient of determination R^2 for the RMA regression of the methods PSAP/TOT and LAHM/TOT.

Correlation	R	R^2
PSAP/TOT	0.85	0.73
LAHM/TOT	0.39	0.16

The regression between the PSAP and TOT data shows the higher R value (0.8519) compared to the RMA model fitted to the LAHM and the TOT data (0.3940) (Table 2). Hence, the relationship between the measurement results of the

PSAP and the TOT method is much stronger than the relationship between the LAHM and TOT method. Computing the Pearson's correlation coefficient for each of the two PSAP datasets (PSAP L_1, PSAP L_2) derived from using the two transmittance coefficients (K_1 and K_2) to calculate the mass loadings, led to the same R and R^2 values, due to the constant ratio of the lower L_1 values to the higher L_2 values ($K_1 > K_2$), which is why only PSAP L_1 has been plotted but is meant to reflect the PSAP method as a whole. With a R^2 value of 0.7256, the RMA model can explain ~73% of the variability in the data that is found between the PSAP/TOT methods, while the percentage of the predictable variance in the LAHM/TOT data lies at only ~16%. The much better agreement between the measurements of the PSAP method and the TOT method with both empirical factors of K_1 and K_2 suggests, that despite the different underlying measurement principles of the optical light transmittance method (PSAP) and the thermal optical method of the TOT seems to arrive at rather similar results when measuring the same filters. The variability in the data which could not be explained by the model may derive from uncertainties in both methods. Regarding the TOT measurements, the high amount of OC on the filters led to a low transmission signal especially for the most enhanced FID 1 signal (carbon species at 100% signal). In the case FID 1 reported no value, FID 2 (carbon species at 25% signal) was recorded and used for calculations. Using FID 2 increased the uncertainty of the exact detection of the OC/EC split point however. Samples which were very dark after the measurements and thus showed only small changes in the laser signal before and after the analysis as well as low signals in general were UM01 A+B, UM01 C+D, and KR01 C+D. Uncertainties were expected to be higher because of the overloaded filters UM02 A+B, UM02 B+C, and KR01 A+B (pers. correspondence Ulla Wideqvist, 2018). The remaining filters were reported to have been lightly pink after the measurements, indicative of the presence of mineral dust on the filters, which could have affected both the transmittance as well as reflectance signal.

The weaker relationship between the LAHM results and the TOT measurements as well as a low R^2 value of ~16% could be based on the fact, that the measurements were carried out on two different filter types. LAHM values were obtained from measurements carried out on the 25 mm filters, which, in some cases, had a higher particle heterogeneity on the filter (dark rims with high particle loading compared to rather light inner part of the filter with less particle loading) than the 50 mm filters did. As particles accumulated on certain parts of the filter, uncertainties might have been introduced by these overloaded spots on the respective filter. As the LAHM method is based on measuring the heat emitted consecutive to the absorption of light by the particles on the filter, a thick layer of particles hinders some of the CP in the lower layers to absorb light, which are subsequently not reflected in the results. To correct for the overloading, the LAHM results were multiplied by an empirical

correction factor based on measurements from snowpacks in the Cordillera Blanca in Peru, which was estimated to carry the possibility to be off by a factor of two as applied to the Alaska filters (pers. correspondence Carl Schmitt, 2019). The high particle loading on the filters of the AK50 dataset measured with the TOT decreased the method's accuracy as well (see above for increase in uncertainty due to overloaded filters, TOT). The filters produced with snow meltwater from Interior Alaska have in fact been so heavily overloaded, that an even smaller filter piece than the usual 1x1cm filter area had to be used in the instrument, which further increased uncertainties (pers. correspondence Ulla Schmitt, 2018). Moreover, as the LAHM method does not provide the actual mass on the filter but rather estimates the black carbon value for the respective sample (equivalent Black Carbon – eBC), the measurements can be strongly influenced by the mass absorption cross section (MAC) of the particles on the filter (Schmitt, 2019). The MAC is strongly related to the mixing state or coating of the CPs, as coating that build up on CP alter the ability of the CP in the core to absorb light and increase or decrease the absorption per mass of BC (Knox et al., 2009). Different types of CPs have been shown to exhibit different MACs and certain forms of mineral dust to have greatly lower mass absorption cross sections than certain soot particles (MAC dust: 0.01-0.5 times that of true black carbon) (Schmitt, 2019). The composition of particles on the filter may therefore alter the absorption and re-emittance of energy. The different MACs are usually accounted for by using corresponding calibration filters and including a reference to the calibration material. If the dust types between the filters are consistent, the relative quantities can be used to understand the relationship and quantities between the different locations. In this case however, samples were taken from many different locations with greatly varying environmental conditions, which may have affected the recording of eBC.

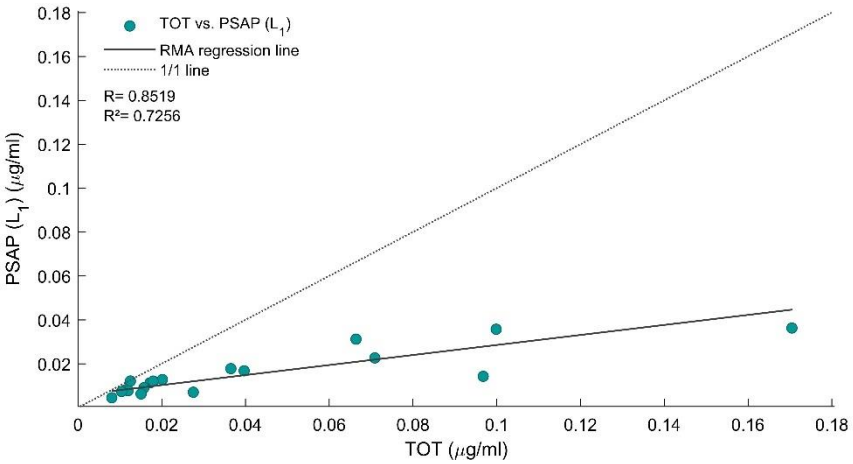

Figure 33. Reduced Major Axis regression fitted to the EC concentration as derived from the TOT method applied to the SW50 filter set and the BCe concentrations as derived from the PSAP (L_1) method applied to the SW50 filter set.

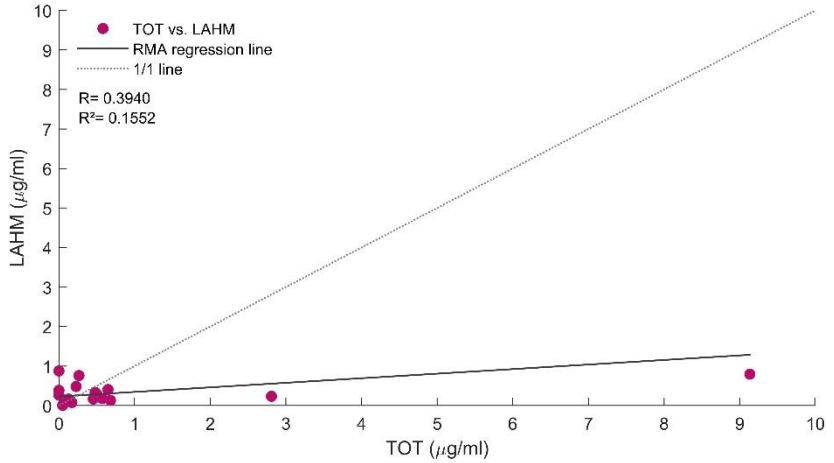

Figure 34. Reduced Major Axis regression fitted to the EC concentration as derived from the TOT method applied to the AK50 filter set and the eBC concentrations as derived from the LAHM method applied to the AK25 filter set.

6.1.2 Comparison of CP levels: Northern Sweden and Interior Alaska

As the TOT method was the only analytical technique applied to both 50 mm filter sets, Alaska (AK50) and Sweden (SW50), the results from the TOT measurements were chosen to compare the two regions. With different uncertainties attached to each of the three methods, choosing two sets of filters analysed by the same method helped to reduce errors to method specific uncertainties only. Several steps were necessary before a comparison of the carbon content of the snow in Northern

Sweden and the carbon content of snow in Interior Alaska was possible. Firstly, the TOT method reported results in µg/cm². To obtain the total mass of particles on the filters retained during the filtration, the loadings obtained from measuring the 1cm x 1cm pieces (some of the AK50 filter pieces had to be reduced in size due to the high CP load) of each filter had to be multiplied by the total area of the filters through which snow meltwater passed, which was that of a circle with a diameter of 34 mm. It was assumed that the particles are evenly distributed on the filter and that no losses occurred during filtration. The mean concentrations of the EC and OC particles in the snowpack were obtained by dividing the mass of particles on the respective filter by the total volume of snow meltwater that was filtered, which resulted in units of µg/ml.

As the environment of the sampling sites within and between the two regions differed strongly, three types of geographic settings were defined to compare and evaluate results from these regions. Due to the greater variability between the sites in Interior Alaska, the Swedish samples were used to define the three geographic groups (a similar approach was undertaken in the study by Zhang et al., 2008). Category 'remote' described sites that were surrounded by forest and with samples collected away from large roads or buildings. 'Rural' sites were not in towns, but close to roads and/or buildings, and 'suburban'/ 'urban' described sites that were on the outskirts of, or within, towns. Some of the Alaskan samples were excluded as they were not taken from natural snowpacks (e.g. from snow dumps, as in A15 JOH). The four samples for which this was the case are marked in italics in table 3. Moreover, some of the remaining Alaskan sites were challenging to assign to a certain category. The sampling in Alaska was rather designed to get as many different chemical signatures as possible instead of acquiring a broad range of samples for the three categories. Furthermore, due to logistical reasons, samples were mostly taken close to roads. Hence, the 'remote' sites in Alaska may still mirror some anthropogenic influence on the snow. An example was sample A12 DPR III. Snow from this pit was indeed taken from a pristine snowpack in the rather remote area of the Denali National Park. However, the newly cleared park road was only ~50 m away, which could have influenced the snow composition in late fall when park staff was still using the road and in the first week of spring after opening the road to the public after the winter closure. Applying the same parameters to assign samples from Alaska to the categories 'rural' and 'suburban' as in the Swedish case was challenging as well. A18 PF, for example, was taken in a rural or remote area, yet was classified as 'suburban' as the sample was taken ~80 m from a road and ~10 m from the facility of the rocket launch site. Table 3 summarizes the OC and EC concentrations measured in the Swedish and Alaskan snowpack samples, along with the type of setting for each sampling site. The last column specifies likely dominant emission sources of CP near each site (e.g. mines). The differentiation of the CP

results into OC and EC is informative for several reasons. Even though EC particles are the strongest light absorbers, OC particles together with dust also absorb both visible and near-infrared light, and therefore contribute to the snow darkening effect (Yasunari et al., 2015). Commonly TC is composed primarily of OC in comparison to EC (Fig. 35c). Additionally, the ratio of OC to EC is often indicative of the relative contribution of anthropogenic emissions to the CP content in a snowpack, as EC particles deposited in winter mainly derive from incompletely combusted fuels (e.g. oil, gas), the high OC/EC ratios of the Alaska samples suggests, that the Alaskan sites were subject to larger anthropogenic OC emissions than the Swedish sites (e.g. wood burning).

Table 3. OC and EC values for Swedish and Alaskan snow samples and their respective environmental setting and CP source categories.

SITE	SAMPLEID	OC (µg/ml)	EC (µg/ml)	SETTING	CP SOURCE
ABISKO	AB01 C+D	0.78	0.02	Remote	Other
ARVIDSJAUR	AR01 A+B	0.53	0.03	Rural	Roads
ARVIDSJAUR	AR01 C+D	0.71	0.04	Rural	Roads
GÄLLIVARE	GA01 A+B+C	0.48	0.03	Suburban	Mines
GÄLLIVARE	GA01 D+E	0.58	0.03	Suburban	Mines
JOKKMOKK	JK01 A+B	0.56	0.02	Rural	Other
JOKKMOKK	JK01 C+D	0.50	0.03	Rural	Other
KIRUNA	KR01 A+B	0.21	0.00	Suburban	Mines
KIRUNA	KR01 C+D	0.54	0.04	Suburban	Mines
LULEÅ	LU01 B+C	0.61	0.11	Suburban	Other
LULEÅ	LU01 D+E	0.91	0.19	Suburban	Other
LYCKSELE	LY01 A+B	1.21	0.05	Rural	Roads
LYCKSELE	LY01 C+D	0.87	0.05	Rural	Roads
PUOLTIKASVAARA	PU01 A+B	0.47	0.02	Rural	Roads
PUOLTIKASVAARA	PU01 C+D	0.31	0.02	Rural	Roads
SVARTBERGET	SV01 A+B	0.52	0.02	Remote	Other
SVARTBERGET	SV01 C+D	1.18	0.06	Remote	Other
UMEÅ	UM01 A+B	1.71	0.05	Suburban	Energy
UMEÅ	UM01 C+D	2.20	0.03	Suburban	Energy
UMEÅ	UM02 A+B	1.19	0.07	Suburban	Energy
UMEÅ	UM02 C+D	1.69	0.09	Suburban	Energy
ALASKA					
CLEARY SUMMIT	A1 CS	1.37	0.02	Rural	Mines
DARK HOLLOW DRIVE	A2 DHD	0.64	0.02	Rural	Mines
RAILROAD	A3 RR	15.26	0.07	Rural	Mines
HEALY SPUR ROAD	A4 HSR	5.41	~0.00	Rural	Energy
GEORGE PARKS HIGHWAY 0	A5 GPH 0	2.25	1.40	Suburban	Roads
GEORGE PARKS HIGHWAY IV	A8 GPH IV	0.76	0.13	Rural	Roads
DENALI PARK ROAD 0	A9 DPR 0	14.95	2.32	Suburban	Roads
DENALI PARK ROAD III	A12 DPR III	0.70	0.02	Remote	Roads
AIRPORT	*A13 AIR*	*72.11*	*~0.00*	*Suburban*	*Airports*
AIRPORT LAKE	A14 AIR_L	11.54	~0.00	Suburban	Airports
JOHANSEN EXPRESS ROAD	*A15 JOH*	*17.43*	*9.23*	*Suburban*	*Roads*
SKILAND	*A17 SKI*	*0.60*	*0.02*	*Rural*	*Other*
POKER FLAT	A18 PF	7.86	0.21	Suburban	Other
DOG KENNEL	A19 DK	33.04	0.24	Suburban	Other
DAVIDSON DITCH	*A20 DD*	*28.12*	*0.20*	*Rural*	*Other*
US CREEK RD	A21 USCR	2.69	0.06	Remote	Other
AIRPORT CENTRAL	A22 AIR_C	8.08	0.06	Remote	Airports
NOAA	A23 NOAA	17.14	~0.00	Rural	Mines

Table 4. Descriptive statistics (mean, range) of OC and EC concentrations (µg/ml) for the geographic categories 'remote', 'rural', 'suburban' of the two regions Alaska and Sweden.

		OC		EC	
	SETTING	**MEAN** (µg/ml)	**RANGE** (µg/ml)	**MEAN** (µg/ml)	**RANGE** (µg/ml)
ALASKA	Remote	3.83	0.70 - 8.08	0.0433	0.0159 - 0.0591
	Rural	12.14	0.64 - 33.04	0.0548	0.0002 - 0.2338
	Suburban	7.47	0.76 - 14.95	0.8125	0.0002 - 2.3219
	Airports	9.81	8.08 - 11.54	0.0296	0.0002 - 0.0591
	Energy	5.41	5.41 - 5.41	0.0002	0.0001 - 0.0002
	Mines	8.60	0.64 - 17.14	0.0236	0.0003 - 0.0699
	Other	14.53	2.69 - 33.04	0.1658	0.0550 - 0.2338
	Roads	4.66	0.70 - 14.95	0.9674	0.0159 - 2.3219
SWEDEN	Remote	0.81	0.78 - 0.85	0.0300	0.0202 - 0.0399
	Rural	0.64	0.39 - 1.04	0.0312	0.0198 - 0.0470
	Suburban	1.01	0.37 - 1.95	0.0624	0.0179 - 0.1489
	Airports	-	-	-	-
	Energy	1.70	1.44 - 1.95	0.0594	0.0387 - 0.0800
	Mines	0.45	0.37 - 0.53	0.0223	0.0179 - 0.0267
	Other	0.73	0.53 - 0.85	0.0588	0.0202 - 0.1489
	Roads	0.68	0.39 - 1.04	0.0328	0.0198 - 0.0470

The OC content differs substantially between the two northern regions. Many of the snowpack samples from Alaska exhibit much higher OC concentrations than their Swedish counterparts taken in comparable settings (Fig. 3a). Comparing the mean OC values of all three categories shows, that category 'rural' displays the greatest differences between Alaska and Sweden with a mean OC concentration of 12.14 µg/ml in Alaska compared to 0.64 µg/ml in Sweden. With mean OC values of 7.47 µg/ml (AK) and 0.81 µg/ml (SW), category 'suburban' displays the second greatest difference followed by category 'remote' with an OC concentration of 3.83 µg/ml for Alaska and 0.81 µg/ml for Sweden. The variability is much greater among the Alaska samples compared to the Swedish samples. For example, the OC contents of the rural sites in Alaska range between 33.04 µg/ml and 0.64 µg/ml compared to 1.04 µg/ml to 0.39 µg/ml at the rural sites in Sweden. The range in OC values also differs significantly between the two regions in the categories 'suburban' and to a lesser extent 'rural' (Table 4). Comparing the three categories of the Swedish samples shows that on average, the OC is highest in the samples taken in suburban/ urban regions of Northern Sweden and is lowest in the 'remote' sites. This does not hold true for the Alaska samples. The highest mean OC content is found in 'rural' regions, followed by samples taken in 'suburban' and 'remote' areas. An explanation for the high OC contents of certain samples in category 'rural' might lie in the habit of many Alaskans to use wood stoves as their main source of heat, releasing significant amounts of OC to the atmosphere (Simpson, 2019). A study by Fine et al. (2002) indeed showed that ambient atmospheric fine particle concentrations can contain up to 20 to 30% of particles derived from wood smoke alone. Locally and under the influence of certain climatic conditions such as strong

temperature inversions as is the case in Fairbanks for example, wood smoke has been found to contribute the majority of the atmospheric PM2.5 burden (Simpson, 2019; Fine et al., 2002). An example of very high OC levels (33.04 µg/ml) is site A19 DK. The snowpack was located close to a dog kennel in a rural area about an hour from Fairbanks and the only house on the large property is mainly heated with a wood stove.

Figure 35b displays the EC content of both northern regions sorted according to the three geographic categories. It is evident that the overall EC content is about two orders of magnitude lower than the OC content for both regions. Additionally, compared to filters from the category 'suburban' in Alaska, which exhibits a great range of values (0.0002 µg/ml - 2.3219 µg/ml), the variance of EC in other categories in both regions is relatively small (see Table 4). In both regions, Alaska and Sweden, the concentration of EC in the snowpacks is lowest in remote sites and highest in the suburban areas. Interestingly, the EC content of snow in remote sites in Alaska (0.06 µg/ml) is on average higher than the EC content of snow in remote sites in Sweden (0.03 µg/ml). Due to the limited number of samples, this difference might however not be significant. Sample pairs A5 GPH 0 – A8 GPH IV and A9 DPR 0 – A12 DPR III from Alaska are worthy of additional discussion. Both sample pairs have been taken on a perpendicular transect from roads with A5 and A9 having been taken directly adjacent to the respective street, whereas A8 and A12 were taken ~50 m from the respective first sample location. A sharp decline in EC levels between the samples A5 (adjacent to road) and A8 (~50 m distant) (1.40 µg/ml – 0.13 µg/ml) and between samples A9 (adjacent to road) and A12 (~50 m distant) (2.32 µg/ml – 0.02 µg/ml) is apparent. The low levels of EC found only ~50 m from the roads suggest, that the effect of traffic on roads is mostly local in character. The magnitude of decline in EC between A9 and A12 taken along the Denali Park Road is slightly greater than the observed decline in EC between A5 and A9. This could be an indicator for the more 'pristine' conditions in Denali Park snow as opposed to the snowpack conditions found alongside George Parks Highway. The high EC values of snow sampled in close proximity to roads and the low EC concentration levels in samples more distant from roads are mirrored in the high variance of points in category 'roads' in Fig. 36b.

A factor which may have led to the greater range of OC and EC values of the Alaska sites in comparison to those of the Swedish samples might have been that two samples were taken per snowpit in Northern Sweden, whereas replicates were not collected for the snowpits in Alaska. Comparing the two values from each site (e.g. Luleå) shows, that the OC and EC levels within the snowpits vary in some cases substantially from each other. A study by Forsström et al. (2013) had shown, that the 'meter-scale variability' in the snowpack can be of the order of ±30 % of the average concentration of EC. Hence, averaging the concentrations of both

samples from one pit as done for the Swedish samples, could thus have levelled-out and masked the uncertainties attached to taking only one sample per site as was not done for the Alaska samples.

Also noteworthy is the fact, that despite the different environmental conditions between the sites in the category 'rural', the range of EC values is relatively low, indicating that the strength of anthropogenic influence is still quite similar. The higher EC content in the rural regions of Alaska might derive from fugitive dust emitted by the two mines, the Usibelli coal mine and the Fort Knox gold mine, as four of the samples in this category were in the proximity of those mines. Another possible cause of higher EC values in rural areas of Interior Alaska as compared to Northern Sweden (Fig. 4b) may be the common practice of having a dual heating system, combining solid fuel burning devices such as coal burners and wood stoves with fuel oil-based heaters (Simpson, 2019; FNSB/APCC, 2016; FNSB, 2014; Wilson, 2014). Especially during the very cold spells in the Interior of Alaska, oil heaters are used to balance the temperature swings of wood stoves and to maintain a stable temperature especially at night, to keep houses/ cabins from freezing (pers. experience).

As figure 35c shows, the ratio of EC to OC is greatest in the 'suburban' samples of Alaska and derives from the high EC content of the road samples. Figures 35d and figure 36d visualize the log-transformed OC/EC values of table 5 sorted according to the two groups of categories. Very high ratios were computed for two samples, A23 NOAA ('mines') and A4 HSR ('energy') in Alaska 'rural', and sample A14 AIR_L ('airports') in 'suburban'. In these cases, the OC content was extremely high in comparison to the EC content leading to high OC/EC ratios. Generally, OC/EC ratios are higher for the Alaska than the Sweden snow samples, reflecting the overall higher OC values in the Alaska region.

Table 5. OC/EC ratios for Interior Alaska and Northern Sweden.

REGION	SAMPLEID	OC/EC	REGION	SAMPLEID	OC/EC
ALASKA	A1 CS	68.79	SWEDEN	AB01	38.56
	A2 DHD	146.81		AR01	19.42
	A3 RR	218.19		GA01	19.80
	A4 HSR	31298.71		JK01	20.19
	A5 GPH 0	1.60		KR01	20.80
	A8 GPH IV	5.78		LU01	5.08
	A9 DPR0	6.44		LY01	22.12
	A12 DPR III	44.39		PU01	19.82
	A13 AIR	47840.45		SV01	21.22
	A14 AIR_L	56638.90		UM01	50.39
	A15 JOH	*1.89*		UM02	18.05
	A17 SKI	*38.18*			
	A18 PF	37.69			
	A19 DK	141.31			
	A20 DD	*143.85*			
	A21 USCR	48.97			
	A22 AIR_C	136.86			

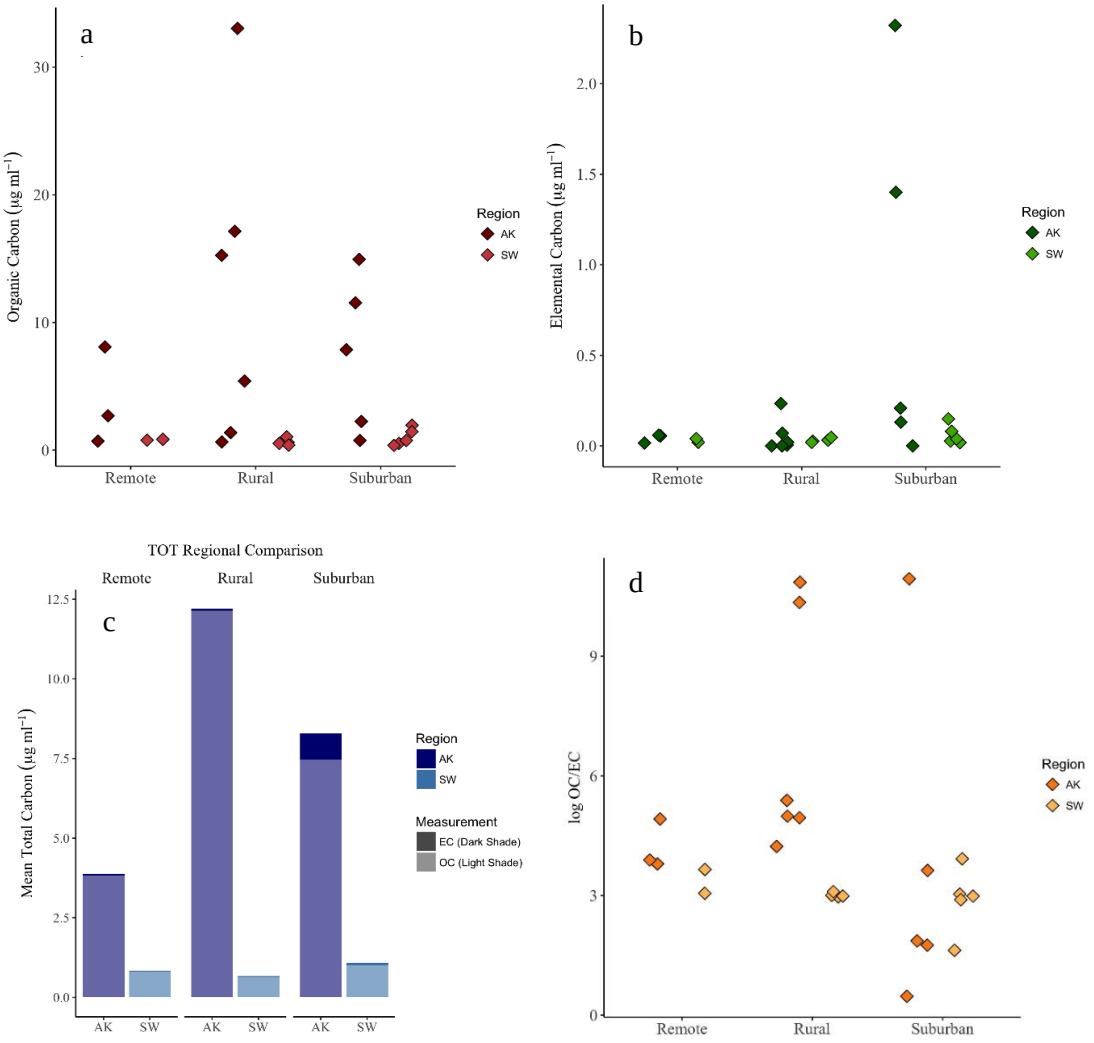

Figure 35. OC (a), EC (b), TC (c), mean TC concentrations and OC/EC ratios of Interior Alaska and Northern Sweden snow samples sorted according to geographic setting categories ‘remote, ‘rural, ‘suburban’.

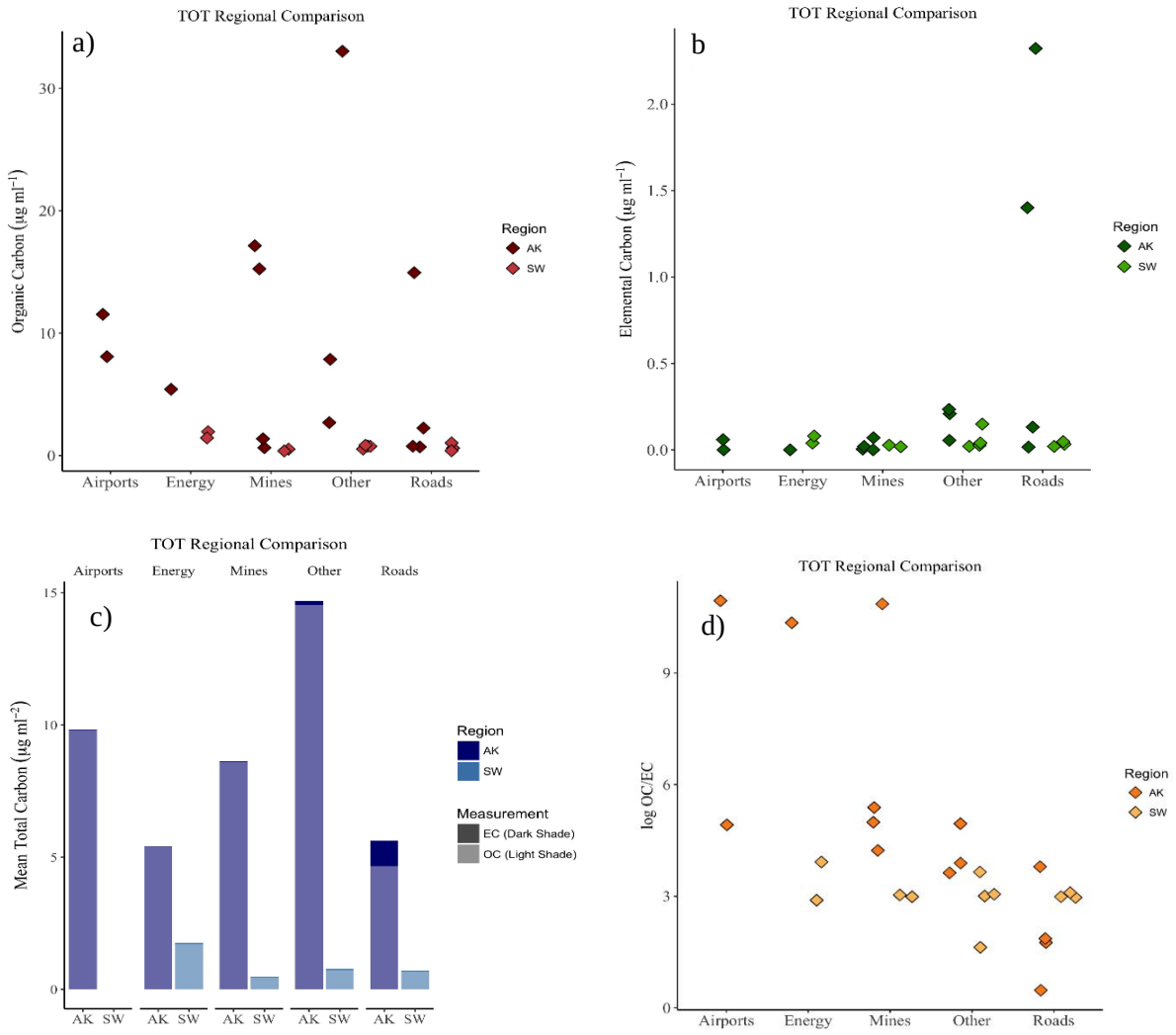

Figure 36. OC (a), EC (b), TC (c), mean TC concentrations and OC/EC ratios of Interior Alaska and Northern Sweden snow samples sorted according to the dominant CP source of emission into categories 'airports', 'energy, 'mines', 'other', 'roads'.

6.1.3 CP in N. Sweden and I. Alaska within the Arctic/subarctic context

Due to growing concerns about the effects of CP on the surface radiation balance in the polar regions, monitoring of CP levels in snow increased significantly since the mid-80s' first large field campaign in the Arctic (see section 2.4). The compilation of data from several field measurements showed that the levels of CP in spring (samples were taken in summer on the Arctic Ocean) in the northern regions are

subject to significant spatial variation. To evaluate how the CP levels in the remote regions of Northern Sweden and Interior Alaska compare to concentrations in other high-latitude sites, the following section will compare the two regions which were the subject of this study to previous published data and corresponding trends and patterns of CP levels in snow in Arctic and subarctic regions.

Table 6. EC concentrations of 'remote' Alaska and Sweden samples as well as mean EC concentration of both regions.

REMOTE	SAMPLEID	EC (ng/g)	MEAN (ng/g)	LATITUDE
ALASKA	A12 DPR III	16		63°42'N
	A21 USCR	55		65°17'N
	A22 AIR_C	59	μ = 43	65°34'N
SWEDEN	AB01 C+D	20		68.22'N
	SV01 A+B	22		64.15'N
	SV01 C+D	57	μ = 33	64.15'N

The mean EC result obtained from remote sampling sites in Interior Alaska for this study of 43 ng/g (based on TOT analysis) is much higher than the mean BC concentration of 7.9 ng/g computed for the samples taken in the Canadian and Alaskan Arctic as presented in the study by Dou and Xiao (2016) (see 2.4) (Fig. 37).

Comparing it to Dou and Xiao's (2016) findings of higher BC levels in lower latitudes (Fig. 7b, 2.4) suggests however, that the values obtained from Interior Alaska (63°42' – 65°34'N) could be higher than the mean concentrations of the cluster 'Canadian and Alaskan Arctic' at higher latitudes (66°10'N – 76°38'N). In this regard, Doherty et al. (2010) provide another dataset derived from snow samples collected on a snowmachine traverse of the Canadian and Alaskan Sub-Arctic by Sturm et al. in 2008 (63°36'N – 67°34'N), which covers the latitudes the remote samples in Interior Alaska were taken at. The mean *estimated* BC value for all subsurface samples collected on this field campaign is 12.5 ng/g. (*Estimated* BC in the paper by Sturm et al. (2008) was defined as the "estimated true mass of black carbon per mass of snow, derived by separating the spectrally-resolved total light absorption into BC and non-BC fractions" (Doherty et al., 2010, p.11651). Even though the mean EC value is still higher than the mean est.BC value of that snowmachine traverse, a look at the individual values shows, that the EC concentration of 16 ng/g taken at sample site A12 in Denali National Park is right around the 16 ng/g est.BC measured at a location at 63°45' during the traverse and is almost 50% lower than the 31 ng/g collected at a site at 63°36'N. As only three samples per region were identified as 'remote' these results might not be representative but especially sample

A12 shows, that the BC content might correlate to the BC content of snow samples at these latitudes derived from earlier sampling. Especially sample A22 taken at the small airstrip in Central may have experienced some slight anthropogenic influence which might explain the higher EC value which is closer to the mean BC values of 33.7 ng/g in Western Russia. Despite these findings, a comparison of values derived from measurements with different instruments should be regarded with caution as each instrument inhibits its own uncertainties and bases its measurements on different concepts.

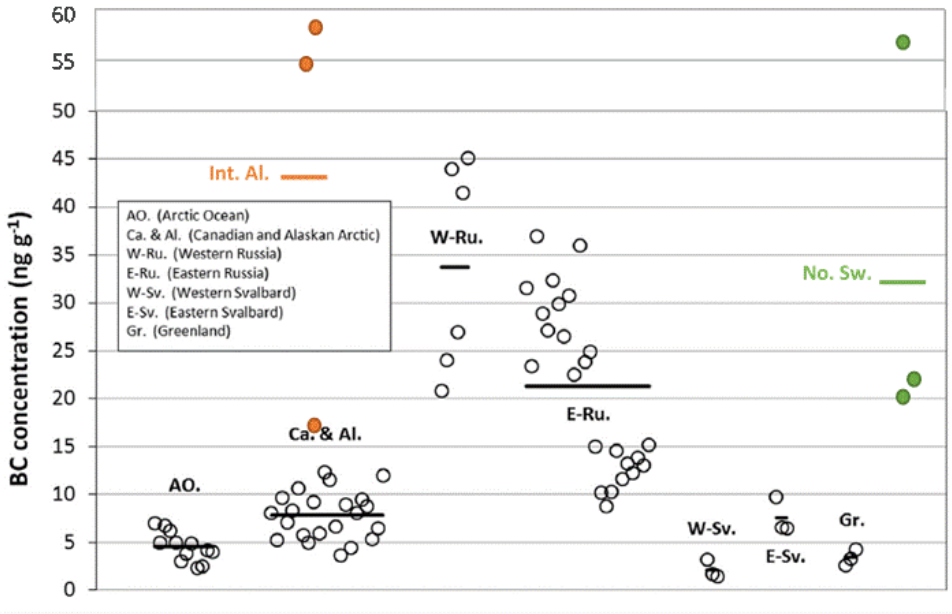

Figure 37. Black circles: the BC concentrations over the Arctic Ocean, Western Russia, Eastern Russia, Western Svalbard, Eastern Svalbard and Greenland as derived from Dou & Xiao, 2016. The horizontal line indicates the mean value of each cluster. The data is based on filter-based absorption photometry. This snow samples of this dataset are the same as the ones shown in Fig. 7/ 2.4 (derived from Dou & Xiao, 2016). Added to the figure are the EC (TOT) values of Interior Alaska (orange) and Northern Sweden (green) as derived from this work, with corresponding mean values indicated by a horizontal line.

The mean EC value of 33 ng/g for samples taken in remote sites in Northern Sweden for this study with 33 ng/g corresponds well with the median EC concentration from Abisko as described in Forsström et al. (2013) (see 2.4) (Fig. 37). As the snow samples of the latter study were measured with the same analytical technique, the TOT, and the same protocol as applied to the Alaskan and Swedish samples collected for this study a comparison of the respective values is feasible. Yet, with only three samples as reference, two of which were taken in the same snowpit, the significance of this finding has only limited significance. What is apparent however, is the great variability of EC concentrations at the sites (42.9 ng/g – 14 ng/g:

Tarfala; 51.4 ng/g – 32.2 ng/g: Abisko). This is in line with the findings outlined in Doherty et al. (2010), that concentrations were more variable in the European Arctic than in the Alaskan/Canadian Arctic, likely caused by the closer proximity to emission sources. The two significantly different EC values in the same snowpit in Svartberget indicate, that a much larger sample size would be necessary to give a comprehensive picture of how the samples taken for this study rank according to data from previous studies.

6.2 Analysis of trace elements

The overarching aim of the second part of this work was to gain more insight into the chemical composition of the samples as well as to test

a) if the method of using filter samples for snow meltwater analyses proves to be reliable, and
b) if the handheld pXRF could be a valuable and economical tool to provide instantaneous results of the chemical composition of PM in the respective snow packs.

Until now, the pXRF instrument has mainly been used on bulk soil samples or hard rock in the field of soil sciences and geology (Lemière, 2018). A first application on filter materials showed successful results when testing for airborne lead on air filter samples (Harper et al. 2007). However, calibrating the pXRF for each analyte (i.e. element) was not possible in this study as in Harper et al. due to the lack of suitable reference materials. For this reason, the following sections will treat the concentrations reported by the instrument mainly as relative levels of trace elements (relative concentration pattern (RCP)). An exception is section 6.2.1, which uses the absolute values as approximate indicators for filter matrix background values.

6.2.1 Element concentration on blank and empty filters

This section presents the results of the analysis of both ‘empty’ and ‘blank’ filters. As mentioned above, the absolute values used for this analysis could not be validated by calibrating the instrument to reference materials of known composition. Hence, the levels of trace metals should be regarded in this light. Yet, a comparison of empty and blank filters to each other as well as the manufacturers information on typical levels of trace elements and the levels of the specific batch used for this analysis is insightful to evaluate whether the background values derived from the filter material is adequate for an analysis of snow meltwater samples.

The term ‘empty’ filter is used for the 50 mm filters which have been baked in a muffle furnace but not treated with distilled (DI) water. The term ‘blank’ filter is used for the 50 mm filters which have been both baked and treated with DI water, as well as the 25 mm filters which have not been baked but treated with DI water.

Ten *empty* 50 mm filters were analysed with the pXRF (empty0 – empty9). Filter ‘empty0’ was measured with calibration M only. Filters ‘empty1’ to ‘empty8’ were measured in the centre of the filter using the GeoExploration (E) calibration, while filter ‘empty9’ was measured in the upper third (E1, M1), the central third (E2, M2) and the lower third (E3, M3) of the filter with both calibrations (GeoExploration = E; GeoMining = M).

In addition, six blank filters were produced during the filtration of snow meltwater from Alaska; three for the 50 mm filters and three for the 25 mm filter. This was done by filtering DI water (50 mm: 1000ml; 25 mm: 100ml) before the filtration of snow meltwater, after 13 samples, and at the end of the filtration procedure. The DI water underwent the same procedure and was in contact with the same filtration set-up as the snow meltwater (zip-lock bag, beakers, mesh strainer, etc.). The three 50 mm Alaska ‘blanks’ were analysed by both the pXRF and the ICP-MS methods. The blank filters for the Swedish set were not available for pXRF analysis and only analysed by ICP-MS.

Two sets of data on the empty MK360 tissuquartz filters used in this analysis were provided by the manufacturer Munktell Ahlstrom: the mean contamination levels of this batch of filters (Batch No. 3167) (Munktell Ahlstrom Falun AB) (Fig. A.2) (ppm) and the list of the typical levels of trace elements in (mg/L) provided in the Munktell Ahlstrom product description catalogue (mg/L) (Fig. A.3).

Comparing the ICP-MS results from the blank filters to levels of empty filters provided by Munktell Ahlstrom to get an approximate idea of element levels before the snow meltwater filtration was not possible. To do so, it would have been necessary to normalize the absolute µg values by the weight of the contaminants on each individual filter. Obtaining the latter information was however not possible for two reasons. Firstly, the filters could not be weighed with an ultra-low readability scale, and secondly, the filters were not get weighed before using them for filtration. An attempt was made to weigh the contaminated filters with a Mettler Toledo AG245 analytical balance (readability of 0.1 mg / 0.01 mg) and subsequently to subtract the mean of ten empty filter halves. However, results showed that the empty filters varied greatly in weight (range: >13 mg), which led to less-contaminated filters (e.g., AB01 A+B) displaying negative values after subtraction of the average empty half-filter weight (82.29 mg) in some cases. The ideal procedure would have been to weigh each individual filter at a certain temperature and humidity before and after filtration.

Instead, we compared the trace element levels between the batch of filters used for this analysis (batch 3167) and the typical levels given in the Munktell Ahlstrom product catalogue. The values from these two sources differed quite substantially. As appendix A.2 and A.3 and figure 38 show, Al (typical level: 25ppm; batch level: 240ppm/ not included in pXRF analysis), Fe (20ppm/26.2ppm), Mn (1ppm/1.46ppm), Na (10ppm/79.6ppm/ not included in pXRF analysis), and Ni (0.5ppm/1.94ppm) in particular, had higher levels than expected. This initial step of the analysis was a first indicator that the trace element levels of the batch of empty filters used for this work were relatively high.

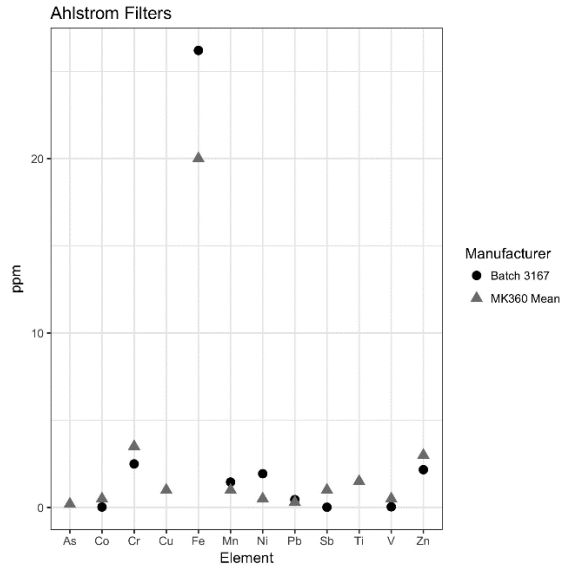

Figure 38. Mean contamination levels of filter batch No. 3167 (black points) (pers. communication, Hanna Olars, Munktell Ahlstrom Falun, 2019) and typical levels of trace elements of MK 360 filters provided by Munktell Ahlstrom product catalogue (Munktell Ahlstrom AB, N.d.) (grey triangles).

Figure 39 shows the pXRF measurement of empty filter (‘empty9’). Comparing these to the trace element levels of the filter batch (B) (Fig. 38) shows that reported levels of many of the elements in filter ‘empty9’ are even higher than the batch levels of the empty filters as delivered from the manufacturer (Cu: E2:218 ppm/ B:<0.04 ppm; Fe: M1:734 ppm/ B:26.2 ppm; Mn: M2:7 ppm/B:1.4 6ppm; Pb: M1:12 ppm/ B:0.455 ppm; Zn: E1:27 ppm/B:2.17 ppm; highest values of each calibration). Ti was not included in the batch information, however the highest pXRF measurement on ‘empty9’(Ti=112 ppm) was much higher than the typical value given in the product catalogue (1.5 ppm). The remaining nine filters show a very similar pattern with very high Fe, Ti, and Cu levels as well as elevated Ni, Pb and Zn levels (Fig. 40). Co and Cr were only elevated for some of the empty filters. A noticeable difference between measurements of the two calibrations was that Cu

values measured with the GeoMining calibration were ~50% lower when compared with GeoExploration measurements, which was noticeable both on the 50 mm filters, as well as the 25 mm filters, as the mean values of both calibrations on both filter types shows (Fig. 41).

As outlined before, as the pXRF didn't undergo a calibration procedure required to work with absolute values, the above described ppm-levels should be regarded with care. However, the reason we chose to describe the exact levels as measured with the pXRF in both calibrations and to compare these to the values provided by Munktell and Ahlstrom is to give an understanding of the scale of diversion from the reported values. Hence, even though the pXRF values might not be accurate, the above description helps to understand the discrepancy of the levels of the levels of trace elements on empty filters as described by 1) the product catalogue from Munktell Ahlstrom, 2) the levels provided by the manufacturer for the respective batch we worked with, and 3) an approximate value of the levels the pXRF is measuring. This comparison showed that the pXRF, with both calibrations, was detecting much higher values on the empty filters than we had initially expected.

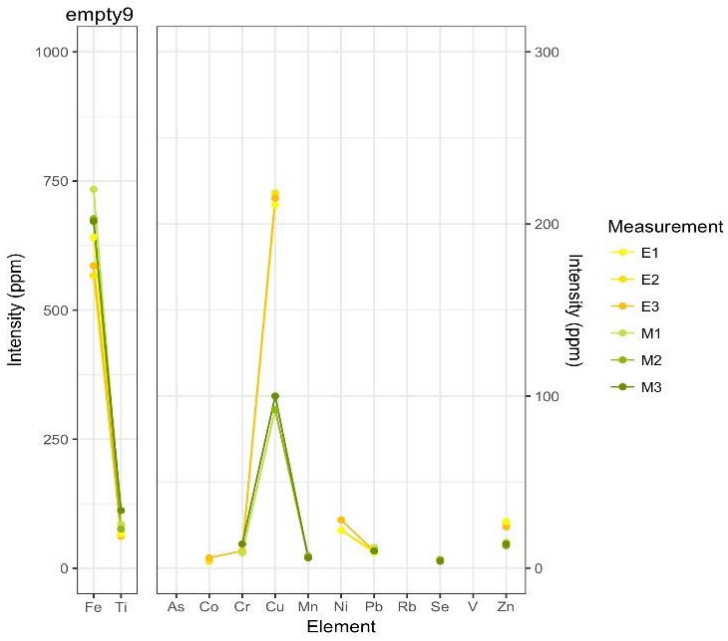

Figure 39. Measurements of empty filter #9. Yellow and orange colors (E) signify measurements with GeoExploration calibration, green shades (M) depict measurements with GeoMining calibration. Numbers 1-3 refer to measurements on the upper, middle, and lower third of the filter.

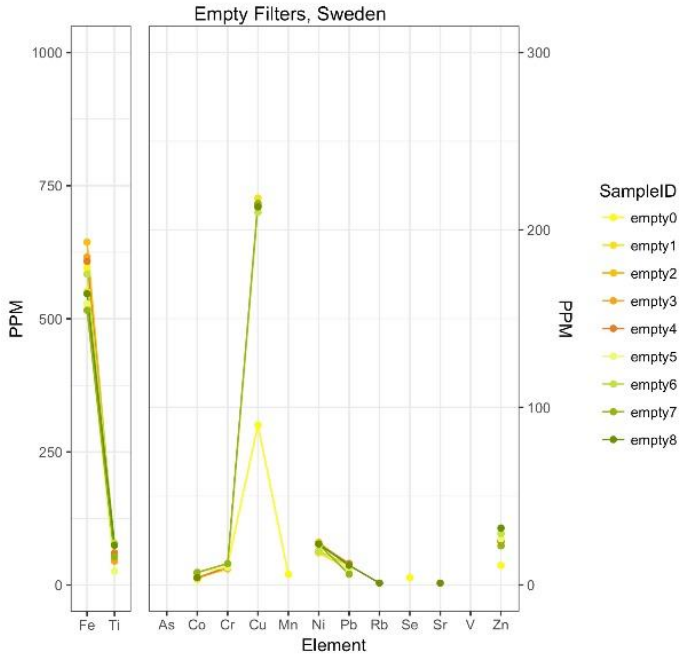

Figure 40. Measurements from nine empty filters measuring with calibration GeoExploration (yellow-red) or calibration GeoMining (green).

The empty filters were additionally compared to the six Alaska blanks (Fig. A4). The same pattern that dominated the empty filters was also clearly visible in these blanks, with particularly high Fe, Ti and Cu levels. The mean values of the two calibrations for both filter sizes showed slightly higher values for most analytes of the 25 mm blanks. The similarity of empty and blank filters suggested that the filtration procedure did lead to higher background trace metal values compared to the empty filters.

The high values of analytes on both empties and blanks remained puzzling. A possible source of contamination could have been the baking procedure of the 50 mm blanks, as the muffle oven showed potential signs of residues from previous usage. However, as the Alaska 25 mm blanks showed very similar ppm-levels for the same analytes and haven't been baked prior to filtration this explanation is rather unlikely. It is therefore assumed that the spikes in certain element are caused by the pXRF instrument itself. As no specific calibration was carried out before the filter analysis, possible disturbing effects such as interelement radiation (primary radiation has enough energy to also excite other atoms) or matrix effects (effect on fluorescent intensity: absorption or enhancement of radiation) could have altered the counts of specific analytes. A common symptom of interelement radiation is the secondary excitation of Cr, Fe, and Ni. Furthermore, as no further homogenization

of the contaminants on the filters were carried out, surface effects or particle-size effects may have affected the element levels as well.

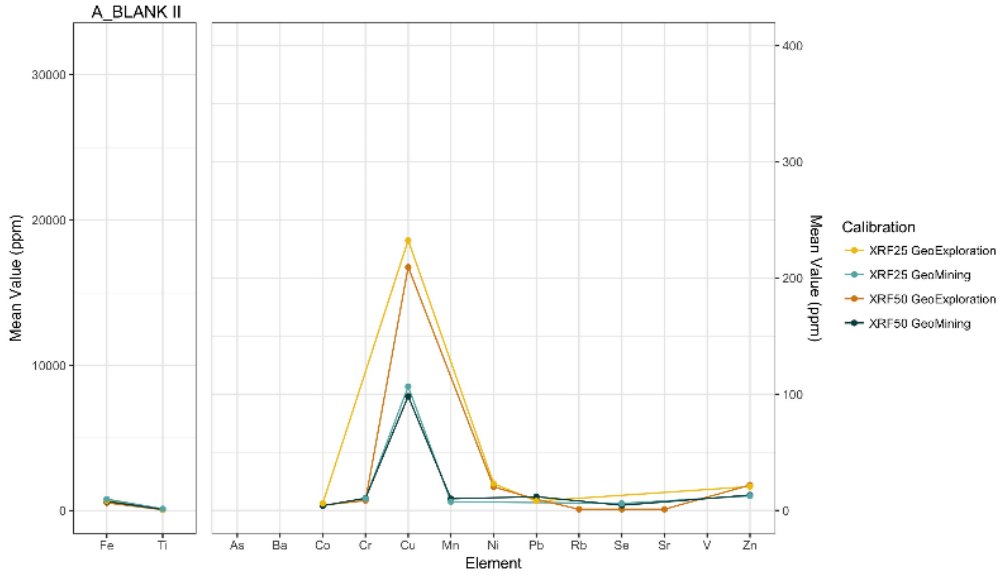

Figure 41. pXRF results from blank II of both filter sizes (25mm, 50 mm) as produced during the filtration of the Alaska snow samples. XRFGeoExploration(orange) describes the measurement of the 25mm tissuquartz filter using GeoExploration calibration. XRF50 GeoExploration (dark orange) describes the pXRF measurement of the blank II filter with 50 mm diameter using calibration GeoExploration. XRF25 GeoMIning (light blue) and XRF50 GeoMining (dark blue) followed the same procedure however using calibration GeoMining.

When necessary for the analysis, empty and blank filter mean values were subtracted from all 'loaded' filters (filters filtered with snow meltwater) to realise a semi-quantitative evaluation. In most cases however, the analysis was based on relative concentration patterns (RCPs), the 'highs' and 'troughs' of the element pattern (lines connecting the values of the elements) of the respective samples. Comparing the patterns of relative concentrations of the samples allows for analysis despite uncertainties in the calibration and without a comparison with independently-determined measurements such as the ICP-MS.

6.2.2 Coefficient of variation analysis of pXRF measurements

To determine the consistency and precision of the pXRF measurements of trace elements in the filtered snow, coefficients of variation (CV), also called relative standard deviation (RSD), were computed for each of the filters. The CV, the ratio of the standard deviation (SD) to the mean (formula (2)), is a measure of relative variability. The lower the CV for a set of measurements on a filter, the less variable or

dispersed were the respective measurements. The CV ranges between 0 and 1 but can also be express as a percentage.

$$CV = \frac{\sigma}{\bar{x}} \quad (2)$$

where

$$\sigma = standard\ deviation, \qquad \bar{x} = sample\ mean$$

The pXRF measurements can be grouped in different 'sets', defined by the region (AK, SW), the filter size (25 mm, 50 mm), and, in case of the Swedish filters, whether each of the filter-halves from one snowpit were analysed separately (SW S), or combined (SW D) as described in 5.3. Each of these 'sets' has additionally been analysed using both calibrations, GeoExploration (E) and GeoMining (M). The results for all sets may be found in appendix table A.1-A.9: empty (EME, EMM) and blank filters (BLE, BLM), AK25, AK50, SW50S, SW50D, and SW50SM. SW50S describes the CV values obtained for the three measurements on each individual half-filter. The CVs of SW50SM were calculated from the six measurements of both filter halves from the same snowpit. SW50D is based on measuring the two corresponding filters from one location arranged on top of each other on the pXRF spectrometer.

Figure 42 and figure A.5 display the CVs of every set, ordered by filter set (Fig. 42) and element (Fig. A.5). The mean of all CVs was computed to be 0.16 (≙16%), including outliers. The CVs of ~96% of all 1765 analyte counts lie below 0.5 (≙ 50%), ~73% are lower than 0.2, and ~46% lie below the 0.1 line, indicating a relatively high precision of measurements on a filter for both calibrations. The highest levels of variation are exhibited by the Alaska sets of both filter sizes and calibrations with a mean of all AK sets of 0.196, compared to a mean of the SW sets of 0.136 (Fig. 42). Since the AK sets of filters were generally carrying a much higher load of contaminants than the SW sets (based on visual analysis), the higher frequency of outliers (esp. for AK50) and higher CV values may result from measurement errors due to high particle loadings. Comparing the average CV values for both AK sets however shows, that the smaller 25 mm filters exhibit much higher CV values for both calibrations: AK25E (GeoExploration): 0.242, AK25M (GeoMining): 0.238, AK50E: 0.136, AK50M: 0.170. The higher variability of the small AK filters may have been the result of the handheld syringe method of filtration. The contaminated 25 mm filters displayed clearly visible darker outer rims on the filter, where material had accumulated in higher amounts as compared to the centre of the filters, while the 50 mm filters looked homogenous. A comparison of the Swedish filter sets' mean CV values for SW50SME and SW50SMM to SW50DE and

SW50DM shows that the variation is higher for the sets in which the measurements from both filters of one snowpit were averaged, SW50SME (0.164) and SW50SMM (0.136) (e.g. AB01A+B and AB01C+D) as compared to 0.142 and 0.131 for SW50DE and SW50DM respectively. As the number of missing values due to LODs is similar in both sets, future measurements might profit from carrying the measurements out using two or more filters at once.

Varying trends between the different analytes are clearly distinguishable in figure A.5. The mean CV values of analytes for each of the different filter sets and calibrations, as well as the averaged value of each element across all filter sets are presented in table 7. Cu exhibits the lowest average CV value (0.058) followed by Zn (0.109), Fe, Pb and Se (0.129, 0.128, 0.133), Ni (0.157), V (0.169), Cr (0.177) and Ti (0.180), Sr (0.186) and Mn (0.190). Analytes with CV values ranging between 0.2 and 0.25 are As, Ba, and Rb. The selection of analytes exhibiting the lowest CVs is worthy of note. Cu, Zn, Fe, Pb, Se and Ni were elements consistently picked up on the empty filters as well as the blanks. Cu displayed one of the most dominant 'spikes' in this regard, with the same ppm intensity counts appearing in all of the blanks and empty filters. This consistency of Cu in particular is mirrored in the very low CV value of 0.01 to 0.07 for the empty and blank filters. With an average CV of 0.084, blanks measured with calibration E are most precise compared to empty filters (EME: 0.123, EMM: 0.133) and blanks measured with calibration M (BLM:0.116) (small sample size n = 4).

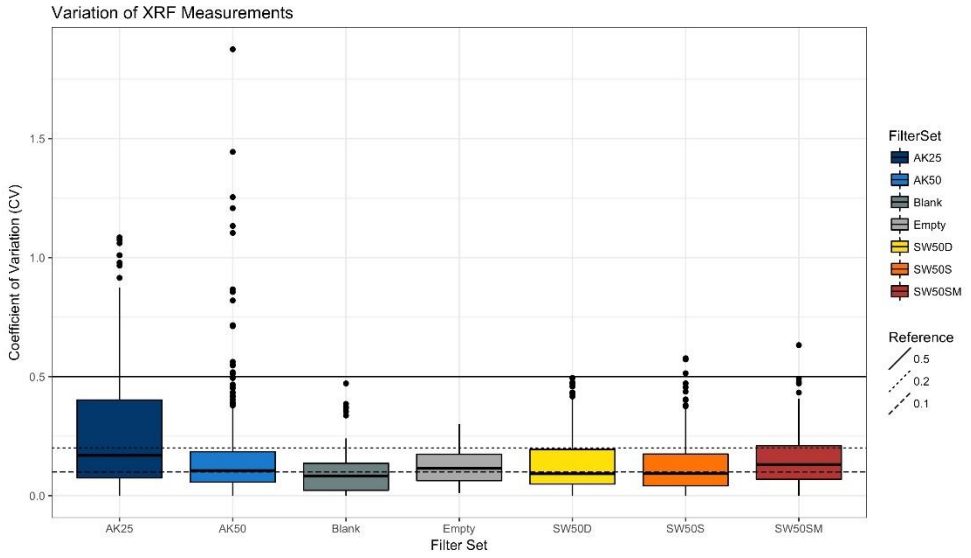

Figure 42. Box-and-Whisker plots of CVs of the different sets of filters; lower and upper end of plots: 25th percentile/ 75th percentile; thick black line: median; black dots: outliers. The number of measurements on each filter varied depending on filter type and set (see 5.3).

Table 7. Presented are the mean CV values of the pXRF measurements sorted according to analyte for each of the different filter sets and calibrations, as well as the averaged value of each element across all filter sets

SET	CAL.	As	Ba	Co	Cr	Cu	Fe	Mn	Ni	Pb	Rb	Se	Sr	Ti	V	Zn	Mean
AK25	E	0.23	0.18	0.36	0.23	0.11	0.25	0.35	0.19	0.17	0.37	0.24	0.44	0.23	0.13	0.20	0.24
AK25	M	0.31	-	0.10	0.19	0.10	0.21	0.24	-	-	0.38	0.13	0.44	0.23	0.06	0.22	0.22
AK50	E	0.19	0.19	0.29	0.13	0.06	0.09	0.15	0.16	0.14	0.15	0.17	0.12	0.09	0.14	0.10	0.14
AK50	M	0.29	0.30	0.28	0.22	0.09	0.09	0.12	0.09	0.17	0.21	0.20	0.24	0.11	-	0.09	0.18
SW50S	E	0.17	-	0.13	0.19	0.03	0.10	0.21	0.17	0.10	0.21	0.00	0.11	0.21	0.07	0.08	0.13
SW50S	M	0.18	-	0.25	0.18	0.06	0.08	0.16	-	0.09	0.16	0.13	0.07	0.15	0.26	0.07	0.14
SW50SM	E	0.15	-	0.16	0.17	0.03	0.19	0.28	0.19	0.14	0.27	0.10	0.17	0.25	0.11	0.10	0.16
SW50SM	M	0.19	-	0.31	0.17	0.07	0.12	0.18	-	0.11	0.18	0.13	0.07	0.19	0.30	0.09	0.16
SW50D	E	0.28	-	0.28	0.18	0.06	0.13	0.18	-	0.11	0.19	0.17	0.11	0.17	-	0.08	0.16
SW50D	M	0.26	-	0.22	0.14	0.03	0.13	0.16	0.15	0.09	0.25	0.10	0.10	0.15	0.26	0.06	0.15
EMPTY	E	-	-	0.28	0.10	0.01	0.07	-	0.13	0.13	-	-	-	0.17	-	0.09	0.12
EMPTY	M	-	-	-	0.22	0.05	0.08	0.08	-	0.16	-	0.13	-	0.21	-	0.13	0.13
BLANK	**E**	-	-	0.29	0.08	0.01	0.01	-	0.09	0.11	0.00	-	0.00	0.18	-	0.06	0.08
BLANK	**M**	-	-	0.28	0.11	0.04	0.03	0.15	-	0.13	-	0.11	0.14	0.19	0.06	0.07	0.12
MEAN		**0.23**	**0.22**	**0.24**	**0.18**	**0.06**	**0.13**	**0.19**	**0.16**	**0.13**	**0.24**	**0.13**	**0.19**	**0.18**	**0.17**	**0.11**	0.24

6.2.3 Effects of pXRF calibrations

The two inbuilt calibrations of the pXRF Tracer 5i 600-800 are GeoExploration (P/N: 730.0187) and GeoMining (P/N: 730.0203). A list of their respective LODs on pure SiO_2 based on 30s measurements with each of the three phases may be found in appendix Table A.10. Calibration GeoExploration (E) exhibits lower LODs for most of the 48 elements and oxides (Heek, 2018). Both calibrations were built on the assumption of a 'geomatrix' meaning, that the calibration curves were adjusted according to tests with bulk samples (pers. communication Tim Heek, Bruker representative, 2018). According to a Bruker representative, this could strongly affect the measurements of a thin material such as the tissuequartz filters used herein (ibid). Furthermore, as the filters are made of pure quartz (SiO_2), the raw data results displayed 100%-values for SiO_2 alongside the percentages of the other elements. According to Mr Heek, both, the thinness of the filters as well as the pure quartz material, led to these erroneous results. He advised to use the quantitative pXRF results with caution but indicated that, despite SiO_2, the remaining analytes may still be accurate and especially semi-quantitative data such as inter-element comparisons of high value (ibid). Moreover, a quantitative comparison to ICP-MS measurements, as planned at the beginning of this work, has not been possible (see 6.2.1). Hence, this section will outline the extent to which the different pXRF calibration settings affect the results but will lack the validation of absolute results of the mass spectrometry data.

The two mean CV values computed for E and M, based on all CV values for the respective calibration, are relatively low. They differ from each other only very slightly between 0.157 for GeoExploration and 0.161 for GeoMining, indicating slightly less variability when utilizing calibration E to analyse trace elements. The mean CV values for each sub-set of measurements of the two calibrations (e.g. AK25E) draws a more detailed picture (Table 7). Differences in the measurement variability of the E and M subsets are apparent. For the small Alaska filters (AK25), calibration M exhibits the lower CV value compared to E (M:0.177/E:0.244). This does however not hold true for the big Alaska filters (AK50). AK50E is less variable than AK50M (E:0.143/M:0.180). In the Swedish sets, the least variability is found in the GeoExploration single filter measurements SW50S (E:0.127/M:0.141), followed by the Swedish double-filter measurements, which exhibited a lower mean CV for M than for E (M:0.161/E:0.150). The averaged measurements of the two snowpit filters, SW50SM E and M (E:0.165/ M:0.163) are almost equal. Comparing the mean CVs of the two calibration-based sub-sets of the AK and SW measurements (e.g. AK25E compared to AK25M) showed, that a higher precision of measurements was not ultimately bound to one calibration but varied depending on the

set of filters. Hence, that determining the more precise and suitable calibration for the pXRF analysis from the mean CVs alone is challenging. It is therefore of value to examine and compare four related variables: 1) the CVs of all filters differentiated by the two calibrations and sorted according to the different analytes (Fig. 43), 2) the corresponding relative concentration pattern (RCP) based on all calibration runs sorted by analytes (AK50: E1-E5, M1-M5; AK25: E1-E2, M1-M2; SW50: E1-E3, M1-M5) (Fig. 44), 3) the individual measurements for each site (google drive [folder: Pinzner_6.2.3(1)]), and 4) the mean values of the two calibrations for each site (google drive [folder: Pinzner_6.2.3(2)]).

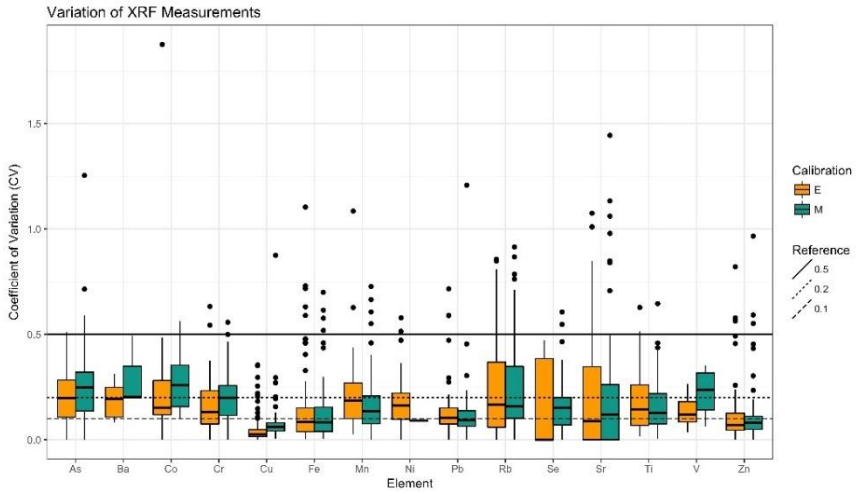

Figure 43. CVs of all filters differentiated by the two calibrations and sorted according to the different analytes. Excluded: high Mn values

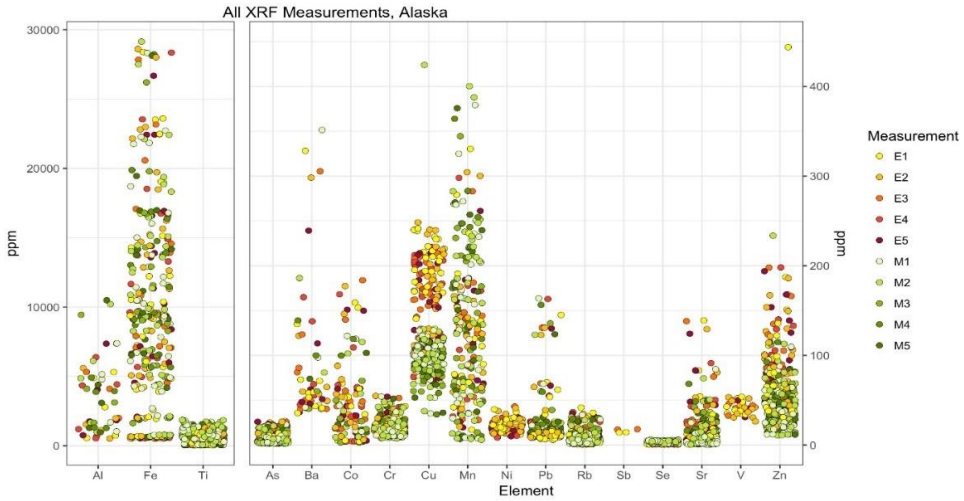

Figure 44. Levels of trace elements (ppm) of all filters of each calibration run sorted by analytes (AK50: E1-E5, M1-M5; AK25: E1-E2, M1-M2; SW50: E1-E3, M1-M5). Excluded: high Mn values)

The comparison of the box-and-whisker plots of the CV values of both calibrations for the different analytes (Fig. 43) showed that the variability between elements and between the calibrations differed in part substantially. Two elements which exhibited lower median CVs for E measurements were Ba and V (Fig. 43). Ni was almost exclusively detected by calibration E (Fig. 44). Another interesting analyte in terms of variation of the filter measurements is Cu. With a high number of measurement counts, most of which are below CVs of 0.2, a differentiation between the two calibrations is apparent, with CVs derived from calibration E generally being lower than CVs derived from calibration M. Lower median CV values of calibration E were further observed for analytes As, Ba, Co, Cr, Se, Sr, V, and Zn. Outliers of CV values occur in measurements of both calibrations. In this regard, the frequency of the occurrence of outliers seems to be more strongly dependent on the element rather than the calibration.

The generally higher detection counts observed for measurement runs in calibration E compared to calibration M may indicate an overall higher sensibility of the calibration E, corresponding to the lower LOD limits of GeoExploration. The trend of obtaining higher measurements with calibration E is more pronounced in the Alaska samples than the Sweden samples. It was not possible to analyse the accuracy of either calibration for the different analytes due to the lack of reference measurements from the ICP-MS. Taking a closer look on the different calibration runs further clarified that especially runs E1 and E2 as well as M1 and M2 seemed to produce higher ppm counts than the following runs (individual filter analysis). The stronger deviations of the first runs from the mean in both calibrations compared to subsequent runs could be related to a heterogeneity of the filter as the runs were always measured at the same point on the filter. It could however also indicate that the instruments measured differently in the first attempts than the following measurements. The level of concentration measured with the different calibrations and filters seemed to be dependent on the analyte. Cu and Zn for example, exhibited higher ppm-value for calibration E in most cases, while Mn displayed higher levels when measured with calibration M.

6.2.4 Geographic categorization – pXRF measurements

To evaluate, whether the pXRF detects differences in the relative abundance of trace metals which can be related to the conditions at each site, the same categorization of sites used in section 6.1.2 was applied to both datasets, Sweden and Alaska: remote, rural, suburban. Included in the Swedish dataset were the mean values of each site (SW50SM) and the measurements from dataset SW50D. The Alaska dataset consists of the data from both AK50 and AK25 filters. As the analysis is meant to compare the patterns of relative concentrations, the trace element levels without

subtracted empty values were used. Yet, the empty filter values were included in the plot to visualize their relationship and possible influence on the levels at the different sampling sites. Figure 45 shows the relative abundance of trace elements of the log-transformed values for better comparability.

Reflecting the findings from section 6.2.1, high levels of Cu, Ni and Se on the empty filters made any assumptions on above-background values of these analytes challenging. The same held true to a lesser extent for Ti, Pb and Zn. Despite these high background values, a pattern becomes apparent in response to forming the three categories: for many of the analytes (not analysed: Cu, Ni, and Se) category 'remote' displays the lowest or no ppm-values (pictured as lowest median value), followed by 'rural'-values, while category 'suburban' exhibits the highest levels of each analyte showing the highest median values expect for analytes As and Co and the highest absolute values over all (Fig. 45). The outliers in the category 'rural' may be due to unnaturally high signals of one or both of the two calibration measurements, which, as in the case of Fe in sample JK01 (GeoExploration: Fe > 30.000ppm) (Fig. 46) or PU01 (GeoExploration: Co >110ppm, Fe > 30.000ppm) may be erroneous (no Co data was found for the soil properties in the region for comparison). As many of the as 'suburban' classified sampling sites are close to one dominant contamination source such as a mine, a road or a power plant, related elements are expected to score high (such as Fe in the case of Kiruna). However, the remainder elements unrelated to the contamination source but still classified as 'suburban' possibly account for the lower values in the category 'suburban'. The relatively clear differentiation between categories follows the expected outcome of lower trace metal levels in snow at remote sites in Northern Sweden as compared to sites affected by anthropogenic activities or in proximity to human settlements. This suggests, that despite the high empty filter values for Cu, Ni, and Se, applying the pXRF method to filters from snow meltwater can at least give a qualitative oversight of the conditions of the sampling sites.

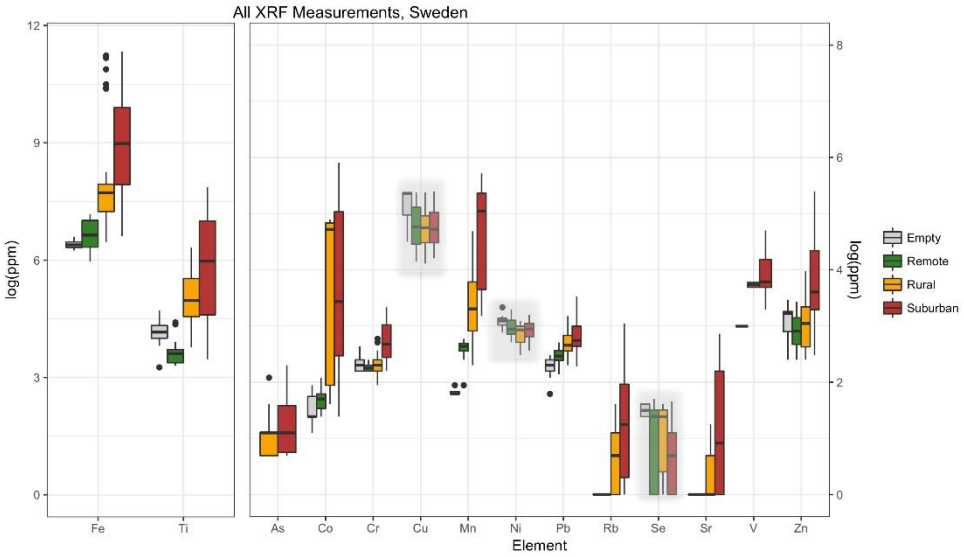

Figure 45. Relative abundance of the log-transformed trace element concentrations for Sweden based on datasets SW50SM and SW50D. Included are the results from empty blanks for comparison. The samples are appointed to the geographic groups 'remote', 'rural', 'suburban' and sorted according to the analytes measured by the pXRF.

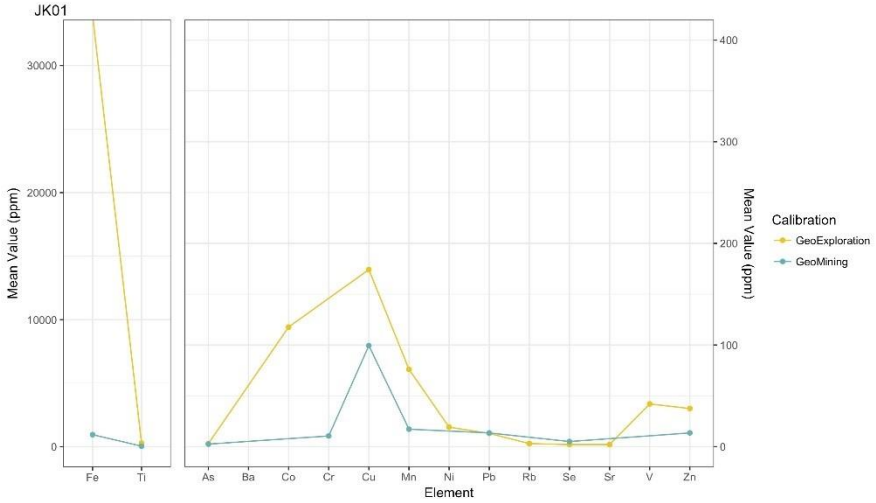

Figure 46. Mean trace element levels of calibrations GeoExploration and GeoMining for sample JK01.

The categorization of sampling sites from the logarithmically transformed Alaska datasets is displayed in figure 47. As was the case for the Swedish datasets, blank

values for Cu, Ni, Se were too high to draw reasonable conclusions from the data. Yet, in this dataset, trends for the clustering of the different categories could be detected as well. Generally, the remote sites register with the lowest values, but the log-values are generally higher than in the Swedish dataset corresponding to the overall higher analyte in the Alaska dataset. As in the Swedish case the lowest median values are related to category ‘remote’ followed by ‘rural’ and the highest median values are exhibited by category ‘suburban’. Exceptions are analytes Co and Pb, which display higher medians in category ‘remote’ compared to the remaining two categories. Higher median values in category ‘remote’ in the AK dataset in comparison to the SW geographic categories could be due to the challenges to definitively assign sampling sites to a certain category in Alaska. As mentioned in 5.1.2, due to logistical reasons snow sampling in Alaska was restricted to sites close to the road system and was mainly designed to obtain a wide range of chemical signatures rather than sampling for pristine sites which would have mirrored elemental background values. If the sampling design would have been different, even lower levels for the category ‘remote’ would have been expected. An example was sample A12 DPR III (Fig. 48). Snow from this pit was indeed taken from a pristine snowpack in the rather remote area of the Denali National Park. However, the newly cleared park road was only about 50 m away, which could have influenced the snow elemental composition in late fall when park staff was still using the road and in the first week of spring after opening the road to the public again after the winter closure. Nevertheless, the pXRF analysis tends to detect trends in trace metal concentrations according to the respective site conditions in the Alaska dataset as well.

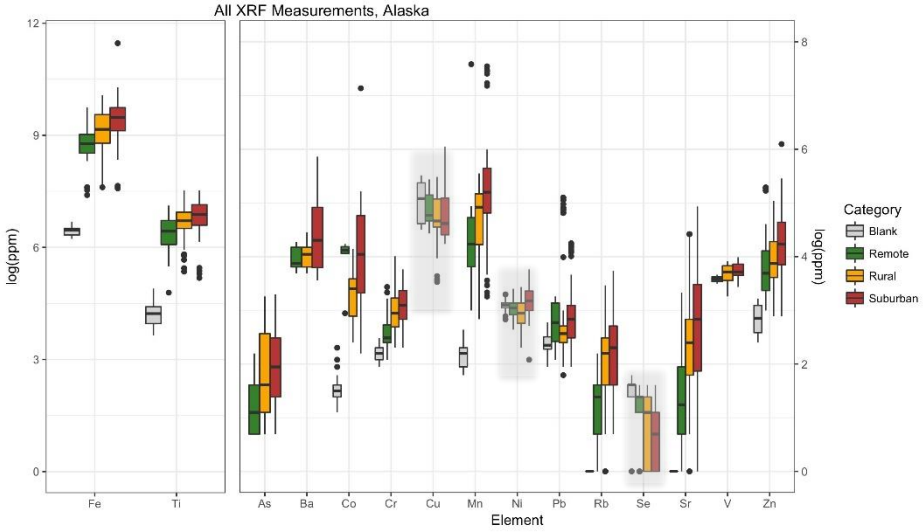

Figure 47. Relative abundance of the log-transformed trace element concentrations for Alaska based on datasets AK25 and AK50. Included are the results from blank filters for comparison. The samples are appointed to the geographic groups 'remote', 'rural', 'suburban' and sorted according to the analytes measured by the pXRF.

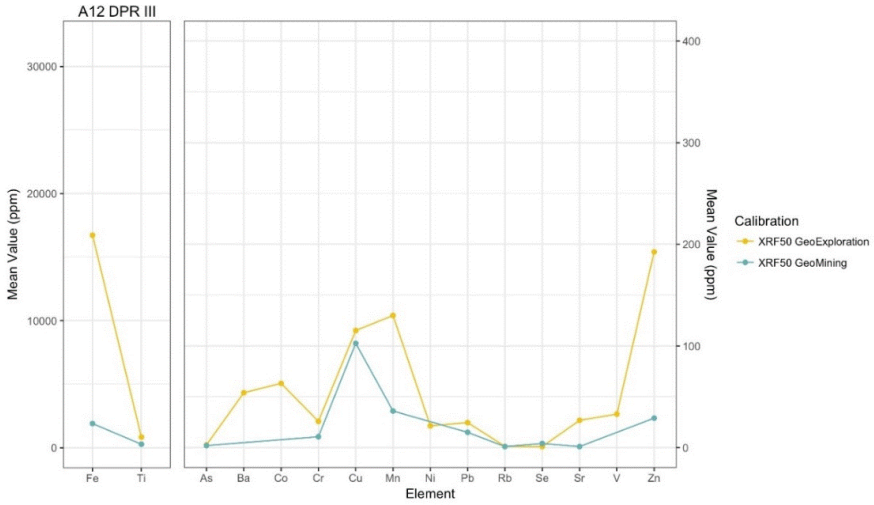

Figure 48. Mean trace element levels of calibrations GeoExploration and GeoMining for sample A12 DPR III.

6.2.5 Source and environmental categorization – pXRF

This section presents the results of the relative concentration patterns (RCPs) of the AK and SW samples organized into groups with similar chemical characteristics which can be related to the types of environments the samples were collected in. Analytes indicative of anthropogenic activities are inter alia: Cr, Mn, Se for coal

combustion, Ni and V for oil combustion, As, Cr, Cu, Mn, Pb and Zn for mining activities, Mn for airports, and As, Co, Cr, Cu, Ni, and Pb for traffic emissions.

Samples from SW50SM and SW50D, which were strongly influenced by a single source of contamination, were assigned to three different categories (Fig. 49, 50; Fig. A.6): 1) Energy: UM01, UM02; 2) Mines: GA01, KR01; 3) Roads: PU01, AR01, LY01. With the two samples from Umea group 1 – 'energy' describes sample locations in the proximity of power plants specifically. These samples have been separated from group 3 – 'roads', to see whether elemental composition differences could be detected between them. The three samples included in this group varied in their proximity to roads, but the aim was to test whether their signatures were similar. Group 2 – 'mines' encompasses the two open-pit Fe ore mines close to Kiruna and Gällivare. All other datapoints were grouped in the category 'other'.

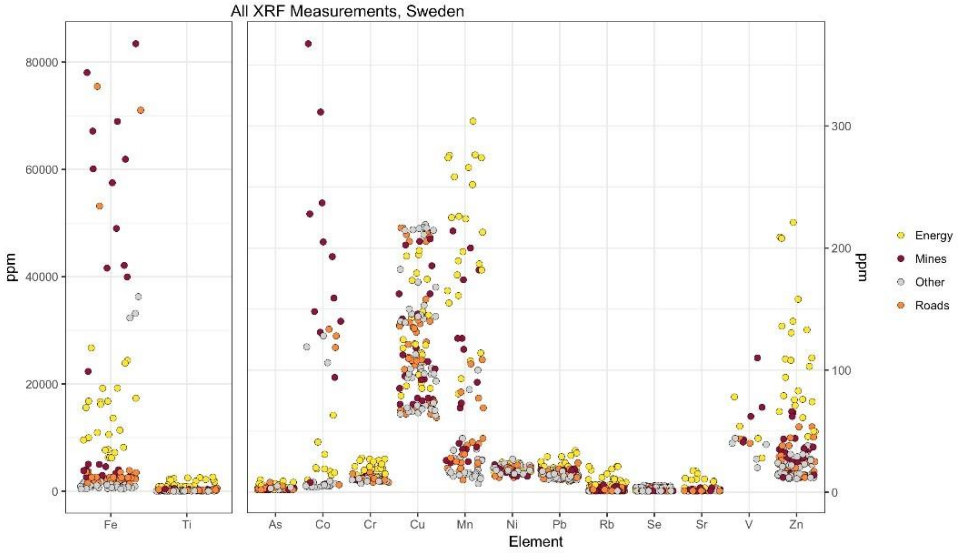

Figure 49. Relative abundance of trace elements for Sweden based on datasets SW50SM and SW50D. The samples are appointed to the source emission groups 'energy, 'mines, 'roads' and sorted according to the analytes measured by the pXRF.

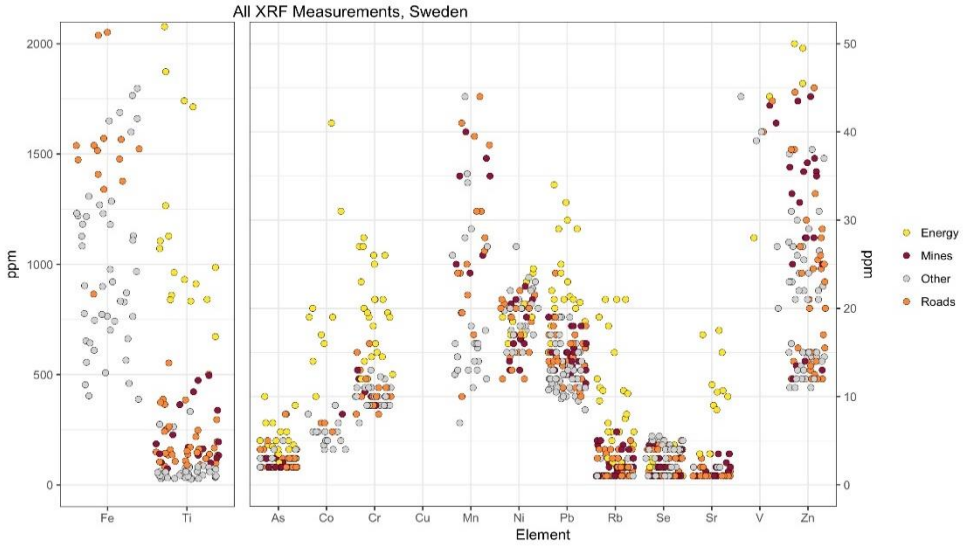

Figure 50. Close-up of figure 49 (see description above).

Figure 49 and A.6 show that the highest Fe levels can be found in snow collected close to the two Fe-ore mines, while the samples grouped in 'energy' exhibit lower Fe values in the range of ~5.000 ppm to 25.000 ppm. In addition, the two mine samples exhibited the highest Co levels of all samples (~150-360 ppm). The high Co levels may have derived from surrounding soil which has been exposed by the mining activities. Indeed, Sweden's largest undeveloped deposit of Co is located only ~48 km east of Kiruna and the Aitik copper mine ~30 km east of Gällivare. Furthermore, Zn levels ranging from ~20 ppm to ~100ppm for the category 'mining' could relate to the Zn levels in the top 50cm soils in the region around both Kiruna and Gällivare of approximately 60 ppm-70 ppm (Fig. 50) (Stendahl, 2019). The same could apply to the levels of Pb, which register at ~10 ppm to 20 ppm. The 50 cm of topsoil in the area are described to contain ~20 ppm (ibid). Worth of note is that category 'energy' exhibits higher ppm-values than category 'road' and 'mining' for Ti, As, Cr, Pb, Rb, and Zn. The combustion category is based on the two samples collected in Umeå in close to the Dåva biofuel power plant, which mainly runs on burning the sorted waste from the city as well as residues from the forest industry. To keep the burning temperature steady, ~700 to 800 m^3 of heating oil were being used (FORCE Technology, 2019). The elevated level of V could be an indicator for the combustion of oil but could also have been a by-product of the burning of waste. As the composition of the burned waste at the power plant is unknown, a source allocation is not possible. However, the high values for the respective elements well above the levels recorded on the empty filters suggests that the emissions of the

power plant increased trace metals in the surrounding snowpack. Category ‘road’ registered elements for the same elements as ‘energy but in lower concentrations (~2500 ppm/ ~150 ppm) except for two Fe values which exceed 7000 ppm. An additional source to emission through fuel combustion are elements eroded off car parts such as brake pads and tires, e.g. Ba, Cr, and Fe, which were detected in the samples. In sum, the pXRF measurements of selected filters from sites in Northern Sweden seemed to give insight into the environmental conditions they were sampled at. However, the interpretation of the possible sources for those elements which are only slightly above the empty filter values has to be understood as such. In those cases, uncertainty remains whether the trace metal levels are based on external environmental influence or rather artefacts in measurements or high loadings due to the filter matrix.

The categorization of the Alaska dataset (AK25 and AK50) had one additional group. In addition to ‘energy, ‘mines’, and ‘roads’, the category ‘airports’ was added as three of the samples contained snow from two airports. The categories contained the following samples: 1) Energy: A4 HSR; 2) Mines: A1 CS, A2 DHD, A3 RR, A23 NOAA; 3) Roads: AK5 GPH0, AK8 GPH IV, AK9 DPR 0, AK12 DPR III; 4) Airports: A13 AIR, AIR14 AIR_L, A22 AIR_C. Figures 51, 52 and A.7 show the clustering of analytes according to their groupings.

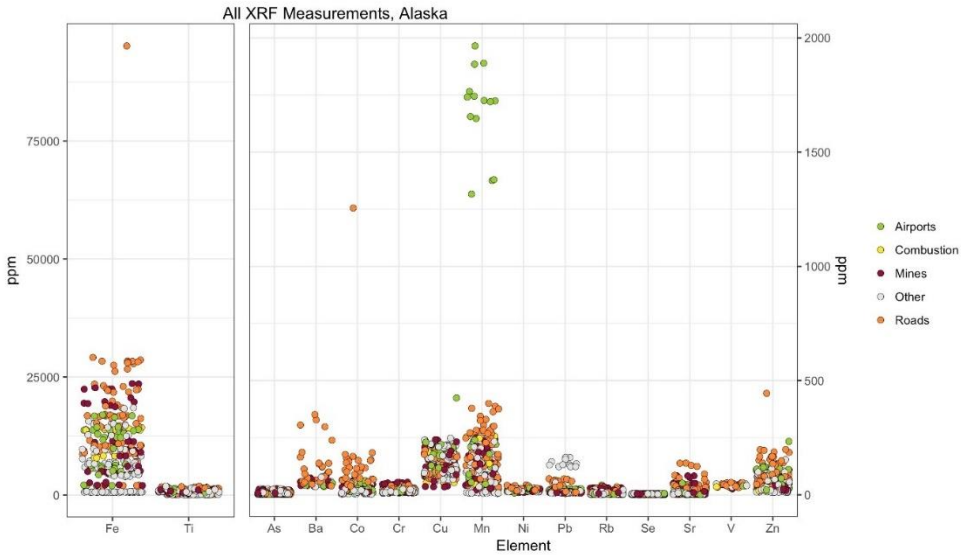

Figure 51. Relative abundance of trace elements for Alaska based on datasets AK25 and AK50. The samples are appointed to the source emission groups ‘combustion’, ‘mines, ‘roads’, and ‘airports’ and are sorted according to the analytes measured by the pXRF.

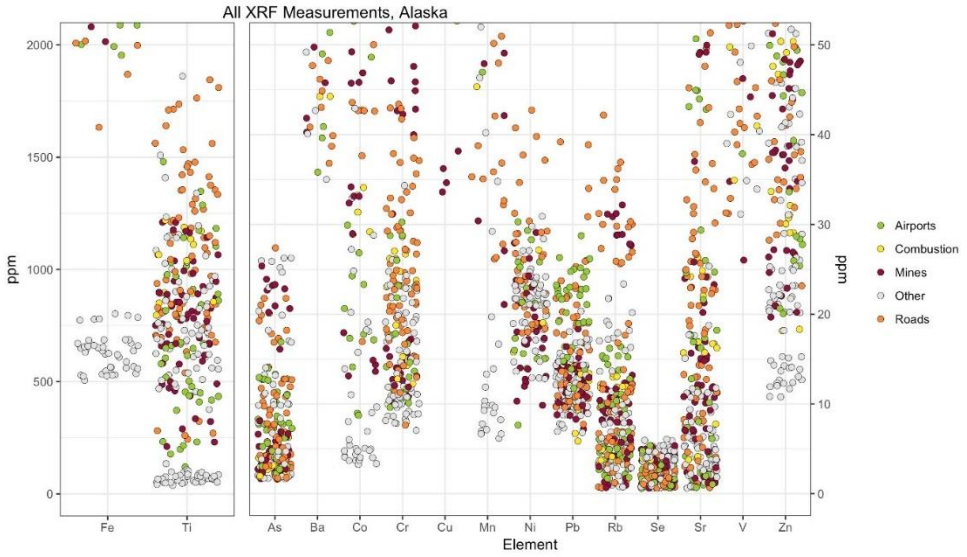

Figure 52. Close-up of figure 51 (see description above).

Outstanding are the extremely high values for Mn (~1300 ppm – 2000 ppm) in the category airports. As figure 56a-c shows, all three samples taken at the airport in Fairbanks (A13 AIR, A14 AIR_L) as well as A22 AIR_C register Mn in high amounts. Yet, A14 shows by far the highest levels. Mn commonly derives from de-icing sprays such as propylene glycol. A possible explanation why the snow on the adjacent lake to the airport registered with such high values is that some of the snow-melt from the snow field which drains into the pond/ lake has been soaked up by the snowpack on the lake. This category further exhibits counts in all remainder elements but displays only elevated levels for Pb in relation to the other categories, a possible indicator for fuel combustion from airplanes as well as the airport fleet.

In contrast to the Swedish RCPs, the analytes of the group 'roads' displayed the highest values for Fe, Ba, Co, Pb, Rb, Se, V, and Zn (Fig. 52), with additional high values for As. Especially Ba, Cr and Fe could have derived from eroded brake pads and other car parts, while the remainder elements are indicative of fuel combustion. The overall higher values for roads, which correlate to the elements detected for roads in the Swedish dataset, could have been the closer proximity to roads. In addition, especially the samples AK5 GPH 0 and AK8 GPH IV were taken close to a major highway in the State which could have increased the trace metal levels in the surrounding snow. The differences in roads as well as the two varying proximities to the roads may be the cause for the wider range of the datapoints as compared to Sweden (~30.000 ppm/ ~500 ppm).

The signature of 'energy' is less dominant in the AK dataset. The only sample in this category (A4 HSR) was collected downwind of the Healy Coal Power Plant.

Even though the signature is lower, it does however show elevated levels for Cr, Se, and specifically for Mn which are indicators for coal combustion (Fig. 54a and b). All remainder analytes also register measurements of ‘combustion’, which could be due to vehicular activities as the sample was taken close to the road leading to the Usibelli coal mine. The category ‘mines’ registered specifically high values for As (except for one datapoint), Co, Cr, Mn, Pb, Rb, Sr. As, Pb, Co, and Zn are often found in mine tailings of gold mines, which could be an indicator of emissions from the samples distributed around the Fort Knox mine north of Fairbanks such as A23 NOAA (Fig. 55).

In conclusion, the comparison of relative concentration pattern of the different sampling sites can yield valuable information about the conditions at the respective sites.

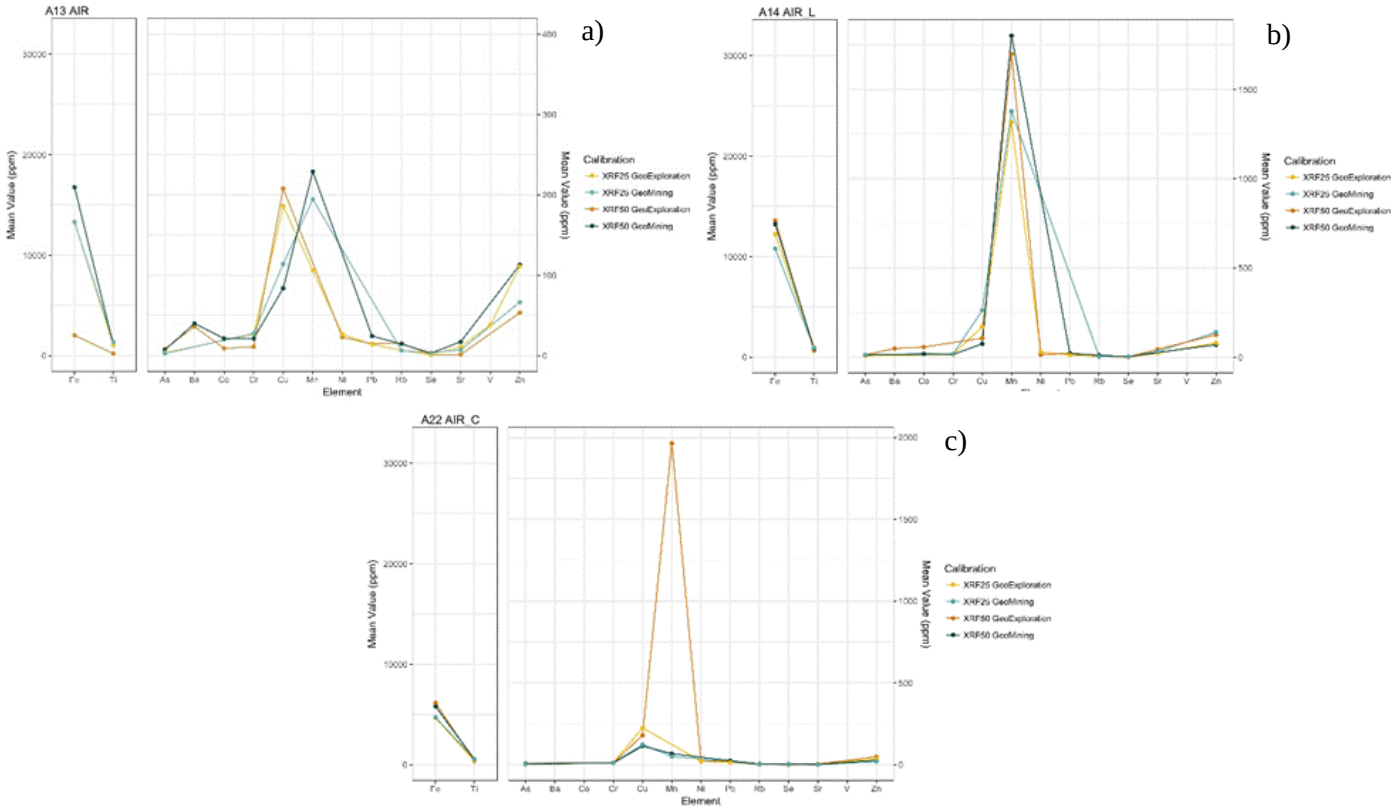

Figure 53. Mean trace element levels of calibrations GeoExploration and GeoMining for samples A13 AIR, A14 AIR_L, and A22 AIR_C for both filter sizes (25mm, 50 mm). No blank values have been subtracted.

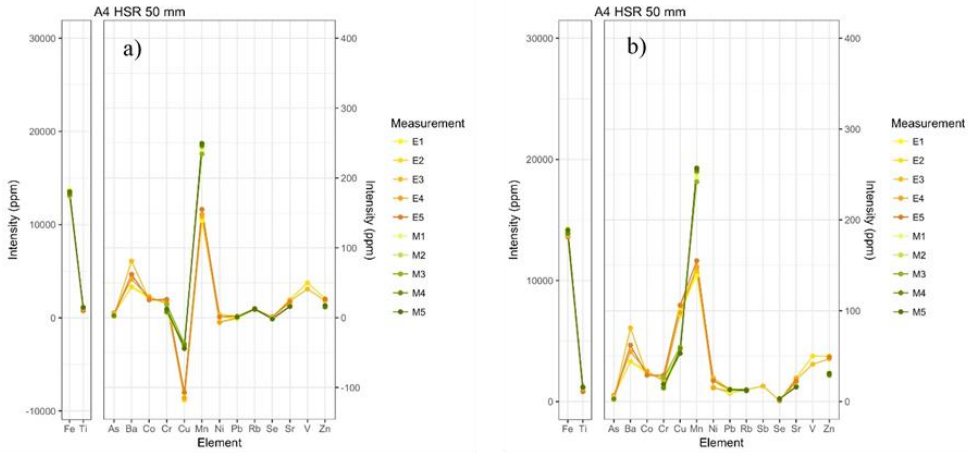

Figure 54. Levels of trace elements measured with all calibration runs for both GeoExploration (E1-E5) and GeoMining (M1-M5) for sample A4 HSR 50 mm a) subtracted blank values b) original pXRF recordings.

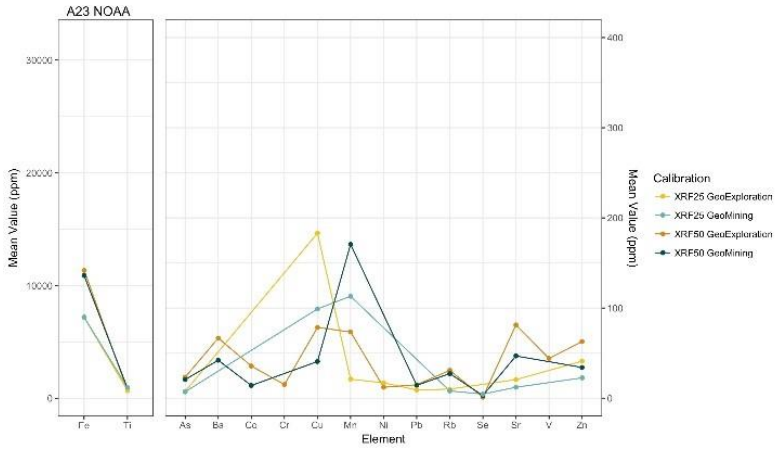

Figure 55. Mean trace element levels of calibrations GeoExploration and GeoMining for sample A23 NOAA for both filter sizes (25 mm, 50 mm). No blank values have been subtracted.

6.2.6 Comparison of pXRF and ICP-MS

ICP Mass Spectrometry is a powerful multi-element trace analysis method, valued for its high sensitivity (Dick et al., 2008). The method is used in a broad range of scientific and commercial fields and can be applied to both liquid and solid samples (ibid). In the cryospheric sciences as well, ICP-MS measurements are a heavily used method of chemical analyses. ICP-MS is, for example, well known to detect even

extremely low concentrations of elements in snow and ice on the Antarctic ice-sheet (e.g., Ardini et al., 2018; Dick et al., 2008, Townsend and Edwards, 1997). For these reasons, both sets of samples (Northern Sweden and Interior Alaska) were sent to the Institute for the Dynamics of Environmental Processes in Venice, Italy. Due to the limited number (n = 20) of Alaska samples, filters 'A8 GPH IV' and 'A12 DPR III' were excluded. The aim was to get ICP-MS reference measurements to which the pXRF results could be compared in order to test the validity of the latter method. The table containing the ICP-MS results may be found in appendix table A.11. As the ICP-MS measures the absolute mass, the results of the analyses are presented in absolute µg. Elements tested for with the ICP-MS but not included in pXRF analysis were excluded from these comparisons.

An initial analysis of the ICP-MS results revealed that the blanks in both datasets displayed not only variable, but often very high absolute values (µg) for many of the elements tested. In the extreme case of Al in the Swedish dataset, one of the blanks exceeded the next highest value of a contaminated filter by more than a factor of 2 (Al: blank3: 5235 µg; KR01C+D: 2154 µg). The initial high elemental loadings on blank filters from both datasets and the high variability between the blanks led to the conclusion that the absolute values of the ICP-MS data could not serve as a comparison for the pXRF method. Measurement or instrument errors were ruled out by Dr. Andrea Spolaor who oversaw the analysis. According to him, both the calibration and cleaning steps were performed successfully and according to standardized protocols (pers. correspondence, Oct 2018). Cross-contamination between the samples and the blanks during transport from Uppsala, Sweden or Fairbanks, Alaska to Venice respectively was also unlikely. All filters were sent separately packaged, in sealed petri-dishes within small, air-tight plastic bags. As indicated in section 6.2.1, a possible explanation for the high blank values could be that the tissue-quartz filters, even though advertised for trace element analysis, may have contained such high elemental concentrations initially that they were too high for the concentrations found on the snow-filters.

As the levels of trace elements on the blank and empty filters were too high for a comparative analysis with absolute values an alternative method, using element ratios, was utilized for comparing the two methods. Using element rations in this regard meant comparing all combinations of analytes of one method to the same combination of element ratios from the other method. An example for element ratios would be Cr/Cu, Cr/Fe from the ICP-MS compared to Cr/Cu, Cr/Fe from the pXRF method. Included in the analysis were all combinations of the following analytes: Ba, Cr, Cu, Fe, Mn, Ni, Pb, Rb, Sr, V, and Z. In this analysis, the data from the two sample sets (Alaska and Sweden) of both methods were compared separately (ICP-MS vs pXRF of the Swedish datasets and ICP-MS vs pXRF of the Alaska datasets). To get insight whether the two different pXRF calibrations might have an effect on

the relation between the two methods, the comparisons were differentiated into comparing the ICP-MS data to the pXRF dataset derived from measuring with calibration E (pXRFE) and from measuring with calibration M (pXRFM). The results are shown as correlation plots in figure 56. For this analysis the sum of ^{56}Fe and ^{57}Fe as measured by the ICP-MS has been used and termed Fe. Same-element ratios (e.g. Sr/Sr) were excluded as well as the redundant ratios (e.g. Cr/Cu, Cu/Cr). For the same assumptions as outlined in 6.1.1 an RMA regression was fitted to the data. The Pearson's correlation coefficient R as well as the coefficient of determination R^2 were determined for each of the four models (Table 8).

Table 8. Pearson's correlation coefficient R and coefficient of determination R^2 for the RMA regression of the methods pXRF and ICP-MS for both regions, Alaska and Sweden, and both calibrations: GeoExploration (pXRFE) and GeoMining (pXRFM).

Correlation / Ratios	**R**	**R^2**
SW: pXRFE/ICP-MS	0.5	0.25
SW: pXRFM/ICP-MS	0.4406	0.1941
AK: pXRFE/ICP-MS	0.5497	0.3022
AK: pXRFM/ICP-MS	0.4997	0.2497

The highest R value is related to the Alaska samples measured with the GeoExploration calibration pXRFE/ICP-MS (0.5497) (Fig. 56c), followed by the Sweden samples measured with the GeoExploration calibration (0.5) (Fig. 56a), while the associations between the two methods is weaker when the samples were measured using the GeoMining calibration of the pXRF. The correlation between the Alaska samples measured with calibration M (pXRF) exhibits the second lowest value of 0.4997 (Fig. 56d) and the Swedish datasets measured with GeoMining (pXRF) show the lowest correlation of 0.4406 (Fig. 56b) (Table 8). The ordering of the R^2 values follows the same pattern, with the highest predictable variance of ~30% (AK) and ~25% (SW) being found for the samples measured with GeoExploration. For the other two method pairs, a slightly lower percentage of the variance in the data can be related to the relationship between the two variables (~25% (AK: pXRFM/ICP-MS); 19% (SW: pXRFM/ICP-MS)). Correlating the elemental ratios and considering the R and R^2 values of the two methods suggests that the relative abundance of elements as measured by the ICP-MS shows a weak association between the ratios of analytes as detected by the pXRF in both calibrations and both regions. Yet, despite the statistical metrics R and R^2 indicating a relationship between the methods, the wide dispersion of datapoints around the regression line rather suggests that the correlation is rather not significant. It appears however, that more of the variability in the datasets measured with the GeoExploration calibration can be related to the

relationship between the two variables as compared to measurements with GeoMining. This finding might be based on the higher sensitivity of calibration E as compared to calibration M. The higher particle loadings of the Alaska filters might also have been advantageous in reducing the counts below the LOD in this dataset and therefore led to a higher correlation to the highly sensitive ICP-MS analysis and the pXRF measurements of the Alaska filters. Future studies studies on the comparison of observed absolute values in analytes between ICP-MS and pXRF would benefit from the use of a more appropriate filter.

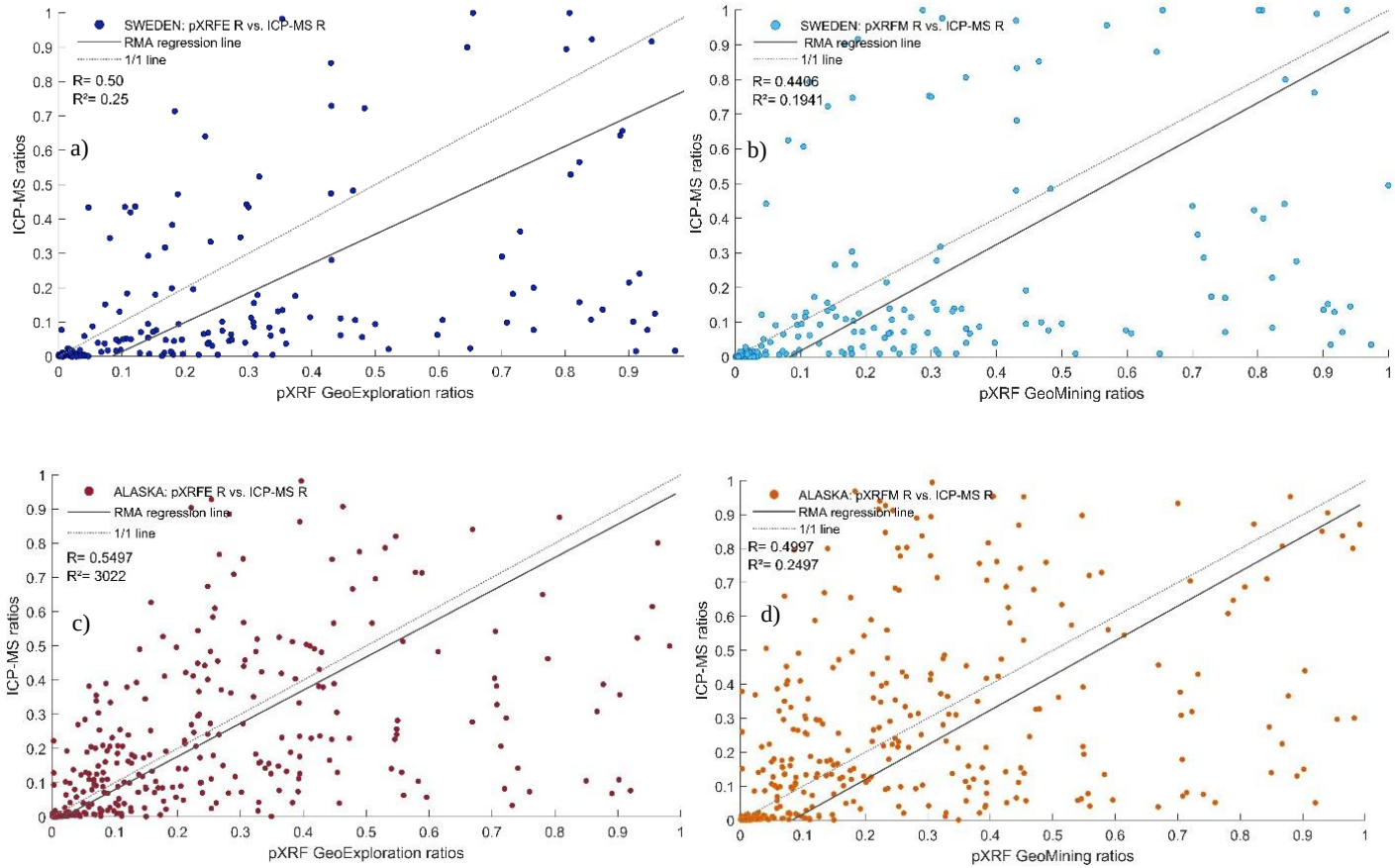

Figure 56. Reduced Major Axis (RMA) regression fitted to the pXRF and ICP-MS analyte ratios from Sweden (a, b) and Alaska (c,d). a) and c) represent the pXRF datasets measured with GeoExploration, b) and d) represent the pXRF datasets measured with GeoMining.

7 Conclusion

This study investigated the carbon and trace metal content of seasonal snowpacks in two Arctic/ subarctic regions: Northern Sweden and Interior Alaska. The comparison of three analytical techniques that measure and characterize CPs filtered from melted snow demonstrated the challenges of using multiple methods to derive the impurity content in snow. Based on the exploitation of different physical principles, the PSAP, TOT, and LAHM methods presented the results in the system-defined expressions BCe, EC/OC, and eBC respectively. A higher correlation was found between the PSAP and TOT method compared to the association of the LAHM and the TOT method. The respective divergences between the methods, particularly the latter two, indicated the importance of using a homogeneous filtration technique prior to the analysis and illustrated the effect of uncertainties inherent to each of the methods. The lower precision of measurements on the 25 mm filters indicated that the 50 mm filters were more homogeneous and therefore better suited. As some analyses such as the TOT only use certain parts of the filters, providing a representative piece of the filter is of importance. Hence, the vacuum-pump filtration setup is thought to be the preferable method of filtration to achieve desired homogeneity in filter loading. However, syringe filtration remains a valuable tool due to its simplicity, portability and low cost. The high level of overloading of the Alaska filters added additional uncertainty to the results.

Comparing the EC and OC levels at different geographic sites in Sweden and Alaska showed that both EC and OC content were generally higher in Alaska than in Sweden. The high OC values in rural sites in Alaska suggested the influence of wood smoke on the snowpacks at those locations. The smaller range of OC and EC mean values for the different geographic regions in Sweden corroborates findings in other studies that advise taking duplicate sample collections at each snowpit to mitigate meter-scale variability in the snowpack. The comparison of EC values of the remote sites of both study areas (Northern Sweden and Interior Alaska) with previously published data suggested a similarity between EC levels measured in the past and those measured for this study, with slightly higher concentrations in Alaska than mean levels derived from field campaigns in the region. A bigger sample size

would have been necessary in order to provide more reliable information in this regard.

Four limitations constrained the chemical analysis of the filters in terms of trace element levels in seasonal snowpacks in the study regions: 1) high background values of trace metals on the empty filter material, 2) the unfeasibility of a calibration of the pXRF instrument to reference materials of known composition for validation of measurements, 3) erroneous 100% SiO_2 measurement of the pXRF due to the thin pure quartz filter matrix, and 4) the inability to obtain the weight of contaminants on the filter in order to normalize the ICP-MS data. Nevertheless, it was possible to establish that the measurements on each of the filters with both default calibrations (GeoExploration and GeoMining) of the pXRF had relatively high precision. Like the CP results, pXRF measurements showed a higher precision for the 50 mm filters as compared to the 25 mm filters. The comparison of both default calibrations showed slightly higher detection counts and levels for most analytes measured with GeoExploration, which is assumed to be due to the lower LOD threshold for this calibration set-up and a resulting better suitability when scanning for trace metals. However, both GeoExploration and GeoMining measure fairly consistently within the respective calibration, with slightly less variability in the filter measurement carried out with GeoExploration. The accuracy of measuring snow meltwater samples with the pXRF could not be proven. Even though the statistical metrics R and R^2 of the correlation between elemental ratios of the ICP-MS and the pXRF measurements indicate an association between the two methods, the dispersion of values around the regression axes are too large to assume a significant correlation between the two methods. Despite slight differences in the precision of pXRF measurements and element counts as well as the limitations mentioned above, analysing snow meltwater filters with both calibrations of the portable XRF instrument gave insight into the environmental conditions and setting of the respective snow sample sites. In this regard, the higher filter loadings on the Alaska filter set as well as the greater particle loads on some of the Swedish filters were advantageous to receive significant signals above the high background values. However, despite the ability of the handheld XRF to give insight into the trace metal composition of snowpacks, further research on the validity of snow measurements with this instrument is necessary to provide a more reliable assertion of trace elements in snow.

From an environmental point of view, the presence of high iron and manganese concentrations at sampling locations close to mines and airports merits further investigation into the effects of these metals on various ecosystems. In addition, the levels of EC values in snow found in both Northern Sweden and Interior Alaska could affect the snowpack's absorption and reflection of solar radiation, which should be impetus for reductions in CP emissions on both global and local scales.

References

Alaska Department of Fish and Game (ADF&G). Where to Go. Wildlife Viewing. Available at: https://www.adfg.alaska.gov/index.cfm?adfg=viewinglocations.main, last accessed 04.03.2019

Alaska Department of Natural Resources (ADNR)/ Division of Mining, Land and Water. 2016. Pogo Mine. Available at: http://dnr.alaska.gov/mlw/mining/largemine/pogo/, last accessed: 10.03.2019

Alaska Department of Natural Resources (ADNR)/ Division of Mining, Land and Water. 2019. Fort Knox Mine. Available at: http://dnr.alaska.gov/mlw/mining/largemine/fortknox/, last accessed: 10.03.2019

Amundsen, P.-A. et al. 2011. Heavy metal contents in whitefish (Coregonus lavaretus) along a pollution gradient in a subarctic watercourse. In: Env. Monitoring and Assessment, Vol.182(1-4), pp.301-306. doi: 10.1007/s10661-011-1877-1
and parameterization. In: Bor. Env. Research, Vol.14, pp.527-538. ISSN 1797-2469 (online)

Andreae, M. O. and Gelencsér, A. 2006. Black carbon or brown carbon? The nature of light-absorbing carbonaceous aerosols. In: Atmos. Chem. Phys., Vol.6, pp.3131–3148. https://doi.org/10.5194/acp-6-3131-2006
Appliance Exchange Program. Total Project Snapshot Report. TPS Report 55302v3. Available at: https://www.omb.alaska.gov//ombfiles/15_budget/CapBackup/proj55302.pdf, last accessed 30.04.2019

Arctic Monitoring and Assessment Programme - AMAP. 1998. AMAP Assessment Report: Arctic Pollution Issues. Arctic Monitoring and Assessment Programme (AMAP), Oslo, Norway. xii+859 pp. Available at: https://www.amap.no/documents/doc/amap-assessment-report-arctic-pollution-issues/68 , last accessed 12.08.2018.

Arctic Monitoring and Assessment Programme - AMAP. 2009. Arctic Pollution 2009. Arctic Monitoring and Assessment Programme, Oslo. xi+83pp. Available at: https://www.amap.no/documents/doc/arctic-pollution-2009/88, last accessed 13.08.2018.

Arctic Monitoring and Assessment Programme (AMAP), 2011. AMAP Assessment 2011: Mercury in the Arctic. Arctic Monitoring and Assessment Programme (AMAP), Oslo, Norway. xiv + 193 pp. ISBN – 13 978-82-7971-068-4

Arctic Monitoring and Assessment Programme (AMAP). 1998. AMAP Assessment Report: Arctic Pollution Issues. Arctic Monitoring and Assessment Programme (AMAP), Oslo, Norway. xii+859 pp. ISBN 82-7655-061-4

Arctic Monitoring and Assessment Programme (AMAP). 2005. AMAP Assessment 2002: Heavy Metals in the Arctic. Arctic Monitoring and Assessment Programme

(AMAP), Oslo, Norway. xvi + 265 pp. (first published as electronic document in 2004). ISBN 82-7971-018-3

Barbante, C. et al. 2017. Man's footprint on the Arctic environment as revealed by analysis of ice and snow. In: Earth-Science Reviews, Vol. 168, pp.218–231. http://dx.doi.org/10.1016/j.earscirev.2017.02.010

Barcan, V. and Sylina, A. 1995. The Appraisal of Snow Sampling for Environmental Pollution Valuation. In: Water, Air, and Soil Pollution, Vol. 89(1-2), pp.49-65. https://doi.org/10.1007/BF00300421

Barrie, L. A. et al. Arctic contaminants: sources, occurrence and pathways. In: Sci. Total Env. Vol. 122 (1-2), pp. 1-74. doi: 10.1016/0048-9697(92)90245-N

Bond, T. C. et al. 1999. Calibration and Intercomparison of Filter-Based Measurements of Visible Light Absorption by Aerosols. In: Aerosol Science and Technology, Vol.30, pp. 582–600. doi: 0278-6826 / 99

Bond, T. C. et al. 2013. Bounding the role of black carbon in the climate system: A scientific assessment. In: Journ. of Geophys. Res., Vol.118, pp. 5380–5552. doi: 10.1002/jgrd.50171, 2013

Bose-O'Reilly, S. et al. 2010. Mercury Exposure and Children's Health. Current Problems in Pediatric and Adolescent Health Care, Vol. 40(8), pp. 186–215. doi: 10.1016/j.cppeds.2010.07.002.

Bourgeois, Q. and Bey, I. 2011. Pollution transport efficiency toward the Arctic: Sensitivity to aerosol scavenging and source regions. Journal of Geophysical Research, Vol.116. D08213, doi:10.1029/2010JD015096

Brouwer, P. 2010. Theory of XRF. 3rd Edition. Almelo, The Netherlands. ISBN: 90-9016758-7.

Brown, R. and Luojus, K. 2018. Snow Assessments. 2018 Snow Assessment. Northern Hemisphere Snow Cover. Available at: http://globalcryospherewatch.org/assessments/snow/2018/, last accessed 07.03.2019
by spectrophotometric analysis of filters. In: Appl. Optics, Vol.50, pp. 2037–2048, 2011. https://doi.org/10.1364/AO.50.002037

CACAR II. 2003. Canadian Arctic Contaminants Assessment Report II. Sources, Occurrence,Trends and Pathways in the Physical Environment. Available at: http://caid.ca/CanArtCon5.2003.pdf, last accessed 07.10.2018

Callaghan, T. V. et al. 2011. Multiple Effects of Changes in Arctic Snow Cover. In. AMBIO, Vol. 40, pp. 32-45. doi: 10.1007/s13280-011-0213-x.
Carbon Aerosol in Relation to Chemical Age. In: Aerosol Science and Technology, Vol.43(6), pp.522-532, doi:10.1080/02786820902777207

Cavalli, F. Et al. 2010. Toward a standardised thermal–optical protocol for measuring atmospheric organic and elemental carbon: The EUSAAR protocol. In: Atmospheric Measurement Techniques, Vol.3, pp.79–89. https://doi.org/10.5194/amt-3-79-2010

Center for Multiscale Modeling of Atmospheric Processes (CMMAP). N.d. Climate. Atmospheric Circulation. Available at: http://kiwi.atmos.colostate.edu/cmmap/learn/climate/circ7.html, last accessed 10.02.2019.

Chai, M. et al. 2012. Organic and Elemental Carbon Filter Sets: Preparation Method and Interlaboratory Results. In: Ann. Occup. Hyg., Vol. 56(8), pp. 959–967. doi:10.1093/annhyg/mes029

Chapman, P. M. 2007. Determining when contamination is pollution – Weight of evidence determinations for sediments and effluents. In: Environmental International, Vol. 33, pp. 492-501. doi:10.1016/j.envint.2006.09.001.

Chemsec. 2016. Hazard vs. Risk – What is best practice when assessing chemicals? Available at: http://chemsec.org/hazard-vs-risk-what-is-best-practice-when-assessing-chemicals/, last accessed 29.07.2018.
Clark, J. 2015. The Mass Spectrometer. Available at: https://www.chemguide.co.uk/analysis/masspec/howitworks.html, last accessed 15.02.2019.
Clarke, A. D. and Noone, K. J. 1985. Soot in the Arctic snowpack: a cause for perturbations in radiative transfer. In: Atmospheric Environment, Vol.19(12), pp. 2045-2053. https://doi.org/10.1016/0004-6981(85)90113-1
combustion: Emissions characterization at a continental scale. In: Journal of Geophysical Research, Vol.107, D21, 8349. doi:10.1029/2001JD000661
Cordillera Blanca, Peru. In: The Cryosphere, Vol.9, pp.331-340. doi:10.5194/tc-9-331-2015
Dahlman, LA/ NOAA 2009. Climate Variability: Arctic Oscillation. Available at: https://www.climate.gov/news-features/understanding-climate/climate-variability-arctic-oscillation, last accessed 17.02.2019
Datz, T. and Perry, C. 2012. Toxic mercury, accumulating in the arctic, springs from a hidden source. Available at: https://www.hsph.harvard.edu/news/press-releases/arctic-rivers-toxic-mercury/, last accessed 06.04.2019
De Caritat, p. et al. 2005. Chemical composition of arctic snow: concentration levels and regional distribution of major elements. In: Science of the Total Environment, Vol. 336, pp. 183-199. DOI: 10.1016/j.scitotenv.2004.05.031.
DeCaritat, P. et al. 2005. Chemical composition of arctic snow: concentration levels and Department of Environmental Conservation (DEC) for Alaska. 2019. Fairbanks PM2.5 – Background. Available at: https://dec.alaska.gov/air/anpms/communities/fbks-pm2-5-background, last accessed: 10.03.2019
Dickhut, R. M. et al. 2000. Automotive Sources of Carcinogenic Polycyclic Aromatic Hydrocarbons Associated with Particulate Matter in the Chesapeake Bay Region. In: Environ. Sci. Technol., Vol. 34 (21), pp 4635–4640. doi: 10.1021/es000971e
Dinis, M. de L. and Fiurza, A. 2010. Exposure Assessment to Heavy Metals in the Environment: Measures to ElimiLODte or Reduce the Exposure to Critical Receptors. In: Environmental Heavy Metal Pollution and Effects on Child Mental Development. DOI 10.1007/978-94-007-0253-0_2.
Doherty, S. J. et al. 2010. Light-absorbing impurities in Arctic snow. In: Atmos. Chem. Phys., Vol.10, pp.11647–11680. doi: 10.5194/acp-10-11647-2010
Dou, T.-F. and Xiao, C.-D. 2016. An overview of black carbon deposition and its radiative forcing over the Arctic. In: Advances in Climate Research, Vol.7, pp.115-122. https://doi.org/10.1016/j.accre.2016.10.003
Dou, T.-F. et al. 2012. The distribution of snow black carbon observed in the Arctic and compared to the GISS-PUCCINI model. In: Atmos. Chem. Phys., Vol.12(17), pp. 7995-8007. https://doi.org/10.5194/acp-12-7995-2012
Douglas, T. A. and Sturm, M. 2004. Arctic haze, mercury and the chemical composition of snow across northwestern Alaska. In: Atm. Env., Vol.38, pp.805-820. doi:10.1016/j.atmosenv.2003.10.042
Duffus, J. H. 2002. “Heavy Metals”—A meaningless term? (IUPAC Technical Report). In. Pure Appl. Chem., Vol. 74, No., pp. 793-807. Available at. https.//old.iupac.org/publications/pac/2002/pdf/7405x0793.pdf, last accessed 05.08.2018.
Dupuis, J. 2017. Melting snow contains a toxic cocktail of pollutants. McGill Newsroom. Available at: https://www.mcgill.ca/newsroom/channels/news/melting-snow-contains-toxic-cocktail-pollutants-267489, last accessed 30.07.2018.

European Environmental Agency (EEA). 2013. Air pollution fact sheet 2013 – Sweden. Available at: https://www.eea.europa.eu/themes/air/air-pollution-country-fact-sheets, last accessed 03.03.2019

European Environmental Agency (EEA). 2018. PM2.5 annual mean in 2015. Available at: https://www.eea.europa.eu/data-and-maps/figures/pm2-5-annual-mean-in, last accessed 03.03.2019

Evangeliou, N. et al. 2018. Origin of elemental carbon in snow from western Siberia and northwestern European Russia during winter-spring 2014, 2015 and 2016. In: Atmos. Chem. Phys., Vol.18, pp.963-977.

Fairbanks North Star Borough (FNSB). 2014. Fairbanks North Star Borough - Enhanced Home Heating

Fairbanks North Star Borough/Air Pollution Control Commission (FNSB/APCC). 2016. Air Quality Comprehensive Plan Framework for Healthy Air, People, and Economy. Available at: http://fnsb.us/transportation/AQDocs/FNSBAPCC%20AQComprehensivePlan2016.pdf, last accessed 30.04.2019

Fine, P. M. et al. 2002. Organic compounds in biomass smoke from residential wood

Fiola, M. L. 2017. Influence of Sample Preparation on Portable XRF-analyses of Aeolian Sediments: a Case Study. Degree Project at the Department of Earth Sciences, Uppsala University. ISSN 1650-6553 Nr 410

Fischer, J. A. 2011. Atmospheric pollution in the Arctic: Sources, transport, and chemical processing. A Doctoral Dissertation. Harvard University, Cambridge Massachusetts. Available at: https://www.uow.edu.au/~jennyf/Fisher_Dissertation.pdf, last accessed 07.10.2018

Fisher Instrumentation. N.d. X-Ray Fluorescence. Available at: http://www.fischergb.co.uk/en/united-kingdom/knowledge/methods/material-testing/x-ray-fluorescence2/, last accessed 03.03.2019

FORCE Technology. 2019. Umeå Energi AB, Dåva, Sweden. Available at: https://biochp.force.dk/downloads/chp-plants-key-figures/umea-energi-ab-dava-sweden/, last accessed 05.05.2019

Forsström, S. et al. 2013. Elemental carbon measurements in European Arctic snow packs. Journ. of Geophys. Res., Vol.118(13), pp.614-627. DOI:10.1002/2013JD019886

Gallet, J. C. et al. 2018. Protocols and recommendations for the measurement of snow physical properties, and sampling of snow for black carbon, water isotopes, major ions and microorganisms. Kortrapport / Brief Report no. 046. Available at: http://www.polarknow.us.edu.pl/wp-content/uploads/Kortrapport46.pdf, last accessed: 12.03.2019

Geochemistry. Available at: https://hal-brgm.archives-ouvertes.fr/hal-01740950/document, last accessed 29.04.2019

Ghaderi, Z.; et al. (2013). From snow skiing to grass skiing. implications of climate change for the ski industry in Dizin, Iran. In. Anatolia, Vol.25, pp.96-107. DOI. 10.1080/13032917.2013.829507

Gogoi, M. M., et a. 2015. Aerosol black carbon over Svalbard regions of Arctic.In: Polar Science, Vol. 10, pp. 60-70. doi: 10.1080/027868290901972.

Gregoris, E. et al. 2015. Impact of maritime traffic on polycyclic aromatic hydrocarbons, metals and particulate matter in Venice air. In: Environ. Sci. Pollut. Res., Vol.23, pp.6951–6959. doi 10.1007/s11356-015-5811-x

Grenfell, T. C., et a. 2011. Light absorption from particulate impurities in snow and ice determined

Groth Grube, A. 2011. Particulate air pollution and its characteristic sources in the high Arctic at Station Nord, N.E. Greenland. Master thesis project. Aarhus University,

DK. Available at: http://www.iceandclimate.nbi.ku.dk/publications/theses/Final_MasterThesis_AnnaGrube.pdf, last accessed 20.04.2019

Hak, C. et al. 2010. Traffic and Air Quality - Contribution of Traffic to Urban Air Quality in European Cities. ETC/ACC Technical Paper. Available at: https://www.researchgate.net/publication/260600460_Traffic_and_Air_Quality_-_Contribution_of_Traffic_to_Urban_Air_Quality_in_European_Cities, last accessed 03.03.2019

Halbach, K. et al. 2017. The presence of mercury and other trace metals in surface soils in the Norwegian Arctic. In: Chemosphere, Vol. 188, pp. 567-574. DOI: 10.1016/j.chemosphere.2017.09.012

Harper, M. and Pacolay, B. 2006. A comparison of X-ray fluorescence and wet chemical analysis for lead on air filters from different personal samplers used in a secondary lead smelter/solder manufacturer. In: J. of Environ Monit., Vol 8(1), pp.140-146. DOI: 10.1039/b504719f

Harper, W. V. 2014. Reduced Major Axis Regression: Teaching Alterntive to Least Squares. ICOTS9 (2014) Contributed Paper. Available at: https://iase-web.org/icots/9/proceedings/pdfs/ICOTS9_C131_HARPER.pdf, last accessed 03.05.2019

Hawkes, S. J. 1997. What is a "Heavy Metal"? In: JourLODl of Chemical Education, Vol. 74, No. 11, p. 1374. Available at: https://pubs.acs.org/doi/pdf/10.1021/ed074p1374?src=recsys, last accessed 05.08.2018.

Heek, T. 2018. Information on pXRF calibration. Email contact on 5th April 2018.

Hegg, D. A. et al. 2009. Source Attribution of Black Carbon in Arctic Snow. In: Environ. Sci. Technol., Vol.43, pp.4016-4022. DOI: 10.1021/es803623f

Hodson, M. E. 2004. Heavy metals – geochemical bogey men? In. Environmental Pollution. Vol. 129, pp. 341-343. DOI. 10.1016/j.envpol.2003.11.003 https://apps.who.int/iris/bitstream/handle/10665/250141/9789241511353-eng.pdf?sequence=1, last accessed 21.03.2019

Huntington, H. P. et al. 2007. The influence of human activity in the Arcticon climate and climate impacts. In: Climate Change. doi 10.1007/s10584-006-9162-y

Hur, S. D. et al. 2007. Seasonal patterns of heavy metal deposition to the snow on Lambert Glacier basin, East Antarctica. In: Atmos. Env., Vol.41(38), pp. 8567-8578. https://doi.org/10.1016/j.atmosenv.2007.07.012

Hustrich, I. 2008. The population of the Arctic, subarctic, and Boreal regions. In. Polar Geography. Vol. 3, pp. 40-48. doi: 10.1080/10889377909377100

Hustrich, I. 2008. The population of the Arctic, subarctic, and Boreal regions. In. Polar Geography. Vol. 3, pp. 40-48. doi: 10.1080/10889377909377100

International Volcanic Health Hazard Network (IVHHN). 2018. Particulate Matter (PM) and Aerosol. Available at: https://www.ivhhn.org/information/information-different-volcanic-gases/particulate-matter, last accessed: 20.01.2019.

Jiao, C. et al. 2014. An AeroCom assessment of black carbon in Arctic snow and sea ice. In: Atmos. Chem. Phys., Vol.14, pp. 2399–2417. doi:10.5194/acp-14-2399-2014

Karanasiou, A. et al. 2015. Thermal-optical analysis for the measurement of elemental carbon (EC) and organic carbon (OC) in ambient air a literature review. In: Atmos. Meas. Tech. Discuss., Vol. 8, pp. 9649–9712. doi: 10.5194/amtd-8-9649-2015

Kashulina, G. et al. 2014. Snow and rain chemistry around the "Severonikel" industrial complex, NW Russia: Current status and retrospective analysis. In: Atm. Env., Vol.89, pp.672-682. doi: 10.1016/j.atmosenv.2014.03.008

Kepski, D. et al. 2016. Progressing Pollutant Elution from Snowpack and Evolution of its Physicochemical Properties During Melting Period—a Case Study From the

Sudetes, Poland. In: Water Air Soil Pollut. Vol.227, pp.112-122. doi:10.1007/s11270-016-2797-z

Khan, A. L. et al. 2017. Impacts of coal dust from an active mine on the spectral reflectance of Arctic surface snow in Svalbard, Norway. In: J. Geophys. Res. Atmos., Vol.122, pp.1767–1778. doi:10.1002/2016JD025757

Knox, A. et al. 2009. Mass Absorption Cross-Section of Ambient Black

Koch, D. et al. 2009. Evaluation of black carbon estimations in global aerosol models. In: Atmos. Chem. Phys., Vol.9, pp. 9001–9026. https://doi.org/10.5194/acp-9-9001-2009

Korosi, J. B. et al. 2016. Assessing the contribution of combustion-derived contaminants to a remote subarctic environment from traffic on the Tibbitt to Contwoyto winter road (Northwest Territories, Canada). In: Sci Total Environ. Vol. 553, pp. 96-106. doi: https://www.sciencedirect.com/science/article/pii/S0048969716302650?via%3Dihub

Krecl, P. et al. 2008. Contribution of residential wood combustion and other sources to hourly winter aerosol in Northern Sweden determined by positive matrix factorization. In: Atmos. Chem. Phys., Vol.8, pp.3639-3653. https://doi.org/10.5194/acp-8-3639-2008

Kyrö, E.-M. et al. 2009. Snow scavenging of ultrafi ne particles: field measurements

Lack, D. A. et al. 2013. Characterizing elemental, equivalent black, and refractory black carbon aerosol particles: a review of techniques, their limitations and uncertainties. In: Anal Bioanal Chem, Vol. 406, pp. 99–122. doi: 10.1007/s00216-013-7402-3

Larose, C. et al. 2013. Interactions between Snow Chemistry, Mercury Inputs and Microbial Population Dynamics in an Arctic Snowpack. In: PLoS ONE, Vol.8(11): e79972. doi:10.1371/journal.pone.0079972

Lary, D. J. et al. 2014. Estimating the global abundance of ground level presence of

Law, K. S. and Stohl, A. 2007. Arctic Air Pollution. Origins and Impacts. In. Science, Vol. 315, Issue 5818, pp. 1537-1540. DOI. 10.1126/science.1137695.

Lee, G. K. et al. 2016. The Geochemical Atlas of Alaska, 2016. In: U.S. Geological Survey Data Series, Vol.908, 25 p., 272 sheets (11”× 17”), GIS database. doi:org/10.3133/ds908

Lemière, B. 2018. A Review of pXRF (Field Portable X-ray Fluorescence) Applications for Applied Geochemistry. Available at: https://hal-brgm.archives-ouvertes.fr/hal-01740950/document, last accessed 29.04.2019

Lindsay, C. et al. 2015. Deriving Snow Cover Metrics for Alaska from MODIS. In: Remote Sens., Vol.7(10), pp. 12961-12985. https://doi.org/10.3390/rs71012961

Maas, R. and Grennfelt, P. (eds), United Nations Economic Commission for Europe (UNECE). 2016. Towards Cleaner Air. Scientific Assessment Report 2016. EMEP Steering Body and Working Group on Effects of the Convention on Long-Range Transboundary Air Pollution, Oslo. xx+50pp

Mankin, S. et al. (2015). The potential for snow to supply human water demand in the present and future. In. Environmental Research Letters 114016. DOI.10.1088/1748-9326/10/11/114016

McAfee, S. 2013. Downscaled projections of rain/snow partitioning for Alaska. Available at: https://casc.alaska.edu/projects/downscaled-projections-rainsnow-partitioning-alaska, last accessed: 05.03.2019

McDowell Group. 2018. The Economic Benefits of Alaska’s Mining Industry. Available at: https://www.mcdowellgroup.net/wp-content/uploads/2018/06/ama-revised-final-report.pdf, last accessed: 10.03.2019

microscopic particulate matter. In: Geospatial Health, Vol.8(3), S611-30. doi: 10.4081/gh.2014.292

Minguillón, M. C. 2012. Description of Automated Technologies for Air Pollutants and Air Quality Metrics. Pollutant Type: Particulate Pollutants, Pollutant Name: Light Absorbing Aerosols Measurement, Technology: Absorption Photometry. Available at: http://db-airmontech.jrc.ec.europa.eu/download/PM_LightAbsorbingAerosol_MMTI_AbsorptionPhotometry.pdf, last accessed 24.03.2019

Moosmüller, H. et al. 2009. Aerosol light absorption and its measurement: A review. In: Journal of Quantitative Spectroscopy and Radiative Transfer. Vol.110(11), pp.844-878. https://doi.org/10.1016/j.jqsrt.2009.02.035

Morabito, E. et al. 2014. Atmospheric Deposition of Inorganic Elements and Organic Compounds at the Inlets of the Venice Lagoon. In: Advances in Meteorology, Vol.2014, Article ID 158902, 10 pages. http://dx.doi.org/10.1155/2014/158902

Mulligan, D. and Cole, C. Tanana Alaska State Soil. Available at: https://www.soils4teachers.org/files/s4t/k12outreach/ak-state-soil-booklet.pdf, last accessed 05.03.2019

Munktell Ahlstrom AB. N.d. Filtration and Separation Technology (product catalogue). Available at: https://www.ahlstrom-munksjo.com/globalassets/munktell-blocks/catalog/en_munktell_filtrationcatalogue.pdf, last accessed 03.05.2019

National Aeronautics and Space Administration (NASA). 2017. Spatial Data AccessTool (SDAT). ABoVE: Last Day of Spring Snow, Alaska, USA, and Yukon Territory, Canada, 2000-2016. Available at: https://webmap.ornl.gov/ogcdown/dataset.jsp?dg_id=1528_17, last accessed: 10.03.2019

National Institute of Environmental Health Services (NIH). 2018. Air pollution. Available at: https://www.niehs.nih.gov/health/topics/agents/air-pollution/index.cfm, last accessed 20.01.2019.

National Oceanic & Atmospheric Administration (NOAA). N.d. Description of Particle Soot Absorption Photometer (PSAP). Available at: https://www.esrl.noaa.gov/gmd/aero/instrumentation/psap.html, last accessed 25.03.2019

National Oceanic and Atmospheric Administration (NOAA). 2019. Interactive graph of monthly values for the Arctic Oscillation index. Available at: https://www.climate.gov/news-features/understanding-climate/climate-variability-arctic-oscillation, last accessed 18.02.2019

National Snow & Ice Data Center (NSIDC) – NOAA. 2019. Snow and Climate. Snow's effect on climate. Available at: https://nsidc.org/cryosphere/snow/climate.html, last accessed 29.07.2018.

North Carolina State University (NCSU). 2018. Global Patterns: Arctic & North Atlantic Oscillations. Arctic Oscillation(AO). Available at: https://climate.ncsu.edu/climate/patterns/nao, last accessed 20.02.2019

Norwegian Polar Insitute. 2014. Transport of pollutants in the atmosphere. Available at: http://www.npolar.no/en/themes/pollutants/transport/atmosphere.html, last accessed 09.08.2018.

Orr, E. et al. (eds) 2019. SESS report 2018, Longyearbyen, Svalbard Integrated Arctic Earth Observing System. Available at: https://www.sios-svalbard.org/SESSreport, last accessed 15.10.2018

Pacyna, J. M. and Pacyna, E. G. 2001. An assessment of global and regional emissions of trace metals to the atmosphere from anthropogenic sources worldwide. In: Env. Reviews, Vol.9(4), pp. 269-298. https://doi.org/10.1139/a01-012

Palter, J. B. 2015. The role of the Gulf Stream in European climate. In: Ann Rev Mar Sci., pp.3-37. doi: 10.1146/annurev-marine-010814-015656
Paramanov, M. et al. 2011. Below-cloud scavenging of aerosol particles by snow at an urban site in Finland. In: Bor. Env. Research, Vol.16, pp.304-320. ISSN: 1797-2469
PerkinElmer Inc. 2011. Technical Note ICP-Mass Spectrometry. The 30-Minute Guide to ICP-MS Available at: https://www.perkinelmer.com/CMSResources/Images/44-74849tch_icpmsthirtyminuteguide.pdf, last accessed 14.02.2019.
Peterson, A. 2016. Köppen climate types of Sweden. Available at: https://commons.wikimedia.org/wiki/File:Sweden_K%C3%B6ppen.svg, last accessed 10.02.2019.
Petiot, C. 2018. What is X-ray fluorescence (XRF)? Available at. https.//hha.hitachi-hightech.com/en/blogs-events/blogs/2017/10/01/what-is-x-ray-fluorescence-xrf/, last accessed 30.07.2018.
Petzold, A. et al. 2013. Recommendations for the Interpretation of "Black Carbon" Measurements. In: Atmos. Chem. Phys., Vol.13, pp. 8365–8379. DOI:10.5194/acp-13-8365-2013
Polar Geospatial Center (PGC). 2018. ArcticDEM Release 7. Available at: https://www.pgc.umn.edu/news/arcticdem-release-7/, last accessed 29.04.2019
Rauch, J. N. and Pacyna, J. M. 2009. Earth's global Ag, Al, Cr, Cu, Fe, Ni, Pb, and Zn cycles. In: Global Biogeochemical Cycles, Vol.23, GB2001, doi:10.1029/2008GB003376
regional distribution of major elements. In: Science of the Total Environment, Vol.336, pp.183-199. doi:10.1016/j.scitotenv.2004.05.03
Reinardy, H. 2018. Arctic Environmental Pollution. The Science of a Stressful Environment. Presentation in course AS301, Longyearbyen.
Revich, B. A. 1995. Public health and ambient air pollution in arctic and subarctic cities of Russia. In: Sci Total Environ. Vol. 160-161(C), pp. 585-594. SSDI: 0048-9697(95)04393-2
Rozell, N. 2018. Fairbanks air earns an unwanted pollution ranking. Available at: https://www.adn.com/alaska-news/science/2018/12/01/fairbanks-air-earns-an-unwanted-pollution-ranking/, last accessed 10.03.2019
Sandström, J. W. N.d. The Snow Cover in Sweden. Available at: http://hydrologie.org/redbooks/a023/023009.pdf, last accessed 01.03.2019
Savinova, T. N. et al. 1995. Chemical Pollution in the Arctic and Sub-Arctic Marine Ecosystems: an Overview of Current Knowledge. NINA-fagrapport 1, pp. 1-68. ISSN: 0805-469X
Schmitt, C. 2019. LAHM. The Light Absorption Heating Method. Instrument manual provided by Dr. Carl Schmitt.
Schmitt, C. G. et al. 2015. Measurements of light-absorbing particles on the glaciers in the
Schoolmeester, T. et al. 2019. Global Linkages – A graphic look at the changing Arctic. UN Environment and GRID-Arendal. ISBN: 978-82-7701-190-5
Sharma, S. et al. 2002. Light absorption and thermal measurements of black carbon in different regions of Canada. In: Jr. of Geoph. Res. Vol. 107(D24), p. 4771. doi:10.1029/2002JD002496
Shaw, G. E. 1987. Chemical Air Mass Systems in Alaska. In: Atmospheric Environment Vol. 22, No. IO, pp. 2239-2248. DOI: doi.org/10.1016/0004-6981(88)90134-5
Sherrel, R.M. et al. 2000. Temporal variability of Cd, Pb, and Pb isotope deposition in central Greenland snow. In: An Electronic Journal of the Earth Sciences, Vol.1. ISSN: 1525-2027

Shindell, D. T. et al. 2008. A multi-model assessment of pollution transport to the Arctic. In: Atmos. Chem. Phys., Vol.8(17), pp.5353–5372. https://doi.org/10.5194/acp-8-5353-2008

Shrivastav, R. 2001. Atmospheric heavy metal pollution. Development of Chronological Records and Geochemical Monitoring. In: Resonance, pp. 62-66. DOI: 10.1007/BF02994594

Shulski, M. and Wendler, G. 2007. The Climate of Alaska. University of Alaska Press, Fairbanks. ISBN: 9781602230071

Simpson, B. 2019. The science of smoke: Fairbanks' particulate problem. Science for Alaska Lectures. January 29th 2019, Fairbanks, AK. Available at: https://www.gi.alaska.edu/events/science-alaska-lecture-series/463, last accessed 05.05.2019

Simpson, B. et al. 2018. Alaskan Layered Pollution And Chemical Analysis (ALPACA) White Paper. Available at: http://www.igacproject.org/publication/other-publications/alaskan-layered-pollution-and-chemical-analysis-alpaca-white-paper, last accessed 05.05.2019

Solbakken, C. F. 2017. Wood burning pollutes the urban air in Norway. Science Nordic. Available at: http://sciencenordic.com/wood-burning-pollutes-urban-air-norway, last accessed 16.09.2018.

Springston, S. R./ ARM Climate Research Facility/ Department of Energy (DOE). 2018. Particle Soot Absorption Photometer (PSAP) Instrument Handbook. Available at: https://www.arm.gov/publications/tech_reports/handbooks/psap_handbook.pdf, last accessed 25.03.2019

Starr, G. and Oberbauer, S. F. (2003). Photosynthesis of Arctic Evergreens under Snow. Implications for Tundra Ecosystem Carbon Balance. In. Ecology, Vol.84(6), pp.1415-1420. DOI. 10.1890/02-3154

Stendahl, J. 2019. About MarkInfo. Available at: https://www.slu.se/miljoanalys/statistik-och-miljodata/miljodata/webbtjanster-miljoanalys/markinfo/markinfo/om-markinfo/, last accessed 02.03.2019

Stuefer, M. 2019. Alaska climate prospects: Some like it hot. Science for Alaska Lectures. Available at: https://www.gi.alaska.edu/events/science-alaska-lecture-series/464, last accessed 02.03.2019

Sturm, M. et al. 2008. A Reconnaissance Snow Survey Across Northwest Territories and Nunavut, Canada, April 2007. ERDC/CRREL Technical Report TR-08-3, US Army Corps of Engineers Cold Regions Research and Engineering Laboratory, 80 pp.

Swedish Commission on Climate and Vulnerability (SCCV). 2007. Sweden facing climate change – threats and opportunities In: Swedish Government Official Reports, Vol. 60. Available at: https://www.government.se/contentassets/5f22ceb87f0d433898c918c2260e51aa/sweden-facing-climate-change-preface-and-chapter-1-to-3-sou-200760, last accessed 28.09.2017.

Swedish Meteorological and Hydrological Institute (SMHI). 2017a. Normalt största snödjup under vintern, medelvärde. Available at: http://www.smhi.se/klimatdata/meteorologi/sno/normalt-storsta-snodjup-under-vintern-medelvarde-1.7931, last accessed 01.03.2019

Swedish Meteorological and Hydrological Institute (SMHI). 2017b. Normal sista dag med snötäcke, medelvärde. Available at: http://www.smhi.se/klimatdata/meteorologi/sno/normal-sista-dag-med-snotacke-medelvarde-1.7935, last accessed 01.03.2019

Swedish Meteorological and Hydrological Institute (SMHI). 2017. Månads-, årstids- och årskartor. Normalt antal dygn med snötäcke per år. Available at:

http://www.smhi.se/klimatdata/meteorologi/sno/normalt-antal-dygn-med-snotacke-per-ar-1.7937, last accessed: 24.02.2019.
Swedish Meteorological and Hydrological Institute (SMHI). 2018a. Klimatindikator – antal dagar med snötäcke. Available at: http://www.smhi.se/klimat/klimatet-da-och-nu/klimatindikatorer/klimatindikator-antal-dagar-med-snotacke-1.91081, last accessed 01.03.2019
Swedish Meteorological and Hydrological Institute (SMHI). 2019a. Månads-, årstids- och årskartor. Normaldygnets medeltemperaturs månadsmedelvärde. Available at: http://www.smhi.se/klimatdata/meteorologi/kartor/monYrTable.php?myn=2001&par=normTmp, last accessed: 23.02.2019
Swedish Meteorological and Hydrological Institute (SMHI). 2019b. Normal uppmätt årsnederbörd, medelvärde 1961-1990. Available at: http://www.smhi.se/klimatdata/meteorologi/nederbord/normal-uppmatt-arsnederbord-medelvarde-1961-1990-1.4160, last accessed: 19.02.2019
Swedish Meteorological and Hydrological Institute (SMHI). 2019c. Månads-, årstids- och årskartor. Normal årsmedeltemperatur för perioden 1961-1990. Available at: https://www.smhi.se/klimatdata/meteorologi/kartor/monYrTable.php?myn=3&par=normYrTmp, last accessed: 19.02.2019
Syk, M. and Vollmer, J. 2018. Characterizing particulate carbon using dielectric property measurements. UPTEC W 18 004, Uppsala University.
Thaillandier, A.-S. et al. 2006. Evolution of the Snow Area Index of the Subarctic Snowpack in Central Alaska over a Whole Season. Consequences for the Air to Snow Transfer of Pollutants. In: Environ. Sci. Technol., Vol.40(24), pp. 7521–7527 DOI: 10.1021/es060842j
The Alaska Climate Research Center (ACRC). 2019. Station Map. Available at: http://akclimate.org/station-map, last accessed 06.04.2019
The Geological Survey of Sweden (Sveriges geologiska undersökning, SGU). 2018. Mines in Sweden. Available at: https://www.sgu.se/en/mining-inspectorate/mines/mines-in-sweden/?acceptCookies=true, last accessed: 02.03.2019
The University of Manchester. 2018. Multi Angle Absorption Photometer (MAAP) and Particulate Soot Absorption Photometer (PSAP). Available at: http://www.cas.manchester.ac.uk/restools/instruments/aerosol/maap/, last accessed 25.03.2019
Thompson, D. W. J. and Wallace, J.M. Annular modes in the extratropical circulation, Part I: Month-to-month variability. In: J.Climate, Vol.13, pp.1000–1016. https://doi.org/10.1175/1520-0442(2000)013<1000:AMITEC>2.0.CO;2
Troedsson, T. and Wiberg, M. 1986. Sveriges jordmåner, Södra bladet, Skala 1:1 000 000, Inst. f. Skoglig marklära, SLU, Uppsala (in Swedish).
Turpin, B. et al. 2007. Relationships of Indoor, Outdoor, and Personal Air (RIOPA): Part II. Analyses of Concentrations of Particulate Matter Species. In: Research Report (Health Effects Institute), Vol.10. Available at: https://www.researchgate.net/publication/5783252_Relationships_of_Indoor_Outdoor_and_Personal_Air_RIOPA_Part_II_Analyses_of_Concentrations_of_Particulate_Matter_Species/figures?lo=1, last accessed 10.05.2019
UK Air Pollution Information System – APIS. 2016. Glossary. Available at: http://www.apis.ac.uk/glossary.htm, last accessed 10.08.2018.
United States Department of Agriculture (USDA)/ Natural Resources Conservation Service (NRCS), Soils. N.d. Gelisols Map. Available at: https://www.nrcs.usda.gov/wps/portal/nrcs/detail/soils/survey/class/maps/?cid=stelprdb1237761, last accessed: 09.03.2019

United States Department of Agriculture (USDA)/ Natural Resources Conservation Service (NRCS). 1999. Soil Taxonomy. A Basic System of Soil Classification for Making and Interpreting Soil Surveys. Sec. Ed. Available at: https://www.nrcs.usda.gov/Internet/FSE_DOCUMENTS/nrcs142p2_051232.pdf, last accessed: 09.03.2019

United States Environmental Protection Agency (EPA). 2018. Particulate Matter (PM) Pollution. Available at: https://www.epa.gov/pm-pollution/particulate-matter-pm-basics#PM, last accessed 20.01.2019.

United States Geological Survey (USGS). 2018. Mineral Resources Online Spatial Data. Interactive maps and downloadable data for regional and global analysis. MRData Alaska. Available at: https://mrdata.usgs.gov/general/map-ak.html#settings, last accessed 10.03.2019

University Corporation for Environmental Research (UCAR). 2019. Aerosols: Tiny Particulates in the Air. Available at: https://scied.ucar.edu/aerosols, last accessed 20.01.2019.

Usibelli Coal Mine. 2015. Usibelli Coal Mine. Cleaner Energy - Brighter Future. Available at: http://www.usibelli.com/, last accessed 10.03.2019

Valavanidis, A. et al. 2008. Airborne Particulate Matter and Human Health: Toxicological Assessment and Importance of Size and Composition of Particles for Oxidative Damage and Carcinogenic Mechanisms. In: J. Env. Science & Health, Part C. Environmental Carcinogenesis and Ecotoxicology Reviews. Vol. 26 (4), pp. 339-362, DOI: 10.1080/10590500802494538

Van der Hoop, J. 2013. Bioamplification, Bioaccumulation and Bioconcentration. Available at: http://mercurypolicy.scripts.mit.edu/blog/?p=499, last accessed: 06.04.2019

Vanasupa, L. 2015. X-ray fluorescence (video). Available at: https://www.youtube.com/watch?v=9V2yRg05a9o, last accessed 16.03.2019

Vouk, V. B. and Piver, W. T. 1983. Metallic elements in fossil fuel combustion products: amounts and form of emissions and evaluation of carcinogenicity and mutagenicity. In: Environmental health perspectives, Vol.47, pp.201-225. doi:10.1289/ehp.8347201

Walsh, J. et al./ Alaska Climate Adaptation Science Center (AK CASC). 2018. New tool offers local climate information. Available at: https://casc.alaska.edu/news/new-tool-offers-local-climate-information, last accessed: 06.03.2019

Western Regional Climate Center (WRCC). 2019. Wind Information. Available at: https://wrcc.dri.edu/Climate/wind.php, last accessed 06.04.2019

Willers, S. et al. 2013. Fine and coarse particulate air pollution in relation to respiratory health in Sweden. In: European Respiratory Journal, Vol.42, pp. 924-934. DOI: 10.1183/09031936.00088212

Wolf, R. E. 2005. What is ICP-MS? ... and more importantly, what can it do? Available at: https://crustal.usgs.gov/laboratories/icpms/intro.html, last accessed 14.02.2019.

World Health Organisation (WHO). 2016. Fine particulate matter of 2.5 microns or less.

World Health Organization (WHO). 2018. Air pollution. Available at: https://www.who.int/airpollution/en/, last accessed 20.01.2019.

Yasunari, T. J. et al. 2012. Correction to “Influence of dust and black carbon on the snow albedo in the NASA Goddard Earth Observing System version 5 land surface model”. In: Journal of Geophysical Research, Vol.117, D18206. doi:10.1029/2012JD018691

Zdanowicz, C. 2018. Data sheet on sample locations. E-mail contact on 27th July 2018.

Zhang, L. et al. 2013. Review and uncertainty assessment of size-resolved scavenging coefficient formulations for below-cloud snow scavenging of atmospheric aerosols. In: Atmos. Chem. Phys., Vol.13, pp.10.005–10.025. doi: 10.5194/acp-13-10005-2013

Zhang, X. Y. et al. Carbonaceous aerosol composition over various regions of China during 2006. In: Journal of Geophysical Research, Vol.113, D14111. doi:10.1029/2007JD009525, 2008

Acknowledgements

I would like to express my heartfelt gratitude to my supervisor Dr. Youen Grusson at the Swedish University of Agricultural Sciences for his unwavering support and engagement throughout the process of writing this thesis, and for answering every one of my emails not only with insightful comments but with continued optimism and encouragement. I would also like to thank my supervisor Dr. Anders Svensson at the University of Copenhagen for his flexibility and understanding for all the twists and turns this thesis took. I also want to thank him for being such an outstanding and engaging teacher. His teaching inspired me to direct the rest of my studies towards the cryospheric sciences. Thank you also to my external supervisor Dr. Christian Zdanowicz at Uppsala University for letting me take a seat in his classes which laid the foundation not only for this thesis but for my amazement with the physical aspects of snow. I further want to thank him for helping me outline the topics within this thesis, and for providing advice and instruments for the field measurements. I also want to thank him for his in-depth advising throughout the writing process. My thanks also go to my second external supervisor and host, Dr. Martin Stuefer at the University of Alaska Fairbanks, for the unique opportunity to conduct my fieldwork and write my thesis in Interior Alaska. I would like to express my gratitude for his flexibility to let me carve out this project and for supporting me in exploring future opportunities.

My gratitude also goes to Dr. Jon-Petter Gustafsson who kindly accepted to be my examiner for this project and for spending days on reading this long document. Thank you very much as well to Dr. Tom Stevens who kindly introduced me to the pXRF laboratory and allowed me to use the instrument, Kiara Költringer for her unwavering enthusiasm in calibrating the pXRF, to Dr. Ulla Wideqvist and Dr. Johan Ström at the ACES laboratory in Stockholm who made the OC/EC measurements possible, and to Carl Schmidt who kindly carried out the LAHM analysis and helped me understand his instrument. Furthermore, I would like to thank Dr. Bill Simpson for giving me advice and access to his laboratory at UAF, Dr. Matthew Sturm for letting me borrow his snow sampling equipment, and Dr. Chris Waigl and Dr. Lea Hartl for driving me around Alaska to hunt for snow, and for keeping the mate supply and plotting advice coming. Thank you also to Kelly Burton, Jodi

Bailey and Thomas Heinrichs, who supported me in acquiring my snow samples and giving me access to sampling sites.

I would also like to acknowledge the German Academic Exchange Service as well as the Swedish Geographic Society for funding me throughout this last year and therefore making this thesis possible.

Finally, thank you to the greatest crew of friends a graduate student could hope to have. Thanks for making the last 3+ years in Copenhagen, Uppsala, and Fairbanks such a fun and wonderful time. Thank you also to my hosts Julie and Bob for the never-ending supply of excellent coffee and for letting me block every freezer in the house with snow samples. Doris and Harald, thank you for the unwavering and unconditional support, and for encouraging me to follow my passions and interests, even though it has meant extended periods of time away from home. My deepest gratitude goes to Duncan. Thank you for your endless support, for making even the longest nights bearable and for never ceasing to make me laugh.

Appendix

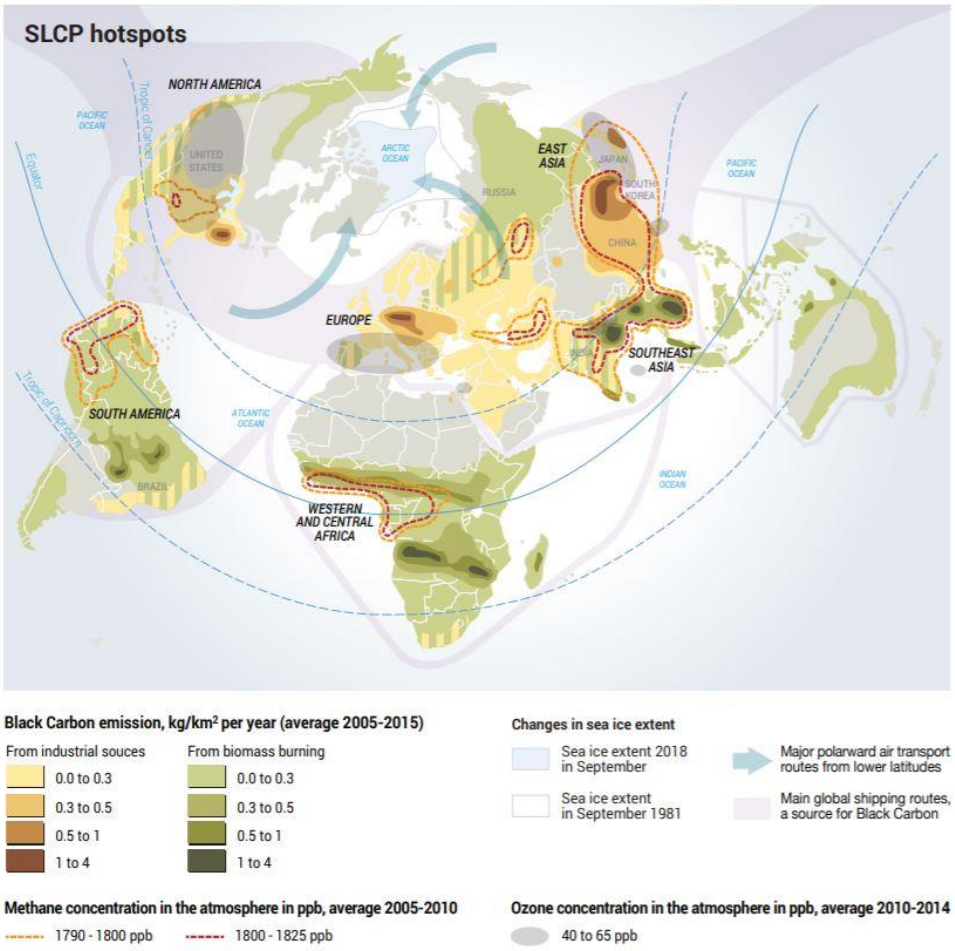

Figure A.1: Global short-lived climate pollutant (SLCP) emissions from industrial sources and biomass burning from 2005-2015 (Schoolmeester et al., 2019).

AHLSTROM

CERTIFICATE

We hereby certify that below product have levels of trace elements as presented below.

Article name: Pre-heated micro quartz fibre paper, MK 360

Batch/ Lot no: 3167
Prod. Date, yymmdd: 160427

Element		
Al	240	ppm
As	<0.3	ppm
Cd	<0.02	ppm
Co	0,03	ppm
Cr	2,5	ppm
Cu	<0.4	ppm
Fe	26,2	ppm
Hg	<0.04	ppm
Mg	22,7	ppm
Mn	1,46	ppm
Na	79,6	ppm
Ni	1,94	ppm
Pb	0,455	ppm
Sb	0,0185	ppm
Sn	<0.08	ppm
Tl	<0.08	ppm
V	0,0424	ppm
Zn	2,17	ppm

Falun 2016-10-25

Peter Fasen
Quality Manager

Figure A.2 Mean contamination levels of filter batch No. 3167 as provided by the manufacturer Munktell Ahlstrom Falun AB (pers. communication Hanna Olars, Customer Service Specialist, Advance Filtration 2019 at Ahlstrom-Munksjö Falun AB, 2019).

Element	MK 360
Al	25
As	0.2
Cd	< 0.02
Co	< 0.5
Cr	3.5
Cu	< 1
Fe	20
Hg	< 0.025
Mg	15
Mn	1
Na	10
Ni	0.5
Pb	0.3
Sb	< 1
Sn	< 0.5
Tl	1.5
V	< 0.5
Zn	3

Figure A.3: Typical Levels of Trace Elements in ppm as provided in the Filtration and Separation Technology Catalogue. Munktell Filter AB, N.d.

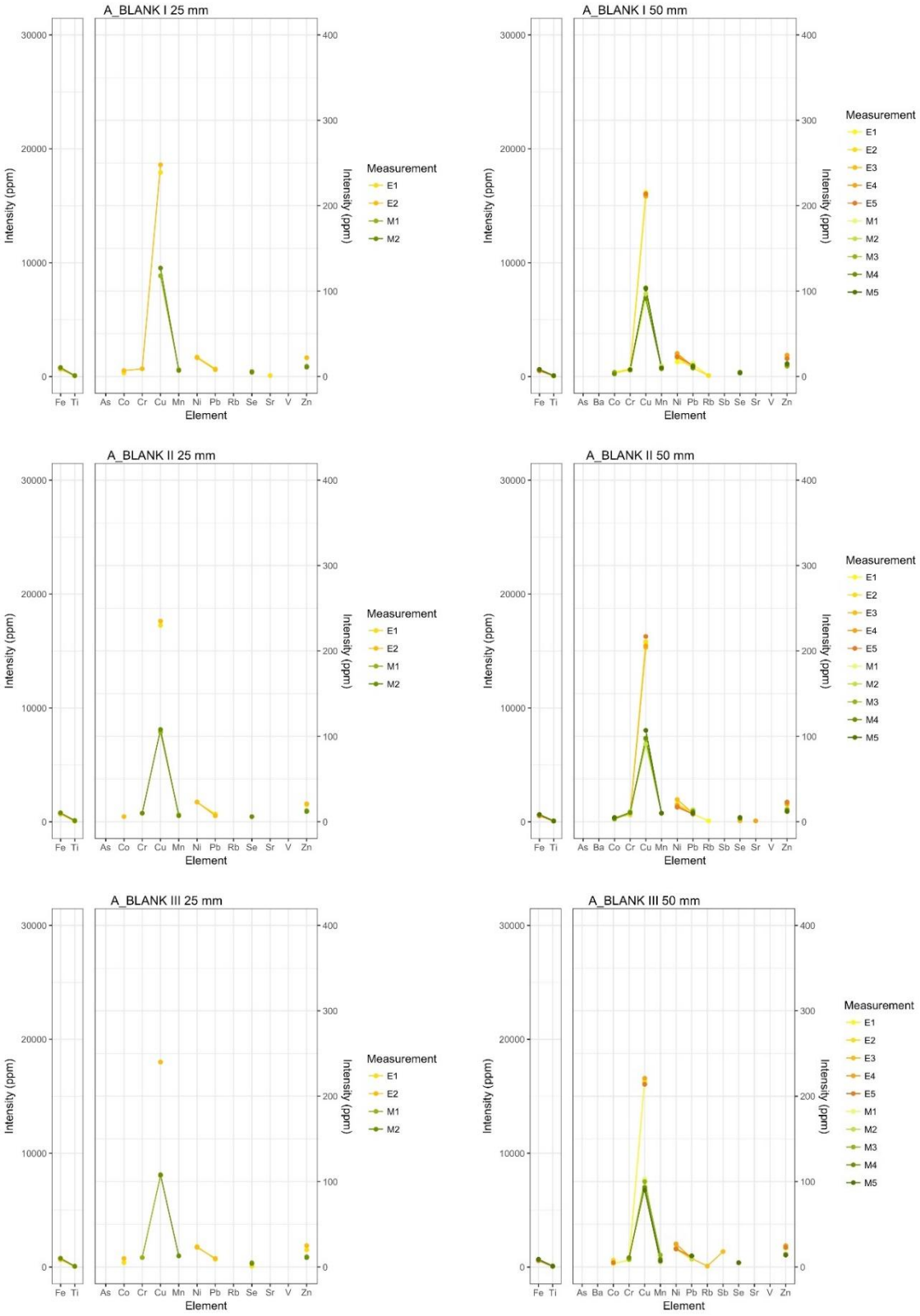

Figure A.4: Results of pXRF measurements of both calibrations on blank filters of both sizes (25mm, 50 mm).

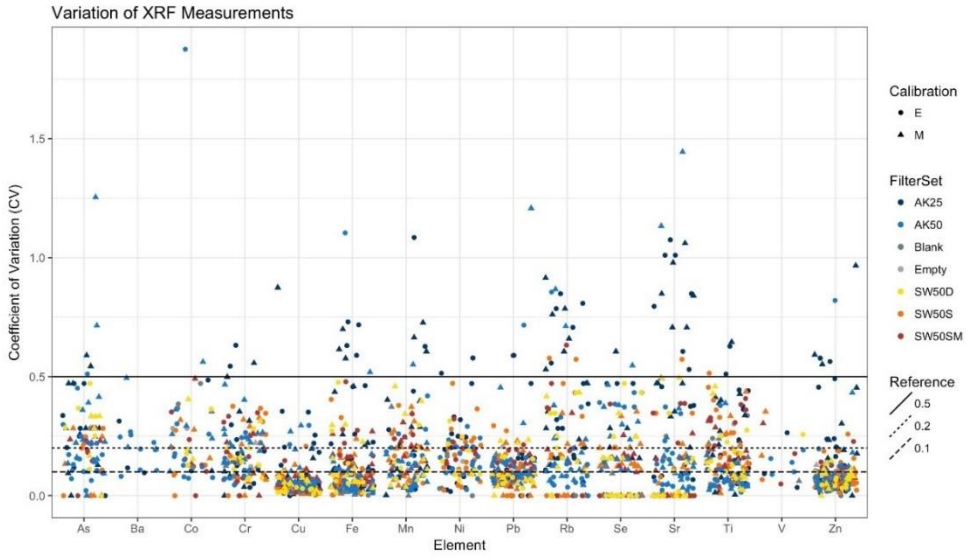

Figure A.5: Coefficient of Variation values of every filter in every set of filters ordered by element. The number of measurements on each filter varied depending on filter type and set (see 5.3).

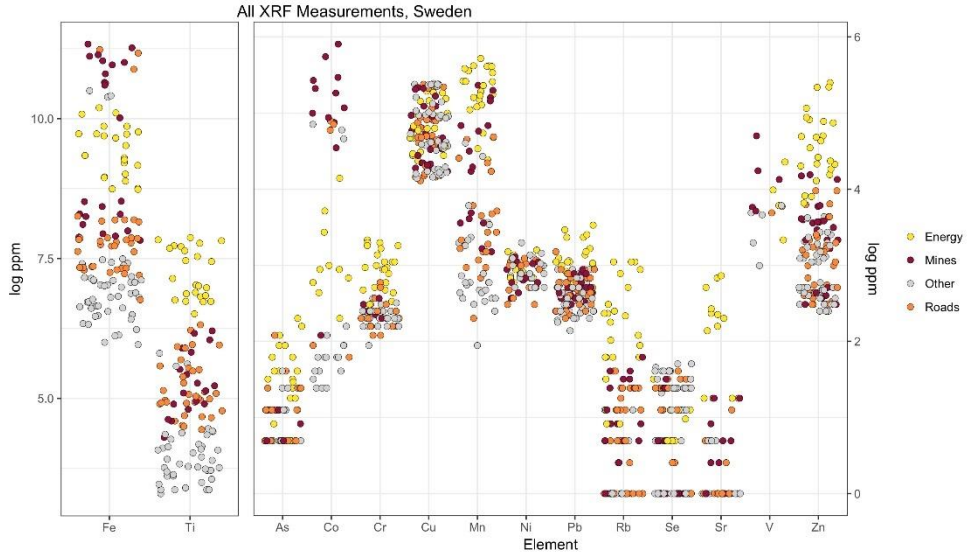

Figure A.6: Log-transformed data of trace elements levels for Sweden based grouped according to emission sources.

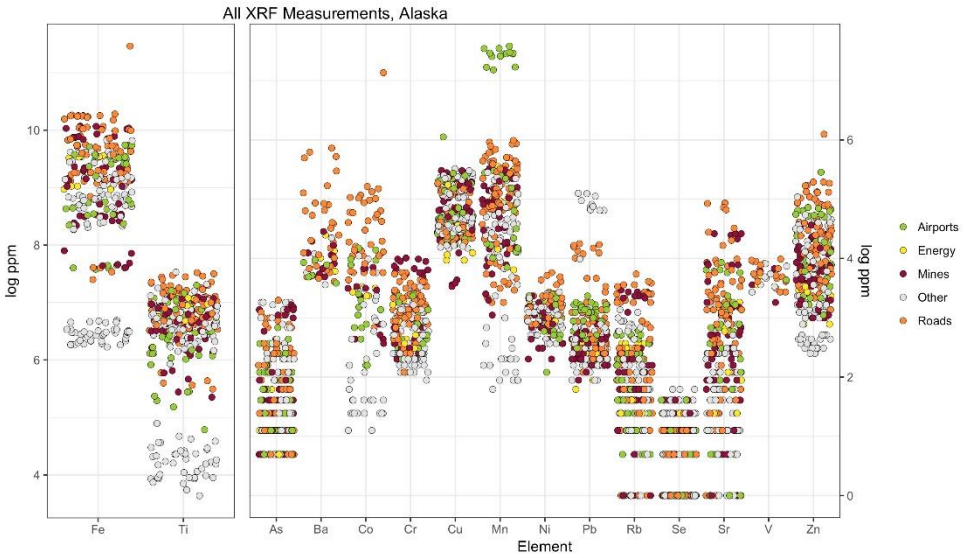

Figure A.7 Log-transformed data of trace elements levels for Alaska based on datasets AK25 and AK50 grouped according to emission sources.

Table A.1: Coefficients of Variation for filter set **AK25E** (snow meltwater from Alaska, 25 mm filters, measured with calibration GeoExploration (E)). Denali III has not been measured, '-' describe <LOD.

SampleID	Cal.	As	Ba	Co	Cr	Cu	Fe	Mn	Ni	Pb	Rb	Se	Sr	Ti	V	Zn
A_BLANK I	**E**	-	-	0.39	-	0.03	0.01	-	0.03	0.08	-	-	-	0.11	-	0.00
A_BLANK II	**E**	-	-	-	-	0.02	0.00	-	0.00	0.18	-	-	-	0.34	-	0.03
A_BLANK III	**E**	-	-	0.47	-	0.00	0.00	-	0.03	0.07	-	-	-	0.15	-	0.16
A1 CS	**E**	-	-	-	-	0.02	0.02	-	0.12	0.07	0.00	-	0.00	0.06	-	0.02
A2 DHD	**E**	-	-	-	-	0.07	0.46	-	0.20	0.18	0.85	-	0.61	0.38	-	0.16
A3 RR	**E**	-	-	-	0.13	0.02	0.03	0.08	0.02	0.07	0.00	-	0.07	0.05	-	0.01
A4 HSR	**E**	-	-	-	0.54	0.00	0.04	0.25	0.25	0.11	0.16	-	0.09	0.05	-	0.07
A5 GPH 0	**E**	0.00	-	-	0.14	0.09	0.22	0.63	0.32	0.00	0.39	0.00	0.53	0.17	0.09	0.20
A8 GPH IV	**E**	0.00	-	-	0.11	0.04	0.04	0.03	0.05	0.16	0.16	-	0.08	0.09	-	0.13
A9 DPR 0	**E**	0.34	0.31	0.49	0.05	0.22	0.15	0.17	0.02	0.06	0.32	0.47	0.38	0.05	0.03	0.19
A12 DPR III	**E**															
A13 AIR	**E**	0.20	-	-	0.19	0.06	0.12	0.21	0.08	0.00	0.11	0.00	0.13	0.12	-	0.13
A14 AIR_L	**E**	0.25	-	-	-	0.13	0.73	-	0.19	0.16	0.20	0.00	1.07	0.63	-	0.46
A15 JOH	**E**	0.12	0.10	0.10	0.03	0.04	0.11	0.28	0.26	0.10	0.17	-	0.08	0.23	-	0.06
A16 JOH_M	**E**	-	0.12	-	0.18	0.25	0.26	0.44	0.33	0.17	0.47	0.47	0.46	0.15	0.26	0.24
A17 SKI	**E**	-	-	-	-	-	-	-	-	-	-	-	-	-	-	-
A18 PF	**E**	0.47	-	-	-	0.35	0.72	-	0.47	0.59	0.79	-	1.01	0.51	-	0.49
A19 DK	**E**	0.28	-	-	0.63	0.18	0.63	-	0.58	0.47	0.81	-	0.85	0.44	-	0.58
A20 DD	**E**	0.47	-	-	0.30	0.35	0.46	1.08	0.11	0.59	0.56	0.47	0.80	0.36	-	0.24
A21 USCR	**E**	-	-	-	-	0.20	0.59	-	0.03	0.08	0.71	-	1.01	0.44	-	0.56
A22 AIR_C	**E**	0.28	-	-	0.24	0.03	0.13	-	0.51	0.00	0.28	-	0.00	0.13	-	0.10
A23 NOAA	**E**	0.09	-	-	-	0.07	0.22	-	0.25	0.16	0.28	-	0.38	0.15	-	0.10
MEAN		**0.23**	**0.18**	**0.36**	**0.23**	**0.11**	**0.25**	**0.35**	**0.19**	**0.17**	**0.37**	**0.24**	**0.44**	**0.23**	**0.13**	**0.20**
MEAN	**0.242**															

Table A.2: Coefficients of Variation for filter set **AK25M** (snow meltwater from Alaska, 25 mm filters, measured with calibration GeoMining (M)). Denali III has not been measured, '-' describes <LOD.

SampleID	Cal.	As	Ba	Co	Cr	Cu	Fe	Mn	Ni	Pb	Rb	Se	Sr	Ti	V	Zn
A_BLANK I	**M**	-	-	-	0.05	0.02	0.09	-	-	-	0.13	-	0.14	-	0.06	-
A_BLANK II	**M**	-	-	-	-	0.02	0.01	0.09	-	-	-	0.00	-	0.22	-	0.06
A_BLANK III	**M**	-	-	-	-	0.01	0.00	-	-	-	-	0.16	-	0.16	-	0.06
A1 CS	**M**	-	-	-	-	0.01	0.02	0.07	-	-	0.47	0.00	0.47	0.08	-	0.03
A2 DHD	**M**	-	-	-	-	0.01	0.44	0.40	-	-	-	0.16	0.71	0.40	-	0.18
A3 RR	**M**	0.28	-	-	0.08	0.04	0.02	0.03	-	-	0.13	0.16	0.00	0.00	-	0.02
A4 HSR	**M**	-	-	-	0.10	0.05	0.04	0.12	-	-	0.00	0.00	0.00	0.02	-	0.00
A5 GPH 0	**M**	0.13	-	-	0.18	0.03	0.22	0.29	-	-	0.47	0.00	0.47	0.27	-	0.19
A8 GPH IV	**M**	0.47	-	-	0.31	0.04	0.04	0.02	-	-	0.16	0.00	0.16	0.15	-	0.12
A9 DPR 0	**M**	0.26	-	-	0.09	0.10	0.15	0.15	-	-	0.24	0.28	0.33	0.01	-	0.23
A12 DPR III	**M**															
A13 AIR	**M**	0.28	-	-	0.08	0.04	0.12	0.11	-	-	0.24	0.20	0.20	0.10	-	0.12
A14 AIR_L	**M**	0.59	-	-	-	0.87	0.12	0.00	-	-	0.61	-	0.84	0.65	-	0.97
A15 JOH	**M**	0.09	-	0.10	0.04	0.07	0.10	0.11	-	-	0.06	0.28	0.09	0.23	-	0.06
A16 JOH_M	**M**	0.28	-	-	0.50	0.06	0.26	0.21	-	-	0.53	0.61	0.49	0.12	-	0.19
A17 SKI	**M**	0.47	-	-	0.00	0.05	0.09	0.19	-	-	0.00	0.00	0.47	0.17	-	0.07
A18 PF	**M**	-	-	-	0.08	0.08	0.70	0.73	-	-	0.92	0.16	0.98	0.41	-	0.45
A19 DK	**M**	-	-	-	0.35	0.09	0.61	0.66	-	-	0.76	0.16	0.85	0.39	-	0.59
A20 DD	**M**	0.54	-	-	0.56	0.20	0.46	0.40	-	-	0.66	0.20	0.71	0.34	-	0.30
A21 USCR	**M**	-	-	-	-	0.08	0.58	0.61	-	-	0.79	0.00	1.06	0.43	-	0.55
A22 AIR_C	**M**	-	-	-	-	0.06	0.12	0.11	-	-	0.28	0.00	0.00	0.21	-	0.03
A23 NOAA	**M**	0.00	-	-	-	0.16	0.21	0.29	-	-	0.35	0.16	0.35	0.16	-	0.16
MEAN		**0.31**	**-**	**0.10**	**0.19**	**0.10**	**0.21**	**0.24**	**-**	**-**	**0.38**	**0.13**	**0.44**	**0.23**	**0.06**	**0.22**
MEAN	**0.238**															

Table A.3: Coefficients of Variation for filter set **AK50E** (snow meltwater from Alaska, 50 mm filters, measured with calibration GeoExploration (E)). '-' describe <LOD.

SampleID	Cal.	As	Ba	Co	Cr	Cu	Fe	Mn	Ni	Pb	Rb	Se	Sr	Ti	V	Zn
A_BLANK I	**E**	-	-	0.12	0.08	0.01	0.02	-	0.17	0.12	0.00	-	-	0.24	-	0.07
A_BLANK II	**E**	-	-	0.13	0.08	0.02	0.03	-	0.18	0.09	-	-	0.00	0.15	-	0.06
A_BLANK III	**E**	-	-	0.37	-	0.01	0.02	-	0.11	0.13	-	-	-	0.06	-	0.06
A1 CS	**E**	0.15	-	-	0.07	0.02	0.05	-	0.29	0.13	0.00	-	0.05	0.05	-	0.04
A2 DHD	**E**	0.25	-	0.15	0.14	0.06	0.02	0.18	0.03	0.16	0.11	0.00	0.15	0.03	0.19	0.05
A3 RR	**E**	0.10	0.20	0.26	0.21	0.06	0.05	0.09	0.09	0.08	0.13	0.37	0.13	0.04	-	0.08
A4 HSR	**E**	0.45	0.27	0.07	0.11	0.05	0.02	0.04	0.23	0.16	0.04	0.00	0.06	0.04	0.14	0.03
A5 GPH 0	**E**	0.51	0.11	1.88	0.14	0.21	1.10	0.42	0.10	0.72	0.86	0.38	0.23	0.11	-	0.82
A8 GPH IV	**E**	0.15	-	-	0.24	0.02	0.11	0.20	0.16	0.07	0.20	-	0.15	0.11	-	0.11
A9 DPR 0	**E**	0.11	0.08	0.08	0.05	0.04	0.03	0.06	0.21	0.09	0.05	0.39	0.05	0.06	0.16	0.05
A12 DPR III	**E**	0.22	0.25	0.08	0.15	0.05	0.02	0.03	0.10	0.06	0.37	-	0.03	0.04	-	0.03
A13 AIR	**E**	0.11	-	-	-	0.02	0.03	-	0.13	0.09	0.06	0.00	0.37	0.11	-	0.14
A14 AIR_L	**E**	0.07	0.11	0.12	-	0.04	0.02	0.03	0.24	0.10	0.05	0.00	0.02	0.01	-	0.02
A15 JOH	**E**	0.13	0.25	0.13	0.11	0.04	0.09	0.11	0.14	0.09	0.13	0.37	0.16	0.05	0.10	0.08
A16 JOH_M	**E**	0.16	-	-	0.14	0.02	0.01	0.28	0.12	0.14	0.08	0.00	0.02	0.03	-	0.02
A17 SKI	**E**	0.17	-	-	0.07	0.02	0.02	-	0.18	0.15	0.10	-	0.07	0.04	-	0.08
A18 PF	**E**	0.22	-	-	0.27	0.03	0.10	-	0.16	0.15	0.07	0.00	0.18	0.07	-	0.06
A19 DK	**E**	0.22	-	0.18	0.11	0.02	0.04	0.13	0.07	0.12	0.08	0.43	0.09	0.04	-	0.09
A20 DD	**E**	0.02	0.19	0.30	0.16	0.04	0.04	0.17	0.21	0.11	0.08	0.43	0.04	0.09	0.09	0.20
A21 USCR	**E**	0.30	-	-	0.08	0.06	0.12	0.26	0.21	0.08	0.14	0.00	0.19	0.06	-	0.12
A22 AIR_C	**E**	0.17	-	-	0.10	0.30	0.06	-	0.11	0.05	0.33	-	0.34	0.38	-	0.02
A23 NOAA	**E**	0.06	0.22	0.16	-	0.05	0.03	0.15	0.20	0.14	0.04	0.00	0.04	0.07	-	0.07
MEAN		**0.19**	**0.19**	**0.29**	**0.13**	**0.06**	**0.09**	**0.15**	**0.16**	**0.14**	**0.15**	**0.17**	**0.12**	**0.09**	**0.14**	**0.10**
MEAN	**0.136**															

Table A.4: Coefficients of Variation for filter set **AK50M** (snow meltwater from Alaska, 50 mm filters, measured with calibration GeoMining (M)). '-' describe <LOD.

SampleID	Cal.	As	Ba	Co	Cr	Cu	Fe	Mn	Ni	Pb	Rb	Se	Sr	Ti	V	Zn
A_BLANK I	**M**	-	-	0.35	0.13	0.06	0.02	0.12	-	0.17	-	0.09	-	0.24	-	0.08
A_BLANK II	**M**	-	-	0.20	0.12	0.06	0.02	0.00	-	0.15	-	0.12	-	0.20	-	0.10
A_BLANK III	**M**	-	-	-	0.14	0.06	0.02	0.37	-	0.11	-	0.00	-	0.14	-	0.04
A1 CS	**M**	0.22	-	-	-	0.06	0.08	0.05	-	0.05	0.12	0.11	0.14	0.09	-	0.09
A2 DHD	**M**	0.39	-	-	0.19	0.10	0.03	0.08	-	0.09	0.07	0.15	0.12	0.02	-	0.04
A3 RR	**M**	0.10	0.20	0.26	0.21	0.06	0.05	0.09	0.09	0.08	0.13	0.37	0.13	0.04	-	0.08
A4 HSR	**M**	0.15	-	-	0.28	0.06	0.01	0.02	-	0.09	0.04	0.14	0.03	0.04	-	0.04
A5 GPH 0	**M**	0.23	-	-	0.15	0.12	0.14	0.17	-	0.04	0.18	0.30	0.17	0.17	-	0.09
A8 GPH IV	**M**	0.16	-	-	0.25	0.05	0.03	0.04	-	0.07	0.24	0.25	0.16	0.03	-	0.08
A9 DPR 0	**M**	0.10	0.20	0.18	0.14	0.02	0.04	0.05	-	0.07	0.06	0.46	0.08	0.07	-	0.06
A12 DPR III	**M**	0.00	-	-	0.24	0.04	0.09	0.22	-	0.09	-	0.00	0.00	0.11	-	0.14
A13 AIR	**M**	0.23	-	0.29	0.27	0.03	0.01	0.04	-	0.12	0.06	0.24	0.05	0.07	-	0.02
A14 AIR_L	**M**	0.13	-	0.36	0.14	0.05	0.03	0.04	-	0.07	0.08	0.38	0.07	0.04	-	0.03
A15 JOH	**M**	0.36	0.49	0.56	0.22	0.08	0.17	0.17	-	0.30	0.38	0.55	0.37	0.09	-	0.13
A16 JOH_M	**M**	0.28	-	-	0.22	0.06	0.11	0.13	-	0.15	0.10	0.15	0.09	0.13	-	0.06
A17 SKI	**M**	0.09	-	-	0.26	0.06	0.06	0.06	-	0.05	0.15	0.11	0.00	0.04	-	0.04
A18 PF	**M**	0.25	-	-	0.40	0.04	0.07	0.14	-	0.09	0.14	0.00	0.16	0.10	-	0.06
A19 DK	**M**	1.25	-	-	0.26	0.29	0.08	0.07	-	0.11	0.71	0.15	1.44	0.06	-	0.18
A20 DD	**M**	0.41	-	0.24	0.19	0.20	0.17	0.08	-	0.45	0.24	0.31	0.24	0.07	-	0.10
A21 USCR	**M**	0.28	-	-	0.22	0.06	0.11	0.13	-	0.15	0.10	0.15	0.09	0.13	-	0.06
A22 AIR_C	**M**	0.71	-	-	0.47	0.19	0.52	0.55	-	1.21	0.87	0.11	1.13	0.39	-	0.43
A23 NOAA	**M**	0.14	-	0.10	-	0.27	0.10	0.11	-	0.08	0.11	0.16	0.12	0.08	-	0.12
MEAN		**0.29**	**0.30**	**0.28**	**0.22**	**0.09**	**0.09**	**0.12**	**0.09**	**0.17**	**0.21**	**0.20**	**0.24**	**0.11**	**-**	**0.09**
MEAN	**0.170**															

Table A.5: Coefficients of Variation for filter set **SW50SE** (snow meltwater from Sweden, 50 mm filters, single filters, measured with calibration GeoExploration (E)). '-' describe <LOD.

SampleID	Cal.	As	Ba	Co	Cr	Cu	Fe	Mn	Ni	Pb	Rb	Se	Sr	Ti	V	Zn
UM01C+D	**E**	0.11	-	0.27	0.37	0.03	0.11	0.18	0.23	0.05	0.09	0.00	0.11	0.18	-	0.10
UM01A+B	**E**	0.20	-	-	0.31	0.01	0.14	0.26	0.15	0.11	0.16	-	0.08	0.18	-	0.16
UM02A+B	**E**	0.25	-	-	0.09	0.01	0.40	0.21	0.20	0.07	0.57	0.00	0.25	0.46	-	0.26
UM02C+D	**E**	0.00	-	-	0.35	0.04	0.03	0.17	0.19	0.11	0.17	-	0.11	0.12	-	0.01
LU01A	**E**	-	-	-	0.07	0.02	0.09	-	0.12	0.06	-	-	-	0.51	-	0.06
LU01A2	**E**	-	-	0.13	0.00	0.02	0.06	-	0.14	0.00	-	-	-	0.26	-	0.06
LU01B+C	**E**	-	-	-	0.17	0.02	0.10	-	0.20	0.12	0.00	-	0.00	0.13	-	0.06
LU01D+E	**E**	0.00	-	-	0.38	0.01	0.05	-	0.23	0.13	-	-	0.00	0.16	-	0.04
AR01C+D	**E**	0.28	-	-	0.22	0.02	0.07	-	0.02	0.14	0.00	-	0.00	0.06	-	0.07
AR01A+B	**E**	0.28	-	-	-	0.01	0.06	-	0.06	0.08	-	-	0.00	0.16	-	0.02
LY01A+B	**E**	0.22	-	-	0.26	0.03	0.10	-	0.09	0.09	0.33	-	0.35	0.13	-	0.14
LY01C+D	**E**	-	-	-	-	0.01	0.00	-	0.11	0.00	0.00	-	0.00	0.12	-	0.02
KR01A+B	**E**	-	-	0.09	-	0.21	0.33	0.05	0.47	0.08	0.58	0.00	0.57	0.26	-	0.19
KR01C+D	**E**	-	-	0.09	-	0.11	0.06	0.38	0.21	0.10	0.17	0.00	0.00	0.11	0.07	0.03
GA01A+B+C	**E**	-	-	-	-	0.00	0.19	-	0.12	0.05	-	-	0.00	0.21	-	0.11
GA01D+E	**E**	-	-	-	-	0.02	0.10	-	0.36	0.10	-	-	0.35	0.15	-	0.04
PU01A+B	**E**	-	-	-	-	0.03	0.11	-	0.28	0.06	0.47	-	0.00	0.21	-	0.07
PU01C+D	**E**	-	-	-	-	0.01	0.06	-	0.22	0.17	-	-	-	0.33	-	0.07
JK01A+B	**E**	-	-	0.13	0.00	0.02	0.11	-	0.17	0.08	0.00	-	-	0.40	-	0.02
JK01C+D	**E**	-	-	-	-	0.01	0.10	-	0.09	0.00	-	-	-	0.08	-	0.07
SV01A+B	**E**	-	-	0.00	-	0.02	0.01	-	0.04	0.06	-	-	-	0.05	-	0.19
SV01C+D	**E**	-	-	0.20	-	0.01	0.05	-	0.04	0.27	-	-	-	-	-	0.07
AB01A+B	**E**	-	-	-	-	0.01	0.07	-	0.18	0.15	-	-	-	-	-	0.03
AB01C+D	**E**	-	-	-	0.07	0.01	0.06	-	0.24	0.29	-	-	0.00	0.36	-	0.05
MEAN		**0.17**	**-**	**0.13**	**0.19**	**0.03**	**0.10**	**0.21**	**0.17**	**0.10**	**0.21**	**0.00**	**0.11**	**0.21**	**0.07**	**0.08**
MEAN	**0.127**															

Table A.6: Coefficients of Variation for filter set **SW50SM** (snow meltwater from Sweden, 50 mm filters, single filters, measured with calibration GeoMining (M)). '-' describe <LOD.

SampleID	Cal.	As	Ba	Co	Cr	Cu	Fe	Mn	Ni	Pb	Rb	Se	Sr	Ti	V	Zn
UM01C+D	M	0.13	-	-	0.15	0.04	0.08	0.09	-	0.05	0.13	0.22	0.05	0.12	-	0.08
UM01A+B	M	0.33	-	-	0.33	0.02	0.07	0.08	-	0.03	0.00	0.33	0.12	0.09	-	0.10
UM02A+B	M	-	-	-	0.32	0.09	0.04	0.14	-	0.04	0.22	0.13	0.16	0.01	-	0.07
UM02C+D	M	0.25	-	-	0.29	0.08	0.04	0.04	-	0.09	0.22	0.00	0.17	0.09	-	0.03
LU01 A	M	-	-	-	0.06	0.09	0.09	0.31	-	0.11	-	0.20	-	0.03	-	0.04
LU01A2	M	-	-	-	0.22	0.07	0.09	0.37	-	0.11	-	0.12	-	0.07	-	0.09
LU01B+C	M	-	-	-	-	0.09	0.11	0.35	-	0.00	-	0.35	0.00	0.44	-	0.04
LU01D+E	M	-	-	-	0.11	0.04	0.05	0.14	-	0.08	0.00	0.11	0.00	0.22	-	0.07
AR01C+D	M	0.00	-	-	-	0.10	0.02	0.16	-	0.04	-	0.20	0.00	0.14	-	0.04
AR01A+B	M	-	-	-	-	0.06	0.05	0.07	-	0.08	-	0.13	0.00	0.12	-	0.04
LY01A+B	M	0.28	-	-	-	0.03	0.08	0.04	-	0.10	0.22	0.13	0.00	0.07	-	0.11
LY01C+D	M	0.00	-	-	-	0.03	0.06	0.06	-	0.19	0.35	0.20	-	0.18	-	0.09
KR01A+B	M	-	-	0.32	-	0.02	0.18	0.13	-	0.04	0.12	0.00	0.16	-	0.17	0.04
KR01C+D	M	-	-	0.28	-	0.13	0.17	0.20	-	0.13	0.16	0.00	0.22	-	0.35	0.10
GA01A+B+C	M	-	-	-	-	0.03	0.16	0.21	-	0.10	-	0.00	-	0.26	-	0.08
GA01D+E	M	-	-	-	0.26	0.08	0.24	0.20	-	0.23	-	0.00	0.00	0.08	-	0.05
PU01A+B	M	-	-	-	-	0.05	0.07	0.07	-	0.05	-	0.12	0.00	0.08	-	0.05
PU01C+D	M	-	-	-	-	0.05	0.07	0.27	-	0.00	-	0.13	-	0.26	-	0.04
JK01C+D	M	0.28	-	-	0.14	0.05	0.01	0.15	-	0.17	-	0.00	-	0.13	-	0.04
JK01A+B	M	-	-	-	0.07	0.05	0.06	0.05	-	0.11	-	0.00	-	0.33	-	0.09
SV01A+B	M	-	-	0.16	-	0.07	0.04	0.20	-	0.09	-	0.20	-	-	-	0.06
SV01C+D	M	-	-	-	0.00	0.07	0.01	0.10	-	0.22	-	0.20	-	0.20	-	0.09
AB01A+B	M	-	-	-	-	0.04	0.05	0.27	-	0.00	-	0.12	-	-	-	0.05
AB01C+D	M	-	-	-	0.26	0.03	0.05	0.20	-	0.10	-	0.12	-	0.15	-	0.08
MEAN		**0.18**	**-**	**0.25**	**0.18**	**0.06**	**0.08**	**0.16**	**-**	**0.09**	**0.16**	**0.13**	**0.07**	**0.15**	**0.26**	**0.07**
MEAN	**0.115**															

Table A.7: Coefficients of Variation for filter set **SW50SME** (snow meltwater from Sweden, 50 mm filters, mean of single filters from each snowpack, measured with calibration GeoExploration (E)) and for filter set **SW50SMM** (see above, measured with calibration GeoMining (M)) '-' describe <LOD.

SampleID	Cal.	As	Ba	Co	Cr	Cu	Fe	Mn	Ni	Pb	Rb	Se	Sr	Ti	V	Zn
AB01	E	-	-	0.24	0.07	0.01	0.17	-	0.19	0.21	-	-	0.00	0.36	-	0.05
AR01	E	0.23	-	0.00	0.16	0.02	0.06	-	0.20	0.14	0.00	-	0.00	0.11	-	0.05
GA01	E	-	-	-	-	0.01	0.14	-	0.24	0.19	0.47	-	0.39	0.16	-	0.07
JK01	E	-	-	0.10	0.06	0.01	0.13	-	0.13	0.07	0.00	-	-	0.33	-	0.04
KR01	E	-	-	0.12	-	0.15	0.22	0.34	0.32	0.12	0.37	0.38	0.35	0.18	0.05	0.12
LU01	E	0.00	-	0.13	0.33	0.02	0.48	-	0.15	0.10	0.00	-	0.00	0.41	-	0.10
LY01	E	0.18	-	-	0.18	0.02	0.28	-	0.14	0.14	0.63	-	0.39	0.31	-	0.10
PU01	E	-	-	-	0.00	0.03	0.17	-	0.23	0.13	0.43	0.00	0.00	0.38	-	0.06
SV01	E	-	-	0.15	0.07	0.02	0.04	-	0.10	0.19	-	-	-	0.04	-	0.14
UM01	E	0.15	-	0.35	0.35	0.03	0.16	0.26	0.17	0.08	0.19	0.00	0.15	0.21	-	0.13
UM02	E	0.19	-	-	0.31	0.02	0.27	0.24	0.20	0.11	0.37	0.00	0.22	0.31	0.18	0.23
MEAN		**0.15**	**-**	**0.16**	**0.17**	**0.03**	**0.19**	**0.28**	**0.19**	**0.14**	**0.27**	**0.10**	**0.17**	**0.25**	**0.11**	**0.10**
MEAN	**0.164**															
AB01	M	-	-	-	0.18	0.06	0.16	0.23	-	0.10	-	0.11	-	0.13	-	0.07
AR01	M	0.00	-	-	-	0.08	0.04	0.17	-	0.06	-	0.17	0.00	0.15	-	0.08
GA01	M	-	-	-	0.22	0.07	0.13	0.21	-	0.17	0.00	0.12	0.00	0.19	-	0.07
JK01	M	0.28	-	-	0.09	0.06	0.07	0.13	-	0.14	-	0.00	-	0.29	-	0.07
KR01	M	-	-	0.49	-	0.11	0.27	0.24	-	0.10	0.20	0.00	0.26	-	0.30	0.11
LU01	M	-	-	-	0.20	0.07	0.08	0.31	-	0.10	-	0.16	-	0.09	-	0.07
LY01	M	0.22	-	-	-	0.06	0.26	0.21	-	0.14	0.35	0.17	0.00	0.31	-	0.10
PU01	M	-	-	-	-	0.05	0.17	0.20	-	0.04	-	0.12	0.00	0.32	-	0.07
SV01	M	-	-	0.13	0.00	0.06	0.04	0.14	-	0.14	-	0.16	-	0.19	-	0.09
UM01	M	0.24	-	-	0.25	0.05	0.10	0.09	-	0.09	0.14	0.25	0.11	0.12	-	0.08
UM02	M	0.23	-	-	0.26	0.08	0.06	0.11	-	0.10	0.19	0.10	0.16	0.06	-	0.12
MEAN		**0.19**	**-**	**0.31**	**0.17**	**0.07**	**0.12**	**0.18**	**-**	**0.11**	**0.18**	**0.13**	**0.07**	**0.19**	**0.30**	**0.09**
MEAN	**0.136**															

Table A.8: Coefficients of Variation for filter set **SW50DE** (snow meltwater from Sweden, 50 mm filters, double filter measurements, measured with calibration Geo-Exploration (E)) and **SW50DM** (see above, measured with calibration GeoMining (M)) '-' describe <LOD.

SampleID	Cal.	As	Ba	Co	Cr	Cu	Fe	Mn	Ni	Pb	Rb	Se	Sr	Ti	V	Zn
UM01	M	0.17	-	0.15	0.20	0.06	0.12	0.11	-	0.23	0.12	0.25	0.14	0.10	-	0.13
UM02	M	0.33	-	-	0.17	0.07	0.03	0.07	-	0.22	0.10	0.25	0.10	0.07	-	0.08
LU01	M	-	-	-	-	0.08	0.07	0.04	-	0.08	-	0.25	-	0.02	-	0.11
AR01	M	0.28	-	-	0.16	0.02	0.30	0.46	-	0.06	0.00	0.16	0.00	0.11	-	0.11
LY01	M	0.33	-	-	0.20	0.09	0.01	0.09	-	0.23	0.25	0.16	0.00	0.03	-	0.03
KR01	M	-	-	0.40	-	0.06	0.23	0.34	-	0.07	0.42	0.35	0.49	-	-	0.15
GA01	M	-	-	-	-	0.04	0.30	0.20	-	0.04	0.43	0.00	0.00	0.43	-	0.09
PU01	M	-	-	-	0.07	0.08	0.03	0.14	-	0.09	0.00	0.16	0.00	0.09	-	0.00
JK01	M	-	-	-	0.31	0.02	0.16	0.15	-	0.00	-	0.16	-	0.25	-	0.05
SV01	M	-	-	-	-	0.08	0.06	0.04	-	0.09	-	0.16	-	-	-	0.08
AB01	M	-	-	-	-	0.05	0.08	0.40	-	0.05	-	0.00	-	0.46	-	0.05
MEAN		**0.28**	**-**	**0.28**	**0.18**	**0.06**	**0.13**	**0.18**	**-**	**0.11**	**0.19**	**0.17**	**0.11**	**0.17**	**-**	**0.08**
MEAN	**0.142**															
UM01	E	0.11	-	0.36	0.13	0.03	0.06	0.07	0.06	0.05	0.00	0.00	0.02	0.13	0.26	0.03
UM02	E	0.29	-	-	0.11	0.02	0.09	0.12	0.09	0.08	0.14	0.47	0.49	0.14	-	0.09
LU01	E	0.47	-	0.18	0.07	0.03	0.27	-	0.19	0.16	0.43	0.00	0.00	0.28	-	0.07
AR01	E	0.33	-	-	0.14	0.03	0.06	-	0.31	0.06	0.35	-	0.35	0.14	-	0.08
LY01	E	0.37	-	-	0.28	0.01	0.05	-	0.25	0.10	0.16	0.00	0.00	0.10	-	0.10
GA01	E	0.00	-	-	-	0.01	0.14	-	0.09	0.16	0.35	0.43	0.00	0.07	-	0.07
KR01	E	-	-	0.20	-	0.10	0.10	0.30	0.11	0.03	0.20	0.00	0.16	0.08	-	0.03
PU01	E	-	-	-	-	0.01	0.01	-	0.22	0.09	0.35	0.00	0.00	0.19	-	0.04
JK01	E	0.25	-	-	-	0.01	0.06	-	0.09	0.07	-	-	0.00	0.18	-	0.05
SV01	E	-	-	-	0.07	0.03	0.09	-	0.15	0.08	-	0.00	-	-	-	0.09
AB01	E	-	-	0.13	-	0.05	0.48	-	0.10	0.15	-	0.00	0.00	0.23	-	0.07
MEAN		**0.26**	**-**	**0.22**	**0.14**	**0.03**	**0.13**	**0.16**	**0.15**	**0.09**	**0.25**	**0.10**	**0.10**	**0.15**	**0.26**	**0.06**
MEAN	**0.131**															

Table A.9: Coefficients of Variation for filter set **AK25BLE** (Alaska, 25 mm filters, blanks measured with calibration GeoExploration (E)), **AK25BLM** (Alaska, 25 mm filters, blanks measured with GeoMining (M)), **AK50BLE** (Alaska, 50 mm filters, blanks measured with calibration GeoExploration (E)), **AK50BLM** (Alaska, 50 mm filters, blanks measured with calibration GeoMining (M)), **EME** (50 mm filters, empty filters measured with GeoExploration (E)), **EMM** (50 mm filters, empty filters measured with GeoMining (M)) '-' describe <LOD.

SampleID	Cal.	As	Ba	Co	Cr	Cu	Fe	Mn	Ni	Pb	Rb	Se	Sr	Ti	V	Zn
A25_BLANK I	**E**	-	-	0.39	-	0.03	0.01	-	0.03	0.08	-	-	-	0.11	-	0.00
A25_BLANK II	**E**	-	-	-	-	0.02	0.00	-	0.00	0.18	-	-	-	0.34	-	0.03
A25_BLANK III	**E**	-	-	0.47	-	0.00	0.00	-	0.03	0.07	-	-	-	0.15	-	0.16
A25_BLANK I	**M**	-	-	-	0.05	0.02	0.09	-	-	-	0.13	-	0.14	-	0.06	-
A25_BLANK II	**M**	-	-	-	-	0.02	0.01	0.09	-	-	-	0.00	-	0.22	-	0.06
A25_BLANK III	**M**	-	-	-	-	0.01	0.00	-	-	-	-	0.16	-	0.16	-	0.06
A50_BLANK I	**E**	-	-	0.12	0.08	0.01	0.02	-	0.17	0.12	0.00	-	-	0.24	-	0.07
A50_BLANK II	**E**	-	-	0.13	0.08	0.02	0.03	-	0.18	0.09	-	-	0.00	0.15	-	0.06
A50_BLANK III	**E**	-	-	0.37	-	0.01	0.02	-	0.11	0.13	-	-	-	0.06	-	0.06
A50_BLANK I	**M**	-	-	0.35	0.13	0.06	0.02	0.12	-	0.17	-	0.09	-	0.24	-	0.08
A50_BLANK II	**M**	-	-	0.20	0.12	0.06	0.02	0.00	-	0.15	-	0.12	-	0.20	-	0.10
A50_BLANK III	**M**	-	-	-	0.14	0.06	0.02	0.37	-	0.11	-	0.00	-	0.14	-	0.04
MEAN	**E**	**-**	**-**	**0.29**	**0.08**	**0.01**	**0.01**	**-**	**0.09**	**0.11**	**0.00**	**-**	**0.00**	**0.18**	**-**	**0.06**
MEAN	**M**	**-**	**-**	**0.28**	**0.11**	**0.04**	**0.03**	**0.15**	**-**	**0.14**	**-**	**0.07**	**0.14**	**0.19**	**0.06**	**0.07**

EMPTY1-8	**E**	-	-	0.28	0.12	0.01	0.08	-	0.11	0.21	-	-	-	0.30	-	0.12
EMPTY9E	**E**	-	-	0.28	0.07	0.02	0.06	-	0.14	0.06	-	-	-	0.04	-	0.06
EMPTY9M/0	**M**	-	-	-	0.22	0.05	0.08	0.08	-	0.16	-	0.13	-	0.21	-	0.13
MEAN	**E**	**-**	**-**	**0.28**	**0.10**	**0.01**	**0.07**	**-**	**0.13**	**0.13**	**-**	**-**	**-**	**0.17**	**-**	**0.09**

Table A.10: TRACER 5i. Geo Exploration Calibration (P/N: 730.0187) and Geo Mining Calibration (P/N: 730.0203). Sample Prep: All calibration samples were prepared as dry sample powders packed into a sample cup and measured through a 4 micron foil. LOD specified for SiO2 matrix in three sigma 99.7% confidence level (3 sigma) and 180 second analysis time in 3-phase mode (60 sec per phase). Calibration range: Is based on available reference materials and can be extrapolated up to 10% (relative) over highest value. Bruker, 2017.

GEO EXPLORATION (3 PHASE RESULTS)	**MgO**	**Al2O3**	**SiO2**	**P**	**S**	**Cl**	**K2O**	**Ca**	**Ti**	**V**	**Cr**	**Mn**	**Fe**	**Co**	**Ni**	**Cu**	**Zn**	**Ga**	**As**	**Se**	**Rb**	**Sr**	**Y**	**Zr**
LOD (ppm) on pure SiO2	5000	1360	N/A	41	73	137	57	30	40	15	9	9	30	4	7	4	10	2	2	1	1	1	1	3
Upper Range (wt %)	70%	69%	100%	13.2%	41%	4%	15.3%	31%	7.1%	10.6%	3.7%	45.4%	67%	0.31%	3%	6.8%	19%	0.02%	2.3%	0.05%	0.05%	0.46%	0.11%	2.5%
Default Reporting as	OX	OX	OX	EL	EL	EL	OX	EL	EL	EL	EL	EL	EL	EL	EL	EL	EL	EL	EL	EL	EL	EL	EL	EL
Conversion factor OX --> EL	0.603	0.529	0.467	-	-	-	0.83	-	-	-	-	-	-	-	-	-	-	-	-	-	-	-	-	-

GEO EXPLORATION (3 PHASE RESULTS)	**Nb**	**Mo**	**Rh**	**Pd**	**Ag**	**Cd**	**In**	**Sn**	**Sb**	**Te**	**Ba(K)**	**La (K)**	**Ce (K)**	**Hf**	**Ta**	**W**	**Pt**	**Au**	**Hg**	**Tl**	**Pb**	**Bi**	**Th**	**U**
LOD (ppm) on pure SiO2	3	5	8*	10*	5	5	29*	15	14	8	48	123	181	11	6	35	7	5*	5	12	3	2	3	5
Upper Range (wt %)	42.4%	1.5%	0.03%	0.08%	0.66%	0.78%	0.06%	1.6%	19%	0.001%	10.7%	0.7%	4.8%	1.05%	0.22%	1.1%	0.16%	0.1%	0.07%	0.02%	4.3%	0.28%	0.68%	0.17%
Default Reporting as	EL	EL	EL	EL	EL	EL	EL	EL	EL	EL	EL	EL	EL	EL	EL	EL	EL	EL	EL	EL	EL	EL	EL	EL

GEO MINING (3 PHASE RESULTS)	**MgO**	**Al2O3**	**SiO2**	**P**	**S**	**Cl**	**K2O**	**Ca**	**Ti**	**V**	**Cr**	**Mn**	**Fe**	**Co**	**Ni**	**Cu**	**Zn**	**Ga**	**As**	**Se**	**Rb**	**Sr**	**Y**	**Zr**
LOD (ppm) on pure SiO2	4900	1200	N/A	30	68	138	60	36	40	18	9	10	10	3	7	4	6		2	1	1	1	1	1
Upper Range (wt %)	70%	69%	100%	13.2%	41%	4%	15.3%	31%	60%	56%	27%	45.4%	70%	72.4%	79%	80%	80%	0.02%	76%	0.05%	0.07%	1.02%	0.22%	39%
Default Reporting as	OX	OX	OX	EL	EL	EL	OX	EL	EL	EL	EL	EL	EL	EL	EL	EL	EL	EL	EL	EL	EL	EL	EL	EL
Conversion factor OX --> EL	0.603	0.529	0.467	-	-	-	0.83	-	-	-	-	-	-	-	-	-	-	-	-	-	-	-	-	-

GEO MINING (3 PHASE RESULTS)	**Nb**	**Mo**	**Rh**	**Pd**	**Ag**	**Cd**	**In**	**Sn**	**Sb**	**Te**	**Ba(K)**	**La (K)**	**Ce (K)**	**Hf**	**Ta**	**W**	**Pt**	**Au**	**Hg**	**Tl**	**Pb**	**Bi**	**Th**	**U**
LOD (ppm) on puer SiO2	1	8	10*	10*	7	7	30*	94	14	8	64	143	118	8	43	29	7	5*	1	11	4	3	3	6
Upper Range (wt %)	70%	67%	0.03%	0.08%	0.66%	0.78%	0.0%	88%	19%	0.02%	10.7%	0.70%	4.8%	1.05%	82%	80%	0.16%	0.1%	86%	0.02%	93%	90%	0.68%	0.17%
Default Reporting as	EL	EL	EL	EL	EL	EL	EL	EL	EL	EL	EL	EL	EL	EL	EL	EL	EL	EL	EL	EL	EL	EL	EL	EL

Table A.11: ICP-MS results (continued on page 141f.)

SAMPLEID SWEDEN	H_2O (g)	Filter weight (mg)	[Cd] absolute µg	[Ba] absolute µg	[Pb] absolute µg	[Na] absolute µg	[Al] absolute u µg	[V] absolute µg	[Cr] absolute µg	[Mn] absolute µg
PU01 C+D	3386	3.42	1.5	2.0	8.7	289.7	520.8	4.7	4.7	2.2
LU01 D+E	1886	5.47	0.7	2.2	1.5	122.2	212.9	5.5	3.2	3.4
BLANK 2	500	N/A	1.6	2.3	9.5	407.3	358.6	6.0	4.9	8.3
BLANK 3	500	N/A	1.7	6.6	7.5	312.5	5234.7	11.7	8.0	85.5
BLANK 4	500	N/A	0.7	2.0	0.9	105.0	944.2	6.3	2.0	14.0
BLANK 1	500	N/A	1.3	2.3	5.8	259.9	996.3	4.0	4.2	15.3
SV01 C+D	3430	13.44	1.4	2.2	8.2	284.6	298.4	3.1	3.3	2.1
LU01 A	736	N/A	1.2	2.2	5.7	252.7	243.6	4.5	4.1	4.1
KR01 C+D	3373	34.34	4.3	25.9	15.3	1034.0	2154.2	27.0	20.5	65.8
PU01 A+B	3384	6.69	1.6	3.3	9.1	371.4	525.1	3.6	5.7	6.6
LU01 A.2	836	4.44	0.5	1.3	1.1	158.0	173.6	3.8	0.9	2.9
SV01 A+B	3349	6.56	0.3	2.1	1.1	83.8	212.8	2.9	2.7	1.4
AR01 A+B	3644	13.77	0.9	1.7	5.5	280.2	525.9	2.9	3.3	4.1
LY01 A+B	3932	15.49	1.2	2.5	8.3	336.2	626.4	2.8	3.4	10.7
AB01 C+D	3656	7.44	0.6	1.4	3.5	201.4	235.0	3.0	1.3	2.7
JK01 C+D	3583	3.52	1.8	1.9	11.2	434.1	338.0	2.4	3.9	4.0
UM01 A+B	3619	35.34	1.6	8.5	11.1	512.6	1295.2	3.9	39.8	24.6
UM02 A+B	3700	16.56	1.7	4.7	11.5	433.1	817.0	3.1	5.0	21.8
AB01 A+B	3646	N/A	1.1	1.6	8.4	348.1	214.4	2.2	2.9	2.8
JK01 A+B	3039	4.77	0.7	1.2	3.1	163.1	209.5	2.2	1.7	2.7
GA01 D+E	3699	10.83	0.9	2.4	2.2	173.2	337.6	2.8	5.1	6.0
KR01 A+B	3352	20.11	1.5	1.6	8.1	366.0	463.0	6.3	8.3	8.2
AR01 C+D	3891	0.13	1.3	1.6	7.3	307.7	317.6	1.9	2.3	3.1
UM02 C+D	3619	25.51	1.8	7.4	11.0	472.5	1265.2	3.3	7.8	38.4
UM01 C+D	4466	47.12	1.2	12.6	9.2	473.9	2053.5	5.1	7.4	32.8
GA01 A+B+C	5336	7.67	1.4	2.7	7.3	347.8	396.7	2.4	2.9	5.3
LY01 C+D	3957	3.78	1.4	2.7	10.5	490.4	556.3	1.9	4.7	9.7
LU01 B+C	3468	0.33	1.6	1.9	10.5	450.0	343.6	3.2	3.7	6.9

SAMPLEID	[56Fe]	[57Fe]	[Ni]	[Cu]	[Zn]	[Sr]	[Ca]	[Rb]	[Mg]	[K]	Total
SWEDEN	absolute µg	absolute µg	absolute µg	absolute µg	absolute u µg	absolute µg	absolute µg	absolute µg	absolute µg	absolute µg	absolute µg
PU01 C+D	62.7	65.5	0.8	31.2	10.7	12.4	445.8	15.4	327.3	250.1	2.06
LU01 D+E	156.9	149.1	-2.1	20.6	15.9	7.4	219.0	14.3	218.7	403.5	1.55
BLANK 2	277.6	284.9	2.0	26.4	26.6	8.5	446.3	13.9	447.5	738.3	3.07
BLANK 3	4295.1	4267.5	1.1	18.4	20.4	9.3	320.1	19.7	590.0	1710.8	16.92
BLANK 4	654.2	661.6	0.2	31.8	18.3	7.8	256.9	13.0	236.2	598.9	3.55
BLANK 1	683.4	651.2	1.2	11.3	17.3	6.4	261.1	12.1	339.2	743.7	4.02
SV01 C+D	75.9	76.8	2.9	29.4	12.6	5.7	225.4	10.2	236.4	134.6	1.41
LU01 A	97.4	99.5	1.7	36.0	38.4	7.2	392.2	9.7	420.6	560.6	2.18
KR01 C+D	13780.8	13676.8	31.5	143.4	477.3	26.2	6562.9	13.8	18613.3	2754.4	59.43
PU01 A+B	378.8	366.5	5.3	6.8	30.6	7.4	455.9	9.3	493.3	697.7	3.38
LU01 A.2	56.5	54.6	0.7	34.4	22.2	5.5	266.7	8.5	278.1	385.8	1.46
SV01 A+B	63.8	57.7	0.6	36.4	7.4	4.7	164.8	7.6	146.2	100.7	0.90
AR01 A+B	143.7	145.1	-0.1	21.8	19.9	5.9	374.1	6.6	309.2	640.2	2.49
LY01 A+B	408.1	408.5	4.4	20.4	25.9	6.2	355.0	8.5	413.8	682.3	3.32
AB01 C+D	118.8	110.4	2.7	21.9	21.1	5.5	280.1	7.9	354.4	427.9	1.80
JK01 C+D	86.8	85.3	1.4	28.4	27.5	6.1	410.9	7.2	418.6	638.1	2.51
UM01 A+B	1438.8	1498.4	5.3	17.7	32.0	11.0	458.2	9.6	698.7	1138.6	7.21
UM02 A+B	689.6	694.8	5.5	25.5	31.4	7.8	421.6	8.3	515.4	760.8	4.46
AB01 A+B	95.9	83.5	2.5	22.3	19.0	4.9	339.6	5.5	334.2	475.2	1.96
JK01 A+B	63.6	69.6	5.9	26.9	22.3	4.2	230.3	5.6	241.4	423.0	1.48
GA01 D+E	350.4	356.2	4.4	37.0	32.5	5.2	348.7	5.2	338.7	442.1	2.45
KR01 A+B	2860.4	2856.3	1.1	13.3	17.2	4.5	267.1	6.3	448.3	464.8	7.80
AR01 C+D	115.9	114.5	3.6	16.4	20.5	3.7	275.8	5.3	265.2	434.3	1.90
UM02 C+D	1241.2	1209.6	6.7	42.1	40.2	10.7	620.4	8.1	699.3	1134.7	6.82
UM01 C+D	2254.8	2197.6	5.2	27.9	33.8	11.8	511.5	10.7	849.4	1552.1	10.05
GA01 A+B+C	418.3	399.2	5.0	24.6	24.0	5.1	403.5	5.8	344.4	791.8	3.19
LY01 C+D	328.3	335.1	5.3	59.2	74.0	5.2	550.3	5.6	521.7	825.4	3.79
LU01 B+C	266.0	273.9	6.9	20.2	28.2	4.5	371.4	5.1	382.9	649.3	2.83

SAMPLEID			[Cd]	[Ba]	[Pb]	[Na]	[Al]	[V]	[Cr]	[Mn]
ALASKA	H_2O (g)	Filter weight (mg)	absolute µg	absolute µg	absolute µg	absolute µg	absolute u µg	absolute µg	absolute µg	absolute µg
A14 AIR_L	1054	186.2	18.5	40.8	34.1	2810.3	4505.7	23.2	13.4	660.2
A20 DD	1291	231.7	30.2	73.8	162.3	6540.4	15706.2	44.6	73.7	165.5
BLANK I	1000	N/A	21.8	15.0	80.4	4577.8	1949.6	19.7	41.4	38.7
A3 RR	883	181.3	25.3	61.4	104.6	5108.7	8871.9	25.2	75.7	137.6
A22 AIR_C	872	107.2	24.1	23.5	96.3	4865.9	4714.3	15.0	35.0	66.9
A23 NOAA	551	200.5	22.3	47.6	106.0	5441.7	10594.6	20.8	32.8	102.9
BLANK III	1000	N/A	27.7	14.4	73.7	4289.0	2748.0	10.8	22.4	45.6
A15 JOH	146	621.4	26.3	86.5	104.5	6232.6	11286.6	63.7	139.7	387.7
A9 DPR 0	1319	441.8	29.0	82.6	122.8	6585.7	10196.5	63.6	99.0	339.6
A17 SKI	2695	108.8	24.5	35.1	88.8	5811.5	4303.4	17.8	40.3	54.0
A18 PF	1637	131.6	21.4	30.2	77.9	4405.8	7218.5	16.5	32.1	78.3
A21 USCR	3137	118.3	27.8	31.0	106.2	5450.5	5128.6	16.7	99.8	76.0
A19 DK	789	145.1	12.0	144.3	31.1	10668.6	8057.8	24.7	29.4	525.8
A4 HSR	511	171.9	16.9	44.7	89.1	4461.3	8039.6	17.2	38.2	96.8
A16 JOH_M	702	N/A	29.7	162.6	505.9	312405.6	11900.0	25.9	875.2	419.4
A5 GPH 0	1063	167.5	16.4	31.2	73.5	4450.1	5093.2	17.6	20.0	99.2
BLANK II	1000	N/A	25.3	12.9	109.9	6044.6	3031.6	8.7	31.0	49.9
A1 CS	2576	103.6	17.7	19.7	74.6	4408.5	4188.5	7.7	23.5	52.7
A13 AIR	193	211.6	23.0	82.3	83.7	5106.3	8001.4	20.3	37.3	145.1
A2 DHD	4264	149.5	19.5	36.6	69.7	4670.7	8616.7	19.5	22.7	97.6

SAMPLEID	[56Fe]	[57Fe]	[Ni]	[Cu]	[Zn]	[Sr]	[Ca]	[Rb]	[Mg]	[K]	Total
ALASKA	H_2O (g)	F. weight (mg)	µg	µg	µg	µg	µg	µg	µg	µg	µg
A14 AIR_L	4484.4	4757.7	25.4	369.3	258.6	83.0	5489.3	45.5	4030.0	6514.3	34
A20 DD	10459.5	10289.6	138.8	580.8	712.6	90.3	8642.7	60.6	8815.2	14158.7	77
BLANK I	506.4	544.6	113.0	407.1	346.0	51.4	5527.5	48.9	5053.5	8655.5	28
A3 RR	8580.8	8377.6	83.4	509.7	300.0	74.3	6027.7	41.5	5607.7	8031.5	52
A22 AIR_C	2177.7	2270.4	84.6	570.7	348.5	60.3	6275.1	34.1	6282.5	7795.6	36
A23 NOAA	4403.3	4225.7	59.2	279.2	269.1	87.1	5295.8	37.6	4812.9	10403.9	46
BLANK III	416.8	412.8	74.2	352.2	317.6	49.3	5915.6	28.1	5387.1	6990.3	27
A15 JOH	25533.7	25743.2	84.5	129.4	421.3	112.2	6735.1	34.1	5825.6	13639.3	97
A9 DPR 0	20542.5	20330.1	113.9	552.7	372.8	87.2	6601.6	39.1	6469.2	12631.3	85
A17 SKI	2054.1	1987.6	180.0	595.6	419.4	62.8	7940.0	34.9	5206.0	11588.0	40
A18 PF	2513.4	2659.3	108.5	477.4	345.0	55.0	5824.4	28.2	5587.5	7826.6	37
A21 USCR	2842.2	2811.8	92.4	-85.6	307.6	50.8	5597.7	32.4	5357.8	7759.7	36
A19 DK	3487.4	3291.1	173.1	854.5	10028.8	2367.2	365469.7	33.5	16050.1	30058.1	451
A4 HSR	4152.5	3991.9	54.2	351.6	216.0	42.8	3670.8	16.4	4148.0	6365.5	36
A16 JOH_M	5559.4	5671.1	1547.6	3683.2	21067.9	1249.5	280389.8	1683.8	43246.2	1836518.8	2527
A5 GPH 0	4914.5	4819.6	36.2	320.7	270.2	39.0	4282.4	19.1	4217.1	7001.5	36
BLANK II	653.6	724.0	79.3	618.3	360.2	51.7	7810.7	20.8	7603.5	9804.1	37
A1 CS	1449.3	1431.2	53.6	83.8	318.0	49.9	5174.8	21.3	5139.6	7230.9	30
A13 AIR	7828.7	8160.0	43.9	349.3	332.0	60.2	5408.1	17.5	5216.6	9414.2	50
A2 DHD	3906.8	4034.3	70.0	783.2	327.2	69.1	6802.5	17.7	6267.1	8742.5	45